สมบัติทางอิเล็กตรอนและสมบัติเชิงกลของสารกึ่งตัวนำคาร์บอนไนเตรตมีเทไดไอด์

นายสรจิตต์ อารีรัตน์

วิทยานิพนธ์นี้เป็นส่วนหนึ่งของการศึกษาตามหลักสูตรปริญญาวิทยาศาสตรมหาบัณฑิต
สาขาวิชาฟิสิกส์ ภาควิชาฟิสิกส์
คณะวิทยาศาสตร์ จุฬาลงกรณ์มหาวิทยาลัย
ปีการศึกษา 2556

ELECTRONIC AND MECHANICAL PROPERTIES OF CARBON NITRIDE METHANEDIIDE

Mr. Sorajit Arrerut

A Thesis Submitted in Partial Fulfillment of the Requirements
for the Degree of Master of Science Program in Physics
Department of Physics
Faculty of Science
Chulalongkorn University
Academic Year 2013

Thesis Title	ELECTRONIC AND MECHANICAL PROPERTIES OF CARBON NITRIDE METHANEDIIDE
By	Mr. Sorajit Arrerut
Field of Study	Physics
Thesis Advisor	Associate Professor Udomsilp Pinsook, Ph.D.

Accepted by the Faculty of Science, Chulalongkorn University in Partial Fulfillment of the Requirements for the Master's Degree

..... Dean of the Faculty of Science
(Professor Supot Hannongbua, Dr.rer.nat.)

THESIS COMMITTEE

..... Chairman
(Sathon Vijarnwannaluk, Ph.D.)

..... Thesis Advisor
(Associate Professor Udomsilp Pinsook, Ph.D.)

..... Thesis Co-advisor
(Assistant Professor Thiti Bovornratanaraks, Ph.D.)

..... Examiner
(Assistant Professor Surachate Limkumnerd, Ph.D.)

..... External Examiner
(Associate Professor Anucha Yangthaisong, Ph.D.)

ส รจิต ต์ อารี รัตน์ : สมบัติ ทาง อิเล็กตรอน และ สมบัติ เชิงกล ของ สาร กึ่ง ตัวนำ คาร์บอน ไน เตร ตมี เท ได ไอด์. (ELECTRONIC AND MECHANICAL PROPERTIES OF CARBON NITRIDE METHANEDIIDE) อ.ที่ปรึกษาวิทยานิพนธ์หลัก : รศ.ดร.อุดมศิลป์ ปิ่นสุข, อ.ที่ปรึกษาวิทยานิพนธ์ร่วม : ผศ.ดร.ธิติ บวรรัตนารักษ์, 74 หน้า.

สารประกอบคาร์บอนไนเตรตมีเทไดไอด์ $C_2N_2(CH_2)$ ถูกสังเคราะห์เป็นครั้งแรกในปี 2011 สารนี้มีพันธะเดียวระหว่าง C-N เหมือนกับสารคาร์บอนไนเตรต C_3N_4 ซึ่งเป็นสารที่มีความแข็งยิ่งยวด (super hard material) สารประกอบ $C_2N_2(CH_2)$ ถูกพบว่ามีช่องว่างแถบพลังงานกว้างประมาณ 6 eV จึงถูกจัดเป็นสารกึ่งตัวนำที่มีแถบช่องว่างพลังงานกว้าง (wide-band gap semiconductor) ซึ่งสามารถนำไปประยุกต์ใช้ได้มากมาย แต่อย่างไรก็ตามยังไม่มีการศึกษาเกี่ยวกับสมบัติของสารนี้มากนัก โดยเฉพาะอย่างยิ่งสมบัติของสารนี้ภายใต้ความดันสูง งานวิทยานิพนธ์ชิ้นนี้จึงมุ่งเน้นศึกษาสมบัติทางอิเล็กตรอนและสมบัติเชิงกลของสาร $C_2N_2(CH_2)$ ภายใต้ความดันระหว่าง 0-50 GPa โดยใช้ทฤษฎีฟังก์ชันนัลของความหนาแน่น (density functional theory) วิทยานิพนธ์นี้ได้ใช้ฟังก์ชัลนัล sX-LDA ซึ่งเป็นฟังก์ชันนัลของพลังงานการแลกเปลี่ยนและสหสัมพันธ์ (exchange-correlation functional) แบบไม่เฉพาะที่ (non-local) ที่เป็นเครื่องมือที่มีความแม่นยำเป็นอย่างมากในการศึกษาวัสดุที่มีแถบช่องว่างพลังงานกว้าง จากการศึกษาโดยใช้ฟังก์ชันนัล sX-LDA พบว่าสาร $C_2N_2(CH_2)$ มีช่องว่างแถบพลังงานกว้าง 6.07 eV และมีค่าลดเมื่อความดันมีค่าเพิ่มขึ้น เรายังพบความสัมพันธ์ระหว่างการเปลี่ยนแปลงของมุม N^1-C^1-N^2 กับแถบช่องว่างพลังงาน จากการคำนวณพบว่าค่ามอดูลัสเชิงปริมาตร (bulk modulus) มีค่า 254 GPa ซึ่งสอดคล้องกับผลการทดลอง เราพบว่าการหดตัวของพันธะ C-N ในสาร $C_2N_2(CH_2)$ ภายใต้ความดันมีความใกล้เคียงกับพันธะชนิดเดียวกันนี้ใน C_3N_4 แต่การหดตัวของพันธะ C-C ในสารนี้มีค่าสูงกว่าในเพชร ซึ่งส่งผลให้สาร $C_2N_2(CH_2)$ มีค่ามอดูลัสเชิงปริมาตรน้อยกว่าเพชร เราได้ทำการตรวจสอบเสถียรภาพของโครงสร้าง $Cmc2_1$ และพบว่ามันมีเสถียรภาพทั้งในเชิงพลวัต (dynamical) และเชิงกล (mechanical) ภายใต้ความดัน รามานสเปกตรัม (Raman spectrum) ของสาร $C_2N_2(CH_2)$ ถูกแสดงและเปรียบกับระบบอื่นเป็นครั้งแรกในงานวิทยานิพนธ์ชิ้นนี้

ภาควิชา ฟิสิกส์ ..... ลายมือชื่อนิสิต .....

สาขาวิชา ฟิสิกส์ ..... ลายมือชื่อ อ.ที่ปรึกษาวิทยานิพนธ์หลัก .....

ปีการศึกษา 2556 ..... ลายมือชื่อ อ.ที่ปรึกษาวิทยานิพนธ์ร่วม .....

5472125423 : MAJOR PHYSICS
KEYWORDS: DENSITY FUNCTIONAL THEORY/$C_2N_2(CH_2)$ /HIGH PRESSURE/ELECTRONIC AND MECHANICAL PROPERTIES

SORAJIT ARRERUT: ELECTRONIC AND MECHANICAL PROPERTIES OF CARBON NITRIDE METHANEDIIDE. ADVISOR: ASSOC. PROF. UDOMSILP PINSOOK, Ph.D., CO-ADVISOR: ASST. PROF. THITI BOVORNRATANARAKS, Ph.D.,74 pp.

The carbon nitride methanediide, $C_2N_2(CH_2)$, has been newly discovered in 2011. This compound contains the C-N single bond, the same as in a super hard material carbon nitride, C_3N_4. The band gap of $C_2N_2(CH_2)$ is around 6 eV. Thus, it is classified as a wide-band gap semiconductor which has many applications. However, the knowledge of $C_2N_2(CH_2)$ is limited; especially, its properties under high pressure. In this thesis, we investigate the mechanical and electronic properties of $C_2N_2(CH_2)$ under high pressure, in the range of 0-50 GPa, using density functional theory (DFT). The non-local exchange-correlation functional calculation, sX-LDA, which is the most accurate tool to simulate wide-band gap materials, is performed. Our result shows that the $C_2N_2(CH_2)$ band gap is 6.07 eV, using the sX-LDA, and it decreases as pressure increases. Moreover, we find the relation between the N^1-C^1-N^2 angle change and the band gap. The bulk modulus of $C_2N_2(CH_2)$ is 254 GPa from our calculation which is in good agreement with the experimental data. The bond contractions of C-N and C-C single bonds are explored. We find that the C-N bond contraction in $C_2N_2(CH_2)$ is the same as those in C_3N_4. However, the C-C bond contraction in $C_2N_2(CH_2)$ is larger than those in diamond. This leads to the lower bulk modulus compared with that of diamond. The $Cmc2_1$ structure stability of $C_2N_2(CH_2)$ is examined and found that it has dynamical and mechanical stabilities. The Raman spectrum of $C_2N_2(CH_2)$ is predicted for the first time in this work, and compared with references from other systems.

Department:.....Physics.....Student's Signature .....

Field of Study:.....Physics.....Advisor's Signature .....

Academic Year:.....2013.....Co-advisor's Signature .....

ACKNOWLEDGEMENTS

First of all, I gratefully thank my advisor, Assoc. Prof. Udomsilp Pinsook, for his always being kindness towards me during Master Program and for his useful advices to make this thesis complete. I highly thank my co-advisor, Asst. Prof. Thiti Bovornratanaraks, for his encouragement and support during my 3 years of Master Program. I would like to thank Dr. Sathon Vijarnwannaluk, Asst. Prof. Surachate Limkumnerd and Dr. Anucha Yangthaisong for his time to examine my thesis. I would like to thank Prof. Rajeev Ahuja for his suggestion on the LDA and the GGA functional. I want to acknowledge Assoc. Prof. Nakorn Phaisangittisakul for his valuable discussions. I want to thank the computing facilities from Chulalongkorn University Centenary Academic Development Project (CU56-FW10) and the Ratchadaphiseksomphot Endowment Fund of Chulalongkorn University (RES560530180-AM) and financial support from the Special Task Force for Activating Research (GSTAR 56-003-23-002), and 90^{th} Year Chulalongkorn Scholarship from Graduate School, Chulalongkorn University. This thesis was partially supported by the National Research Council of Thailand (NRCT). Finally, I profoundly thank all members of ECPRL for their encouragement, friendship and very helpful discussion.

CONTENTS

page

LIST OF TABLES

Table **page**

LIST OF FIGURES

Figure **page**

Chapter I

INTRODUCTION

The carbon nitride methanediide, $C_2N_2(CH_2)$, was synthesized successfully in 2011 [1]. A few years later many researchers studied the mechanical and electronic properties of this compound [2, 3, 4, 5, 6]. They showed that $C_2N_2(CH_2)$ consisted of the C-N single bond which had compressibility comparable with those of super hard material carbon nitride, C_3N_4. In addition, Sougawa [2] claimed that the C-C single bond in this compound also had compressibility comparable with the C-C bond in diamond. This made the mechanical properties of the $C_2N_2(CH_2)$ compound attractive. For the electronic property, its band gap was over 6 eV predicted using first principle method so it was classified as a wide-band gap semiconductor. The wide-band gap semiconductor has a band gap wider than a material in general use [7], i.e. the band gap of Si. It possesses many interesting optical and electrical properties. For the optical property, a semiconductor with a band gap between 1.9-3.1 eV and more than 3.1 eV emits photon in the range of visible light and UV [8, 9], respectively. A UV emitting semiconductor has many applications, such as solar UV measurement, missile plume detection, bactericidal and vitamin-synthesizing [9, 10]. The electronic property is more advantageous than that of Si, for example, the maximum junction temperature limit for most Si devices is 150 °C but the wide band gap device can be operated at higher temperatures. An explicit example is SiC which has a band gap between 2.00-7.00 eV. A SiC device can be operated at 350 °C up to 500 °C [11].

In 1989, Liu and Cohen proposed an empirical model to calculate the bulk modulus of covalent solids [12]. This model showed that the bulk modulus was a function of iconicity parameter (λ) and bond length (d)

$$B = \frac{19.71 - 2.20\lambda}{d^{3.5}} \tag{1.1}$$

It can describe the bulk modulus of diamond and zine-blende solids precisely. Then Liu and Cohen proposed the β-C_3N_4 structure (as shown in FIG.1.1a) based on Eq.(1.1) and the β-Si_3N_4 structure. They found that the bulk modulus of

this material is 427 ± 15 GPa which was compareable to that of diamond (442 GPa) [13]. They explained in more detail that the bond length of C-N in the β-C_3N_4 is shorter than C-C in diamond, resulting in lower compressibility. After the structure of β-C_3N_4 was proposed, many researches about this material, both theoretical and experimental work, were employed. From theoretical researches, the other phases of C_3N_4 were predicted, such as α-C_3N_4 [14, 15], g-C_3N_4[10], pseudocubic-C_3N_4 [15, 16], cubic- C_3N_4 [15, 17] etc.. The highest bulk modulus of C_3N_4 is 496 GPa [15] in the cubic-C_3N_4 phase which is higher than that of diamond. They also predicted the phase transition of this material under pressure [18]. The results showed that the cubic-C_3N_4 can arise at high pressure. However, this material has not been successfully synthesized yet because the N_2 molecule also has strong stability so it is hard to form the C-N single bond.

In 2011, Sougawa and his team tried to synthesize C_3N_4 using $C_3N_4H_xO_y$ nanoparticles as a substance [1]. They expected that the chemical reaction of $C_3N_4H_xO_y \rightarrow C_3N_4 + H_xO_y$ might occur under extreme condition. If this chemical reaction occurs, superhard C_3N_4 will be discovered. In that experiment, they used the laser heating diamond anvil cell (LHDAC) to control temperature and pressure. A new crystalline phase was detected at the pressure of 40 GPa and the temperature of 1200-2000 K. The researchers used many methods to analyze this crystal, i.e., X-ray diffraction (XRD), transmission electron microscopy (TEM), selected area electron diffraction (SAED), energy dispersive X-ray spectroscopy (EDS), Rietveld analysis and first-principle calculation. They reported that the chemical formula of this compound is $C_2N_2(CH_2)$ and the structure is orthorhombic with the space group $Cmc2_1$ as shown in FIG.1.2 . In addition, they found that this compound, like C_3N_4, contains the C-N single bond. The compressibility of the single bonds, i.e. C-N and C-C, and the bulk modulus of this compound were reported [2, 3]. They examined the compressibility of the single bonds by calculating single bond length at 30 GPa relative to those at 0 GPa. Then they compared with those of β-C_3N_4 and diamond. They concluded that the compressibility of the single bonds in this material is comparable with those of β-C_3N_4 and diamond. However, the bulk modulus of the $C_2N_2(CH_2)$ is 258 ± 3.4 GPa by fitting the experimental data of the volume under pressure with the Birch-Murnaghan equation of state (EOS). This value was about 40% less than that of diamond. They explained that the low bulk modulus in this compound was due to the rotation of tetrahedral $C^1N_3C_b$ which does not exist in diamond. The electronic structure was calculated using the density function theory (DFT) with a non-local exchange correlation, sX-LDA [4]. The results showed that this compound has band gap

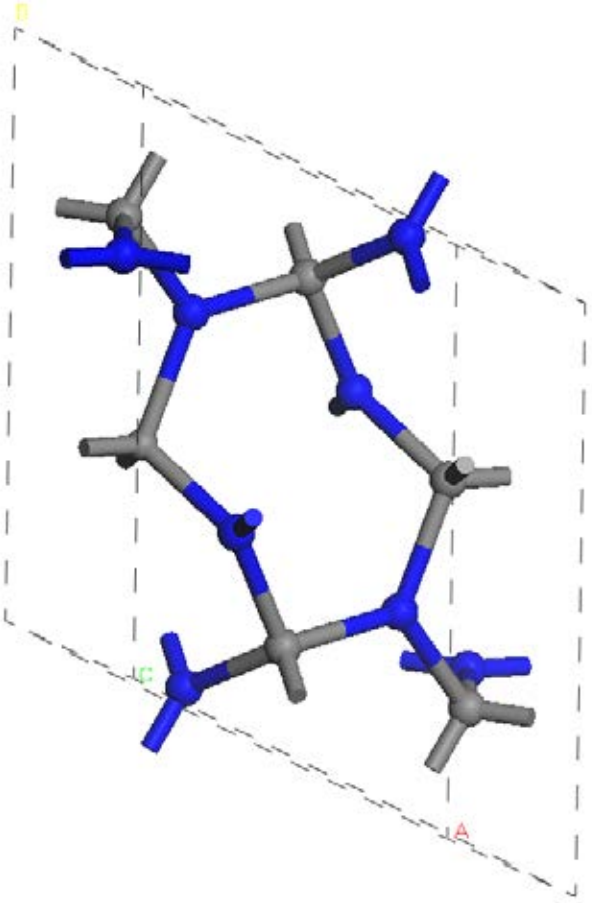

(a)

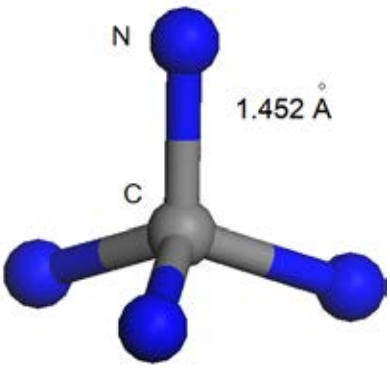

(b)

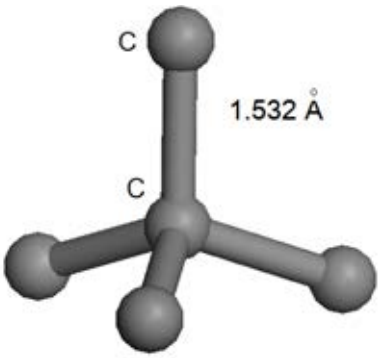

(c)

Figure 1.1: (a) The β-C_3N_4 structure. (b) The C-N single bond in β-C_3N_4 and (c) the C-C single bond in diamond. Carbon in grey and Nitrogen in blue.

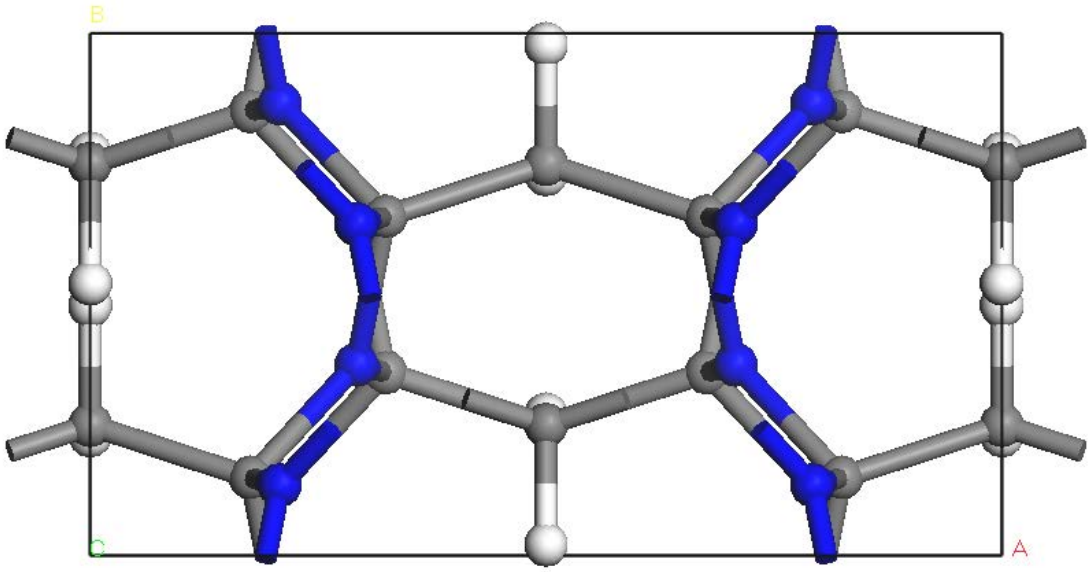

Figure 1.2: Structure of $C_2N_2(CH_2)$ with $Cmc2_1$ space group.

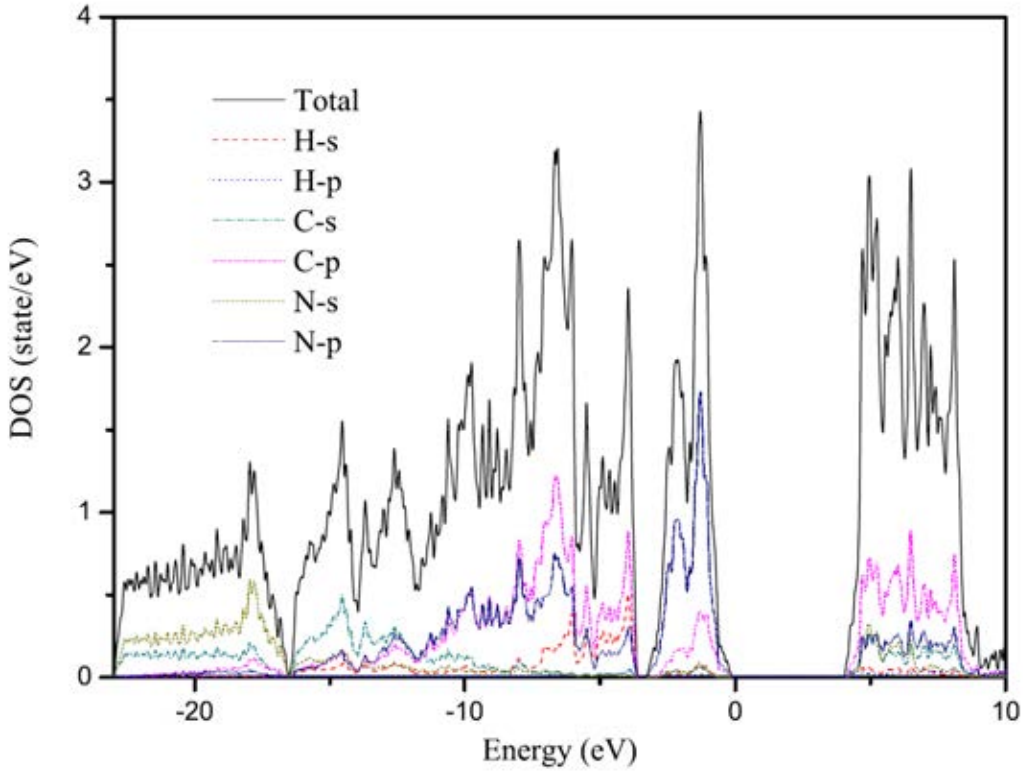

Figure 1.3: The partial density of state of $C_2N_2(CH_2)$ was calculated by Qun [15]

around 6 eV so it is classified as a wide-band gap semiconductor.

Its Youngs modulus and shear modulus were predicted by Qun Wei [5]. He found that the highest Youngs modulus is 686 GPa and the lowest is 376 GPa when the tensile axis is in the [001] and [120] directions, respectively. The shear modulus of the $C_2N_2(CH_2)$ is the largest on the (001) plane with [010] stress direction and on (010) plane with the [001] shear stress direction. The electronic structure was analyzed by examining the partial wave density of states (PDOS) projected onto different atoms, i.e., C, N and H (some typical results are shown in FIG.1.3). This showed that the valence band maximum (VBM) was mainly originated from C-p and N-p orbitals, and the conduction band minimum (CBM) was mainly superimposed of the C-p orbitals.

Yingchun Ding [6] examined the hardness of the $C_2N_2(CH_2)$ using two semiempirical hardness models, i.e., Gao's model [19] and Simuneks's model [20]. The Vickers hardness [18] should be more than 40 GPa for a super hard compound but is 30.53 GPa and 38.49 GPa, respectively for this compound so it was not a super hard compound. Moreover, the hardness of the C-C bond in the $C_2N_2(CH_2)$ was calculated and found that it is only 20.28 GPa which is very low compared with the hardness of the C-N single bond ($\sim$35 GPa) in that work. It could imply that the compressibility of the C-C bond in the $C_2N_2(CH_2)$ is higher than that of diamond. This result contrasts with the Sougwa's work which claimed that it has compressibility comparable with that of diamond.

According to our review, the knowledge about the properties of the $C_2N_2(CH_2)$ under pressure needs more investigation; especially, the contraction of the C-C bond, the structure stability and the band structure. Therefore, we will focus on these issues. In this thesis, the $C_2N_2(CH_2)$ compound is simulated using Cambridge serial total energy package (CASTEP) code based on the DFT with three different exchange-correlation functional, i.e., LDA, GGA and sX-LDA. The mechanical and electronic properties of this compound under high pressure, from 0 to 50 GPa, are studied. For the mechanical property, we compare the lattice parameters and volume under pressure from our calculation with the experimental and previous theoretical work [1, 5]. The bulk modulus is calculated using the third-order Birch-Murnaghan equation of states. The contraction of the single bonds, i.e. C-N and C-C, are examined in the same way as Sougawa's work [2]. The effect of pressure on the interatomic angle is studied. The Raman spectrum is calculated and compared with the experimental data for the first time in this work. For the electronic property, the change of band gap and the density of states

under pressure are studied. The direct-indirect band gap crossing over effect is tested. The effect of interatomic angle on the band gap is analyzed.

The organization of the thesis is as follows: In Chapter 2 we describe the theory is used in this work. Chapter 3 contains the results for structure property, phonon and raman spectrum under high pressure. We present, in Chapter 4, electronic property, i.e., band structure, density of state and relation between interatomic angle and band gap. Finally, Chapter 5 gives the conclusions.

Chapter II

THEORETICAL BACKGROUND

The comprehension of electrons behavior plays an important role to predict property of the condensed matter. The electrons behavior is studied by solving the Schrödinger's equation. However it is hardly to find the exact solution of it due to a number of electron and Coulomb interaction. There are two approaches to overcome this problem. First approach is solving the Schrödinger's equation directly using approximation method, i.e., Hartree approximation, Hartree-Fock approximation and perturbation theory. The second method, which is used in our work, is the density functional theory (DFT).

In 1964, Hohenberg and Kohn proposed that a total energy of the condensed matter can be written in terms of functional of electron's density. This leads to DFT which is a power approach to study a property of a solid. In this chapter, a traditional method, i.e., Hartree and Hartree-Fock approximation, used to solve the many body problems is introduced. Next the Kohn-Sham equation, which is the core equation of the DFT, and the method to solve it is explained. Finally, we show a method to calculate a property, i.e., bulk modulus, phonon dispersion, Raman spectrum and band structure, from the DFT.

2.1 Many body problems

Quantum mechanics is an important tool to study property of solid because it explains a behavior of a small unit such as electrons and nuclei which are the cause of macroscopic properties of condensed matter. If we can find exact solution of Schrödinger's equation of the solid system,

$$\hat{H}\Psi = E\Psi, \tag{2.1}$$

we will know all their features. Here E is the energy of the system, Ψ is the wavefunction and $\hat{H}$ is the Hamiltonian operator of the system which can be

written as

$$\hat{H} = \hat{T}_{\text{e}} + \hat{V}_{\text{e-e}} + \hat{V}_{\text{n-e}} + \hat{T}_{\text{n}} + \hat{V}_{\text{n-n}}. \tag{2.2}$$

$\hat{T}_{\text{e}}$ represents the operator for the kinetic energy of the electrons, the second term, $\hat{V}_{\text{e-e}}$ represents the operator for the Coulomb potential between the electron and the electron, the third term, $\hat{V}_{\text{n-e}}$ represents the operator for the Coulomb potential between the electron and the nucleus, the next term, $\hat{T}_{\text{n}}$ represents the operator for the kinetic energy of the nuclei and the last term, $\hat{V}_{\text{n-n}}$, represents the operator for Coulomb potential between the nucleus and the nucleus.

The solid system consists of millions of electrons and nuclei so Eq.(2.1) is too complicated to find an exact solution. In 1927, M. Born and J. R. Oppenheimer proposed that the solution of Eq.(2.1) can be separated into two parts; the electron and the nucleus wavefunctions, under adiabatic condition. To calculate the electron part, the third and the fourth term in Eq.(2.2) are solved separately. This approximation is called Born-Opppenheimer approximation. If we choose to focus on the electron, the Hamiltonian can be reduced to

$$\hat{H} = \hat{T}_{\text{e}} + \hat{V}_{\text{e-e}} + \hat{V}_{\text{n-e}}. \tag{2.3}$$

The exact solution for the Hamiltonian in Eq.(2.3) is still unknown even when Born-Opppenheimer approximation is used to reduce the nucleus part from the problem. There are two methods to find a solution of Eq.(2.3). The first method, the Schrödinger's equation is solved directly by solving an eigenvalue problem. Hartree proposed that if the wavefunction of the n-body system can be written as the superposition of a one-body wavefunction, the problem will reduced to the one-body problem (n-equations), called Hartree approximation,

$$\Psi_{\text{H}} = \varphi\left(\mathbf{r_1}\right)\varphi\left(\mathbf{r_2}\right)...\varphi\left(\mathbf{r_n}\right). \tag{2.4}$$

He found that the ground state energy calculated by using Eq.(2.4) is always an overestimation to the true ground state energy.

To overcome this problem, we include some electron properties directly into the wavefunction. Electron is a fermion, it must satisfy Pauli's exclusion principle, and for identical particles, electron can permute. The wavefunction which is a solution to equation Eq.(2.3) must be antisymmetric to accord with the property of electron; this approximation is called Hartree-Fock approximation. The antisymmetric wavefunction can be satisfied using Slater determinant

$$\Psi_{\text{HF}} = \frac{1}{\sqrt{N!}}\det[\varphi_1\varphi_2...\varphi_N]. \tag{2.5}$$

The ground state energy calculated by this approximation is lower than Hartree approximation but is still higher than the exact ground state energy. The difference in the ground state energy calculated by Hartree-Fock approximation and Hartree approximation is called the exchange energy, while the difference between Hartree-Fock energy and the exact ground energy is called the correlation energy. The accuracy of the total energy calculation can be improved if the perturbation theory is applied. However, this method requires a lot of computing resources.

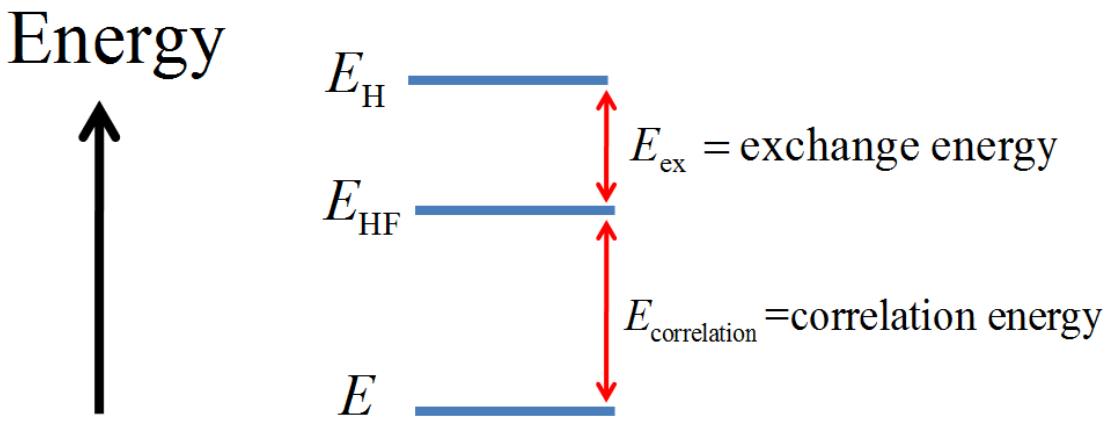

Figure 2.1: The ground state energy calculated by Hartree approximation and Hartree-Fock approximation.

2.2 Density functional theory

This theory proposed by Hohenberg and Kohn states that the total energy, Eq.(2.3), of the solid system can be represented in terms of functionals of electron density,

$$E[n] = T[n] + V_{\text{e-e}}[n] + V_{\text{n-e}} = F_{\text{HK}}[n] + V_{\text{n-e}}[n]. \tag{2.6}$$

$n \equiv n(\mathbf{r})$ is the electronic density and $F_{\text{HK}}[n]$ is a Hohenberg-Kohn functional. To simplify Eq.(2.6), the exact electron kinetic energy, T, is replaced by the electron kinetic energy of a non-interacting system, T_{s}. The Coulomb potential, $V_{\text{e-e}}$, between electron and electron is replaced by the classical Coulomb potential or Hartree pontential, V_{H}. The Coulomb potential between nucleus and electron is redefined as external potential, V_{ext}, and the correction term due to electron-electron interaction is included in exchange-correlation energy, E_{xc},

$$E[n] = T_{\text{s}}[n] + V_{\text{H}}[n] + V_{\text{ext}} + E_{\text{xc}}[n]. \tag{2.7}$$

The detail of the exchange-correlation energy will be discussed later. Hohenberg and Kohn proved two important theorems which are

1. There is only one exact ground density, $n_0(\mathbf{r})$, that corresponds to an external potential, $V_{\text{ext}}[n]$.

2. The total energy can be represented in terms of the functionals of the electron density. The energy functional gives minimum value if and only if the density is the exact ground state density.

$$E_0 = \sum_n E[n] = E[n_0] < E[n] \tag{2.8}$$

These two theorems imply that if the variational principle is applied to the energy functional, the variation will be zero when the energy is lowest; in other words, the density is the ground state density. This leads to Kohn-Sham equation which is the most important equation in the density functional theory,

$$\frac{\delta E[n_0]}{\delta n(\mathbf{r})} = 0. \tag{2.9}$$

2.3 Kohn-Sham equation

According to Eq.(2.7), the kinetic energy in term of the electron density was first proposed by Thomas-Fermi which was based on the uniform electron gas,

$$T_{\text{TF}}[n] = \frac{3}{10}\left(3\pi^2\right)\int n^{5/3} d\mathbf{r}. \tag{2.10}$$

However, this formula is not used in this calculation because its performance is really inaccurate. The electron's kinetic energy used in our calculation was proposed by Kohn and Sham in 1965,

$$T_{\text{s}}[n] = \sum_{i=1}^{N}\int \varphi_i^*(\mathbf{r})\left(-\frac{\hbar^2}{2m}\nabla^2\right)\varphi_i(\mathbf{r})d\mathbf{r}, \tag{2.11}$$

where the φ_i are the orbitals of the non-interacting system and the electron density can be defined by

$$n(\mathbf{r}) = \sum_{i=1}^{N}\left|\varphi_i(\mathbf{r})^2\right| = \sum_{i=1}^{N}\varphi_i^*\varphi_i. \tag{2.12}$$

The second term of Eq.(2.7) is the classical Coulomb potential or Hartree's potential. The constant $\frac{1}{4\pi\varepsilon_0}$ is omitted. Eq.(2.7) can be expressed explicitly as

$$V_{\mathrm{H}}[n] = \int\int \varphi_i(\mathbf{r})\varphi_i(\mathbf{r})^* \frac{1}{|\mathbf{r}-\mathbf{r}'|}\varphi_j(\mathbf{r}')\varphi_j(\mathbf{r}')^* d\mathbf{r}d\mathbf{r}'$$
$$V_{\mathrm{H}}[n] = \int \varphi_i(\mathbf{r})\varphi_i(\mathbf{r})^* \int \frac{\varphi_j(\mathbf{r}')\varphi_j(\mathbf{r}')^*}{|\mathbf{r}-\mathbf{r}'|} d\mathbf{r}'d\mathbf{r}. \tag{2.13}$$

From electrostatics, the scalar potential, $\Phi(\mathbf{r})$, is generated by $\int \frac{n(\mathbf{r}')}{|\mathbf{r}-\mathbf{r}'|}d\mathbf{r}'$ so

$$V_{\mathrm{H}}[n] = \frac{1}{2}\int \varphi_i(\mathbf{r})\varphi_i(\mathbf{r})^*\Phi(\mathbf{r}) = \frac{1}{2}\int n(\mathbf{r})\Phi(\mathbf{r})d\mathbf{r}. \tag{2.14}$$

The factor $\frac{1}{2}$ is included to take care of double-counting. The third of Eq.(2.7) is the external potential which can be written as

$$V_{\mathrm{ext}}[n] = \int v_{\mathrm{ext}}(\mathbf{r})n(\mathbf{r})d\mathbf{r}. \tag{2.15}$$

The last term of Eq.(2.7) is the exchange-correlation term. As we have explained before, it is a correction term to our approximation. In more detail, it is the difference between the exact many-body energy and the non-interacting kinetic energy and the Hartree's energy,

$$E_{\mathrm{xc}}[n] = (T - T_{\mathrm{s}}) + (V_{\mathrm{ee}} - V_{\mathrm{H}}). \tag{2.16}$$

There is no explicit form for E_{xc}. Thus there are only proposed models which we will talk about later. The simplest form of this term can be written as

$$E_{\mathrm{xc}} = \int v_{\mathrm{xc}}n(\mathbf{r})d\mathbf{r}. \tag{2.17}$$

From Eq.(2.9) and Eq.(2.12), the electron density is defined from a complex function but the value is always real. To find the extremum value in this case, not only must the condition in Eq.(B.3) be satisfied but also the constraint that the number of electrons must be conserved, $\sum_i \int \varphi_i\varphi_i^* d\mathbf{r} = N$. The Euler's equation with Lagrange multiplier ε_i can be represented by

$$\frac{\delta}{\delta n}[E(n)] = \frac{\delta}{\delta\varphi_i^*}[E\{\varphi_i\}] = 0,$$
$$\frac{\delta}{\delta\varphi_i^*}[T_{\mathrm{s}} + V_{\mathrm{H}} + V_{\mathrm{ext}} + E_{\mathrm{xc}} - \sum_i \varepsilon_i \left(\int \varphi_i\varphi_i^* d\mathbf{r} - N\right)] = 0. \tag{2.18}$$

The derivatives of kinetic energy, external potential, exchange-correlation energy and the constraint, the first, the third, the fourth and the last term of Eq.(2.18),

respectively are written as

$$\begin{aligned}
\frac{\delta}{\delta\varphi_i^*}T_{\rm s} &= -\frac{\hbar^2}{2m}\nabla^2\varphi_i, \\
\frac{\delta}{\delta\varphi_i^*}V_{\rm ext} &= v_{\rm ext}(\mathbf{r})\varphi_i, \\
\frac{\delta}{\delta\varphi_i^*}E_{\rm xc} &= v_{\rm xc}\varphi_i, \\
-\varepsilon_i\varphi_i &= -\sum_i \varepsilon_i \frac{\delta}{\delta\varphi_i^*}\left(\int \varphi_i\varphi_i^* d\mathbf{r} - N\right).
\end{aligned} \tag{2.19}$$

The derivative of the Hartree potential is more complicated than the other terms because both density and scalar potential depend on φ_i^*. The changing of density is calculated in the same way as the other terms but the changing of scalar potential is more complicated. To consider the changing of a scalar potential, we recalled that Poissons equation is $\nabla^2\Phi(\mathbf{r}) = -n(\mathbf{r})$, where the factor 4π is omitted, and it is implied that $\nabla^2\delta\Phi(\mathbf{r}) = -\delta n(\mathbf{r})$,

$$\int (\delta\Phi) n d\mathbf{r} = \int (\delta\Phi)\left(-\nabla^2\Phi\right) d\mathbf{r}.$$

If we integrate by parts this equation twice, we have,

$$\begin{aligned}
\int (\delta\Phi)\left(-\nabla^2\Phi\right) d\mathbf{r} &= -(\delta\Phi)\nabla\cdot\Phi + \Phi\nabla\cdot(\delta\Phi) - \int \Phi\nabla^2(\delta\Phi) d\mathbf{r}, \\
&= \int \Phi\delta n d\mathbf{r}.
\end{aligned} \tag{2.20}$$

The first and second term in this equation vanish because the change of scalar potential at the boundary must be zero. Then the derivative of the functional $V_{\rm H}$ is

$$\begin{aligned}
\frac{\delta}{\delta\varphi_i^*}V_{\rm H} &= \frac{1}{2}\left[\Phi(\mathbf{r})\frac{\delta}{\delta\varphi_i^*}n(\mathbf{r}) + n(\mathbf{r})\frac{\delta}{\delta\varphi_i^*}\Phi(\mathbf{r})\right], \\
&= \Phi(\mathbf{r})\frac{\delta}{\delta\varphi_i^*}n(\mathbf{r}), \\
&= \Phi(\mathbf{r})\varphi_i.
\end{aligned} \tag{2.21}$$

By replacing Eq.(2.19) and Eq.(2.21) in Eq.(2.18). We get the final result,

$$\begin{aligned}
-\frac{\hbar^2}{2m}\nabla^2\varphi_i + \Phi(\mathbf{r})\varphi_i + v_{\rm ext}(\mathbf{r})\varphi_i + v_{\rm xc}\varphi_i - \varepsilon_i\varphi_i = 0, \\
\left[-\frac{\hbar^2}{2m}\nabla^2 + v_{\rm eff}\right]\varphi_i = \varepsilon_i\varphi_i.
\end{aligned} \tag{2.22}$$

This is the Kohn-Sham equation and the $v_{\rm eff}$ is the effective potential which is defined by

$$v_{\rm eff} = \Phi(\mathbf{r}) + v_{\rm ext} + v_{\rm xc}.$$

2.4 Exchange-correlation energy

As we explained before, The Hohenberg-Kohn theorem stated that the total energy of the solid system can be represented in terms of functionals of the electron's density, $E = E[n]$. However, the exact energy functional is not known and, may be, it does not have an explicit form. This means that the exact mapping from n to E cannot be written as a formula with E on the left-hand side and n on the right. In the Kohn-Sham method, the exchange-correlation is only one unknown term and must be modeled. Indeed, this term is very important for the precision of the Kohn-Sham method. The exchange-correlation energy can be separated into two terms, the exchange energy and the correlation energy,

$$E_{\mathrm{xc}}[n] = E_{\mathrm{x}}[n] + E_{\mathrm{c}}[n]. \tag{2.23}$$

Hartree-Fock approximation shows that the exchange energy arises from the fact that the electron wavefunction must be an antisymmetric wavefunction. Actually the explicit form of the exchange energy is,

$$E_{\mathrm{x}}^{\mathrm{exact}}[n] = -\int\int \varphi_j(\mathbf{r})\varphi_j^*(\mathbf{r}')\frac{1}{|\mathbf{r}-\mathbf{r}'|}\varphi_i^*(\mathbf{r})\varphi_i^*(\mathbf{r}')d\mathbf{r}d\mathbf{r}', \tag{2.24}$$

but this exact form is not used in the DFT calculation because it is non-local, i.e. $\mathbf{r}'$ dependent. There are many form of the exchange-correlation energy that has been proposed but the functionals widely used in physics calculations are the local density approximation (LDA), the generalized gradient approximation (GGA) and the screened-exchange local density method (sX-LDA).

The local density approximation or LDA is the simplest exchange-correlation energy. This method supposes that the exchange-correlation energy takes the forms of that of the uniform electron gas system. In the uniform electron gas or homogeneous electron gas system, the exact exchange energy can be defined by

$$E_{\mathrm{x}}[n(\mathbf{r})] = \int n\left(C_{\mathrm{x}}n^{1/3}\right)d\mathbf{r}, \tag{2.25}$$

where the C_{x} is a constant. The exact correlation energy does not exist, even in a very simple system, although approximations in the high-density and low-density limits can be ascertained. Thus it assumes the form

$$E_{\mathrm{c}}\left[n(\mathbf{r})\right] = -B\int n(1+\alpha_1 r_{\mathrm{s}}) \ln\left[1+\frac{1}{B\left(\beta_1 r_{\mathrm{s}}^{1/2}+\beta_2 r_{\mathrm{s}}+\beta_3 r_{\mathrm{s}}^{3/2}+\beta_4 r_{\mathrm{s}}^2\right)}\right]d\mathbf{r}, \tag{2.26}$$

which arises from interpolations between those two limits. Where the r_{s}, defined from $\frac{4}{3}\pi r_{\mathrm{s}}^3 = \frac{1}{n}$, is the radius of a sphere whose volume is the effective volume of an electron. The variables B, α_1 and β_i, in Eq.(2.26) are fitting constants. Normally, they are fit to known properties, i.e., atomic spectra, etc. As in Eq.(2.25) and Eq.(2.26), the exchange and the correlation functionals depend on the electron density at the observing position and the exchange-correlation energy in uniform electron gas can be written as an integral of the exchange-correlation potential, v_{xc}, as

$$E_{\mathrm{xc}}^{\mathrm{LDA}}[n] = E_{\mathrm{xc}}^{\mathrm{uniform}}[n] = \int v_{\mathrm{xc}}^{\mathrm{uniform}}(n) n d\mathbf{r} \tag{2.27}$$

The LDA is reasonably accurate for the prediction of bond lengths and lattice constants, but has some significant errors, for example in atomic energy, molecular energy and band gap. The problem of the LDA calculation is due to the fact that the electron density in a real system is far from that of the uniform electron gas. To improve the LDA, the generalized gradient approximation, GGA, is developed by added the gradient of the electrons density; in order to, contain some information of the environmental detail around an observing position. This, to some extent, can cover the non-local behavior of the electrons.

The generalized gradient approximation or GGA explicitly includes the gradient of electron density into the exchange-correlation energy,

$$E_{\mathrm{xc}}^{\mathrm{GGA}}[n] = \int v_{\mathrm{xc}}\left(n, |\nabla n|\right) n d\mathbf{r}. \tag{2.28}$$

We chose the model that is proposed by Perdew-Burke-Ernzerfof (PBE). The GGA-PBE is good in the prediction of atomic and molecular energy but the band gap problem still remains, the same as LDA. The band gap calculated by LDA and GGA always underestimates the experimental data, especially, in a wide-band gap semiconductor and an insulator. There are two reasons for this problem. First, the ground state density calculated by using Kohn-Sham equation can predict only the ground state property. The electron at the ground state occupies upto the Fermi level so the states that are higher than Fermi level might not have physical meaning. Second, the exchange-correlation energy is a non-local potential in the real system but, in the LDA and GGA approximation, this term becomes local and semi-local, respectively. The generalized Kohn-Sham (GKS) schemes and screened, nonlocal exchange are proposed to overcome this problem.

The generalized Kohn-Sham method is a more precision of the density functional theory. This method proposes [21] that the ground state energy can be calculated by

$$E_0[n] = \min_n \left\{ F^{\mathrm{S}}[n] + R^{\mathrm{S}}[n] + V_{\mathrm{ext}} \right\}, \tag{2.29}$$

where

$$R^{\mathrm{S}}[n] = F_{\mathrm{HK}}[n] - F^{\mathrm{S}}[n]. \tag{2.30}$$

The $F^{\mathrm{S}}[n]$ functional is the energy functional that can be chosen. This is the main difference between the Kohn-Sham and generalized Kohn-Sham methods. This method reduces to Kohn-Sham method if we chose the $F^{\mathrm{S}}[n]$ functional to be the kinetic energy. The functional $R^{\mathrm{S}}[n]$ can be written as

$$\begin{aligned} R^{\mathrm{S}}[n] &= \{T[n] + V_{\text{e-e}}[n]\} - T[n], \\ &= V_{\mathrm{H}} + E_{\mathrm{x}} + E_{\mathrm{c}}. \end{aligned}$$

In this case, Eq.(2.29) reduces to

$$E_0[n] = \min_n \{T[n] + V_{\mathrm{H}}[n] + V_{\mathrm{ext}}[n] + E_{\mathrm{xc}}[n]\}$$

The solution of this equation is the Kohn-Sham equation. In the sX-LDA method, the $F^{\mathrm{S}}[n]$ consists of the kinetic energy, Hartree energy and the Thomas-Fermi screening exchange energy which is the simplest version of Eq.(2.24);

$$E_{\mathrm{x}}^{\mathrm{sX}}[\{\varphi\}] = -\int\int \varphi_j(\mathbf{r}_1)\varphi_j^*(\mathbf{r}_2)\frac{1}{|\mathbf{r}_1 - \mathbf{r}_2|}\varphi_i^*(\mathbf{r}_1)\varphi_i^*(\mathbf{r}_2)e^{-k_{\mathrm{TF}}|\mathbf{r}_1-\mathbf{r}_2|}d\mathbf{r}_1 d\mathbf{r}_2, \tag{2.31}$$

where k_{TF} is the Thomas-Fermi screening constant. The F^{S} in this case can be expressed as

$$F^{\mathrm{S}}[n] = T[n] + V_{\mathrm{H}}[n] + E_{\mathrm{x}}^{\mathrm{sX}}[\{\varphi\}],$$

thus the $R[n]$ is the difference between the true exchange-correlation energy and the screened-exchange energy. In sX-LDA method, the widely acceptable LDA exchange-correlation energy is chosen to replace the true exchange-correlation energy,

$$R^{\mathrm{S}}[n] = E_{\mathrm{xc}}^{\text{sX-LDA}}[n] = E_{\mathrm{xc}}^{\mathrm{LDA}}[n] - E_{\mathrm{x}}^{\mathrm{sX,LDA}}[n].$$

The $E_{\mathrm{x}}^{\mathrm{sX,LDA}}[n]$ is the local density approximation of $E_{\mathrm{x}}^{\mathrm{sX}}[\{\varphi\}]$ [22, 23]. The sX-LDA equation, generalized Kohn-Sham equation, is

$$\begin{aligned} \varepsilon_i\varphi_i(\mathbf{r}) = &-\frac{\hbar^2}{2m}\nabla^2\varphi_i(\mathbf{r}_1) + \Phi(\mathbf{r}_1)\varphi_i(\mathbf{r}_1) + v_{\mathrm{ext}}(\mathbf{r}_1)\varphi_i(\mathbf{r}_1) \\ &+ \int v_{\mathrm{x}}^{\mathrm{sX}}(\mathbf{r}_1, \mathbf{r}_2)\varphi_i(\mathbf{r}_2)d\mathbf{r}_2 + v_{\mathrm{xc}}^{\text{sX-LDA}}(\mathbf{r}_1)\varphi((\mathbf{r}_1)) \end{aligned} \tag{2.32}$$

Where $v_{\mathrm{x}}^{\mathrm{sX}}$ and $v_{\mathrm{xc}}^{\text{sX-LDA}}$ are the derivatives of $E_{\mathrm{x}}^{\mathrm{sX}}[\{\varphi\}]$ and $E_{\mathrm{xc}}^{\text{sX-LDA}}$ respectively. The sX-LDA method is more accurate than LDA and GGA[21]; however, this method requires numerous computing resources compared to the others.

2.5 Kohn-Sham orbital representation

The Kohn-Sham orbital can be expressed as a linear combination of basis functions as

$$\varphi_i = \sum_{\mu=1}^{L} c_{\mu i}\phi_\mu. \tag{2.33}$$

For $L \to \infty$, it would give the exact expression for φ_i for given basis functions ϕ_μ. However, if suitable basis functions were chosen, a few number of basis functions are required in calculations. There are three methods to expand basis functions, i.e. orthogonal plane wave (OPW) [24], linear combination of atomic orbital (LCAO) [25] and augmented plane wave (APW) [26]. Each method has different advantages and disadvantages. The CASTEP code [27], which we used in this work, chose the OPW method. One of the favourable properties of the plane wave basis is that it is a complete and orthogonal set, but the most advantage, of this basis is its periodicity which satisfies the Bloch theorem. In this basis, the Kohn-Sham orbital can be written as

$$\varphi_i(\mathbf{r}) = \sum_{\mathbf{q}} c_{i,\mathbf{q}} e^{i\mathbf{q}\cdot\mathbf{r}}, \tag{2.34}$$

where $\mathbf{q}$ is a wave vector. This method has a problem when it is used to calculate core electrons. The plane wave basis is good for describing the nearly free electron but core electrons have strong interactions with the nucleus, resulting in localized states around the nucleus. Therefore, the core electrons' behavior is far from that of the nearly free electrons. In order to describe the core electrons, a large number of the plane waves are required. In addition to the core electrons, the wavefunctions of the valence electrons also distribute themselves in the core region, which is the area between nucleus and core radius (r_c). Fortunately, it is found that only the valence electrons play an important role in the prediction of the chemical property and the crystal structure so the core effect can be neglected (only after some careful treatment [28, 29]). In 1959, Phillips and Kleinman [30] proposed that the valence wavefunctions ϕ_i^{v} can be divided into two parts,

$$\phi_i^{\mathrm{v}} = \phi_i^{\mathrm{ps}} + \sum_n a_{ni}\phi_{ni}^{\mathrm{c}}, \tag{2.35}$$

the first term ϕ_i^{ps} is called pseudo-wavefunctions which is a smooth part of the valence wavefunctions and the second term is the oscillating part in the core region of the valence wavefunctions, while ϕ_i^{c} is the core wavefunctions. If the valence wavefunction is operated by the Hamiltonian operator, we have

$$\hat{H}\phi_i^{\mathrm{v}} = \varepsilon^{\mathrm{v}}\phi_i^{\mathrm{v}}, \tag{2.36}$$

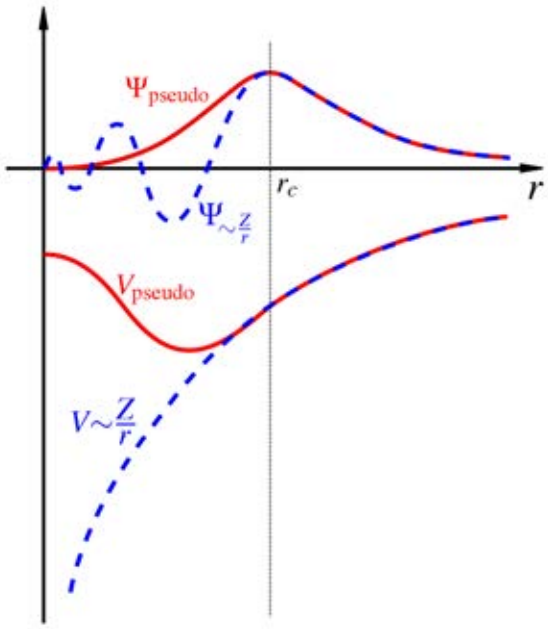

Figure 2.2: pseudo wavefunction and pseudo potential

and replace the valence wavefunction by Eq.(2.35) to obtain

$$\left[-\frac{\hbar^2}{2m}\nabla^2 + v_{\text{eff}}\right]\phi_i^{\text{ps}} + \sum_n a_{ni}\left(\varepsilon_n^{\text{c}} - \varepsilon^{\text{v}}\right)\phi_{ni}^{\text{c}} = \varepsilon^{\text{v}}\phi_i^{\text{ps}},$$

$$\begin{aligned}\hat{H}_{\text{ps}}\phi_i^{\text{ps}} &= \left[-\frac{\hbar^2}{2m}\nabla^2 + v'_{\text{eff}}\right]\phi_i^{\text{ps}}, \\ &= \varepsilon^{\text{v}}\phi_i^{\text{ps}},\end{aligned} \tag{2.37}$$

when a_{ni} and v_{ps} are defined by,

$$\begin{aligned}a_{ni} &= -\int \phi_i^{\text{ps}*}\phi_{ni}^{\text{c}} d\mathbf{r}, \\ v'_{\text{eff}} &= v_{\text{eff}} + \sum_n a_{ni}\left(\varepsilon_n^{\text{c}} - \varepsilon^{\text{v}}\right)\frac{\phi_{ni}^{\text{c}}}{\phi_i^{\text{ps}}} \\ &= \Phi(\mathbf{r}) + v_{\text{ext}}(\mathbf{r}) + v_{\text{xc}} + \sum_n a_{ni}\left(\varepsilon_n^{\text{c}} - \varepsilon^{\text{v}}\right)\frac{\phi_{ni}^{\text{c}}}{\phi_i^{\text{ps}}}, \\ v'_{\text{eff}} &= \Phi(\mathbf{r}) + v_{\text{ps}} + v_{\text{xc}}.\end{aligned} \tag{2.38}$$

This means that the pseudo wavefunction can be used instead of the true valence wavefunctions but the potential of the system must also be modified. In more detail, the second term in Eq.(2.38) is always positive so it is a repulsive potential. Thus, the psudopotential, v_{ps}, is weaker than the original potential and cannot represent the original potential in the core region, as shown in a FIG.2.2.

In conclusion, the OPW is a good method to represent the Kohn-Sham orbital but the problem is that it requires a large basis set. However, Phillips and

Kleinman showed that the number of the basis set can be reduced, if the external potential, which is Coulomb potential between nucleus and electron, is modified.

2.6 Pseudopotential

The pseudopotential is a modified potential derived from the true Coulomb potential between nucleus and electron, for using with the OPW method. A good pseudopotential must be transferable [31]. It means that if we have a pseudopotential in a reference atomic system, this potential can be applied to any system, i.e., solids, molecules, insulators and metals. The pseudopotential can be called the "norm-conserving pseudo-potential" [32], if it satisfies the following conditions:

1. The pseudo wavefunction is smooth.
2. The pseudo wavefunction and all electron wavefunctions, ϕ^{ae}, are the same beyond r_c,
$$\phi_i^{\text{ps}}(r) = \phi_i^{\text{ae}}(r) \text{ for } r > r_c, \quad \text{where ae stands for "all electrons".}$$
3. The integrals from 0 to r_c of the psuedo and all electron charge densities are equal,
$$\int\limits_{r<r_c} |\phi_l^{\text{ps}}(r)|^2 \, r^2 dr = \int\limits_{r<r_c} |\phi_l^{\text{ae}}(r)|^2 \, r^2 dr.$$
4. The pseudo and all electron eigenvalues are equal,
$$\varepsilon_l^{\text{ps}} = \varepsilon_l^{\text{ae}}.$$

In order to generate pseudopotential [33], the Kohn-Sham equation in the reference system must be solved with all electrons (core and valence electrons). The ground state of the atomic system has a spherical symmetry so the Kohn-Sham equation can only have the radial part which is easy to be solved as

$$\left[-\frac{\hbar^2}{2m}\frac{d^2}{dr^2} + \left(\frac{\hbar^2}{2m}\frac{l(l+1)}{r^2} + v_{\text{eff}}(r) - \varepsilon_l \right) \right] \phi_l(r) = 0, \tag{2.39}$$

where l is a angular momentum. Note that the exchange correlation energy can be used to calculate in Eq.(2.39) so it is clear that the exchange correlation energy affects the pseudopotential even within the same atom. The all electron energy levels, $\varepsilon_i^{\text{ae}}$, and wavefunctions, ϕ_l^{ae}, can be obtained after solving Eq.(2.39). The core radius is chosen in order to separate the oscillating and smooth parts of all electron wavefunctions. The pseudo wavefunctions with the norm-conservation conditions can be generated and then the potential can be constructed.

2.7 The characteristic equation

In order to solve Eq.(2.22), we substituted the plane wave in Eq.(2.34) for the Kohn-Sham orbital,

$$\left[-\frac{\hbar^2}{2m}\nabla^2 + v_{\text{eff}}\right]\sum_{\mathbf{q}} c_{i,\mathbf{q}}|\mathbf{q}\rangle = \varepsilon_i \sum_{\mathbf{q}} c_{i,\mathbf{q}}|\mathbf{q}\rangle, \tag{2.40}$$

when we defined $|\mathbf{q}\rangle = e^{i\mathbf{q}\cdot\mathbf{r}}$. Then we operate on Eq.(2.40) with the conjugate of the basis, $\langle\mathbf{q}'|$,

$$\sum_{\mathbf{q}}\langle\mathbf{q}'|\left[-\frac{\hbar^2}{2m}\nabla^2 + v_{\text{eff}}\right]|\mathbf{q}\rangle c_{i,\mathbf{q}} = \varepsilon_i \sum_{\mathbf{q}} \delta_{\mathbf{q},\mathbf{q}'} c_{i,\mathbf{q}}. \tag{2.41}$$

Consider the first term on the left hand side in Eq.(2.41), it is the kinetic operator which operates on the plane wave basis so this kinetic energy is the non-interacting, free electron, kinetic energy, or explicitly written as

$$\langle\mathbf{q}'|\left[-\frac{\hbar^2}{2m}\nabla^2\right]|\mathbf{q}\rangle = \frac{\hbar^2}{2m}|\mathbf{q}|^2\delta_{\mathbf{q},\mathbf{q}'}c_{i,\mathbf{q}}. \tag{2.42}$$

The second term is the effective potential. The Bloch theorem states that the potential in a crystal system is periodic so the effective potential can be expressed as a sum of Fourier components,

$$v_{\text{eff}}(\mathbf{r}) = \sum_m v_{\text{eff}}(\mathbf{G}_m)e^{i\mathbf{G}_m\cdot\mathbf{r}}.$$

Thus,

$$\langle\mathbf{q}'|v_{\text{eff}}|\mathbf{q}\rangle = \sum_m v_{\text{eff}}(\mathbf{G}_m)\delta_{\mathbf{q}'-\mathbf{q},\mathbf{G}_m}, \tag{2.43}$$

this term is non-zero only if $\mathbf{q}$ and $\mathbf{q}'$ differ by some reciprocal lattice vector $\mathbf{G}_m$. If we define $\mathbf{q} = \mathbf{k} + \mathbf{G}_m$ and $\mathbf{q}' = \mathbf{k} + \mathbf{G}_{m'}$, when $\mathbf{k}$ is the vector pointing only within the first Brillouin zone, then the Konh-Sham equation can be written as a matrix equation as

$$\sum_m H_{m',m}(\mathbf{k})c_{i,m}(\mathbf{k}) = \varepsilon_i(\mathbf{k})c_{i,m'}(\mathbf{k}), \tag{2.44}$$

where,

$$H_{m',m}(\mathbf{k}) = \langle\mathbf{k}+\mathbf{G}_{m'}|\left[-\frac{\hbar^2}{2m}\nabla^2 + v_{\text{eff}}\right]|\mathbf{k}+\mathbf{G}_m\rangle.$$

This is the characteristic equation of the Kohn-Sham equation with the OPW method. This equation is solved in each sampling k-point that is carefully chosen

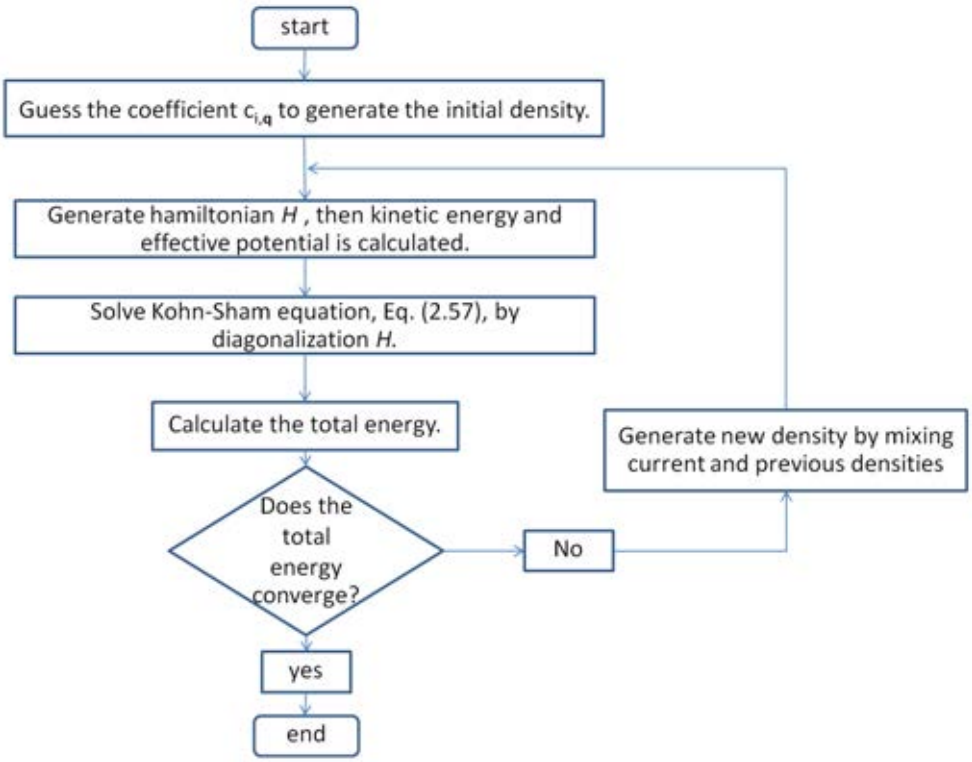

Figure 2.3: The scheme of self consistent field (SCF) method to solve the Kohn-Sham equation.

and the dimensions of this matrix depend on the index which relates to the number of the basis set. FIG.2.3 shows an algorithm for solving self-consistent Kohn-Sham equation, (2.44). First, the initial density is generated by randomly assigning the coefficients of the plane wave basis. Second, the kinetic energy, Eq.(2.42), and the effective potential, Eq.(2.43), are calculated. Next, the Eq.(2.44) can be solved to obtain the Kohn-Sham orbital, and the total energy is calculated by

$$E_{\rm tot} = \sum_{i}^{\rm occ} \varepsilon_i - V_{\rm H}[n] + E_{\rm xc}[n] - \int \frac{\delta E_{\rm xc}[n]}{\delta n} n(\mathbf{r}) d\mathbf{r}. \tag{2.45}$$

If the total energy converges, the calculation stops. If not, the new density must be generated by mixing the current and previous densities and the calculation must be repeated until the total energy converges.

2.8 Energy cut-off and k-point

In the numerical calculation of the Kohn-Sham equation with the OPW method, there are two parameters, energy cut-off and number of k-point, which are very important. First parameter, the energy cut-off related to the number of the plane

wave basis set is set from the highest kinetic energy of the plane wave basis

$$-\frac{\hbar^2}{2m}\nabla^2\phi_i = \frac{\hbar^2}{2m}(\mathbf{k}+\mathbf{G})^2\phi_i. \tag{2.46}$$

The energy cut-off is defined by,

$$E_{\text{cut}} \leq \frac{\hbar^2}{2m}(\mathbf{k}+\mathbf{G})^2. \tag{2.47}$$

As we mentioned before, infinite number of terms of the plane wave basis are required to represent the Kohn-Sham orbital completely, i.e., set $E_{\text{cut}} = \infty$. However, due to the limited resources of calculation we must find an optimum value of E_{cut}. The second parameter, the number of k-point is the parameter that is related to the number of sampling points in the k-space which is used in the calculation. In the calculation, the Kohn-Sham equation is solved in k-space. The potential, in the crystal system, is periodic so the first Brillouin zone is a good representative of the system. The sampling of the k-points in first Brillouin zone can be chosen by using the Monkhorst-Pack method [34]. They proposed that the sampling k-points are distributed homogeneously in the Brillouin zone, with rows or columns of k-points running parallel to the reciprocal lattice vectors that span the Brillouin zone,

$$\mathbf{k} = x_1\hat{\mathbf{b}}_1 + x_2\hat{\mathbf{b}}_2 + x_3\hat{\mathbf{b}}_3,$$

when $\mathbf{b}_i$ are the reciprocal lattice vectors. The higher number of the sampling k-points gives more accurate calculation but it also requires more resources. Thus the two parameters much be tested to find suitable values for the system before other properties are calculated. Normally, we choose the values that give the convergent of the ground state energy within an acceptable tolerance, e.g., 1 meV.

2.9 Geometry optimization

In our calculation, the temperature effect is ignored, $T = 0K$, Then the enthalpy must be minimized with respect to all structure parameters, if pressure p is applied, then

$$\mathcal{H} = E + pV, \tag{2.48}$$

when E is the total energy and V is volume of the system. The enthalpy can be a function of strain tensor ϵ and atomics positions R_i [35],

$$\mathcal{H} = \mathcal{H}(\epsilon, R_1, \ldots, R_N),$$

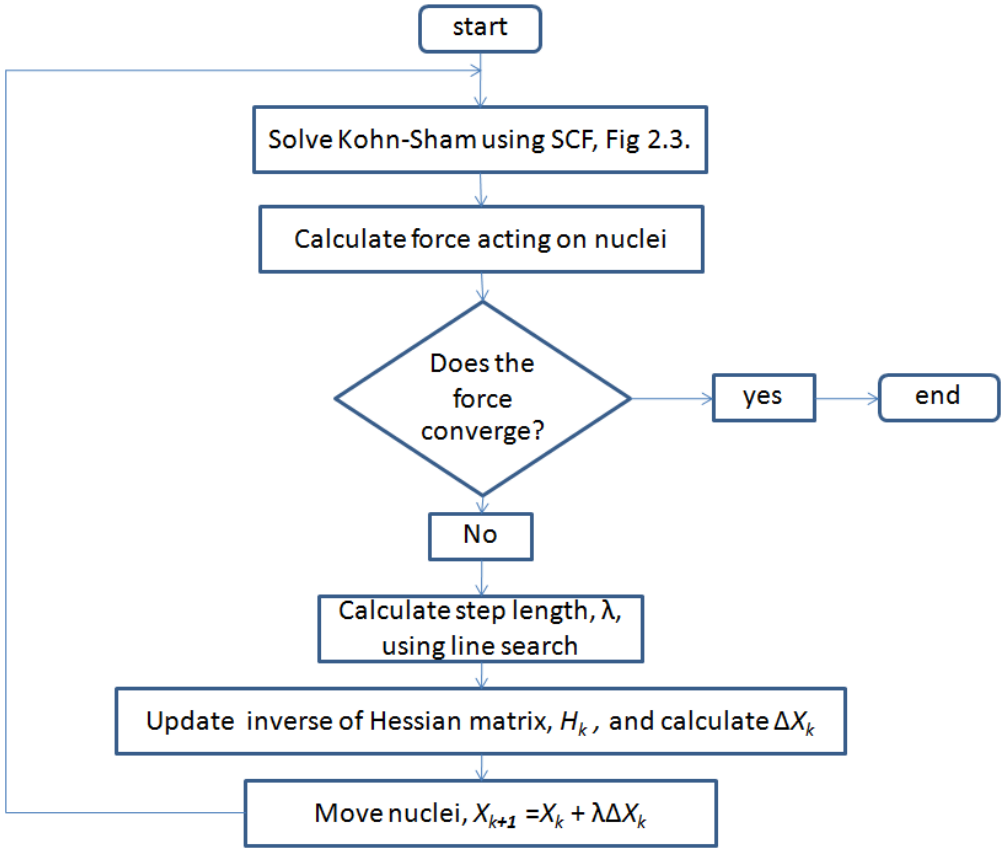

Figure 2.4: The scheme of geometry optimization.

so, in unit cell with N atoms, the enthalpy has $9+3N$ dimensions. The negative of the first derivative of the enthalpy is called the force vector,

$$F = -\left.\frac{\partial \mathcal{H}}{\partial X}\right|_p , \tag{2.49}$$

where X is a column vector. The first nine components is strain which is defined as

$$X_{3(i-1)+j} = \epsilon_{ij} \qquad ; i,j = 1,2,3, \tag{2.50}$$

and the follows are atomic positions in the unit cell,

$$X_k = R_k \qquad ; k = 1,2,\ldots,N. \tag{2.51}$$

At the minimum $X_{\min}$, the gradient of the enthalpy is zero. This implies that the force vector is zero. In order to search for $X_{\min}$ we used the quasi-Newton method where X in $(k+1)^{\text{th}}$ step is updated according to:

$$\begin{aligned} X_{k+1} &= X_k + \lambda \Delta X_k, \\ \Delta X_k &= H_k F_k \end{aligned} \tag{2.52}$$

where H_k is the inverse of the Hessian matrix A_k , $H_k = A_k^{-1}$ and λ is the step length. In the calculation, the initial H_0 is unknown so it must be from a guess, usually $H_0 = I$, and then updated using the algorithm that was proposed by Broyden-Fletcher-Goldfarb-Shanno (BFGS scheme [36, 37]). The diagram of the Kohn-Sham calculation with geometry optimization method is shown in FIG.2.4.

2.10 Bulk modulus

The bulk modulus (B_0) is calculated using the third-order Birch-Murnaghan isothermal equation of state (EOS) [38]. In 1944, Murnaghan [39] assumed that the bulk modulus is a linear function of pressure, $B = B_0 + B_0' P$, where B_0 and B_0' are the bulk modulus and its derivative at 0 GPa. Then he proposed the Murnaghan's EOS based on the principle of conservation of mass and Hooke's law,

$$P(V) = \frac{B}{B_0'}\left(\left(\frac{V}{V_0}\right)^{-B_0'} - 1\right), \tag{2.53}$$

where V_0 is the volume at 0 GPa. Later, Birch developed Eq.(2.53) to use in a hydrostatic compression case [38] which is of the form

$$P(V) = \frac{3B_0}{2}\left[\left(\frac{V_0}{V}\right)^{\frac{7}{3}} - \left(\frac{V_0}{V}\right)^{\frac{5}{3}}\right]\left\{1 + \frac{3}{4}(B_0' - 4)\left[\left(\frac{V_0}{V}\right)^{\frac{2}{3}} - 1\right]\right\}, \tag{2.54}$$

and

$$E(V) = E_0 + \frac{9V_0B_0}{16}\left\{\left[\left(\frac{V_0}{V}\right)^{\frac{2}{3}} - 1\right]^3 B_0' + \left[\left(\frac{V_0}{V}\right)^{\frac{2}{3}} - 1\right]^2\left[6 - 4\left(\frac{V_0}{V}\right)^{\frac{2}{3}}\right]^3\right\}, \tag{2.55}$$

where E_0 is the total energy at 0 GPa. The Eq.(2.54) and Eq.(2.55) are called the third-order Birch-Murnghan isothermal EOS. From the solution of the Kohn-Sham equation with the geometry optimization, we can obtain the set of the ground state energy and the corresponding volume. Therefore, we can use the Eq.(2.54) to calculate the bulk modulus by fitting to our data.

2.11 Structure stability

The structure stability can be examined by considering phonon frequencies. If nuclei are perturbed slightly, they can oscillate around their equilibrium positions.

In this case, the harmonic approximation is used to describe the total energy of the system:

$$E_{\text{tot}}(\{\mathbf{u}\}) = E_{\text{tot}}^{(0)} + \sum_k \sum_j \frac{1}{2} A_{k,j} u_k u_j,$$
$$A_{k,j} = \frac{\partial^2 E_{\text{tot}}}{\partial u_k \partial u_j}; \tag{2.56}$$

where u_k is a small deviation of the nuclei from equilibrium, $k = 1, \ldots, 3N$. Note that the first derivative of the E with respect to u_k is zero at equilibrium point. A is Hessian matrix or force constant matrix [40]. The Fourier transform of Hessian matrix is related to the dynamical matrix D according to

$$\tilde{A}_{k,j} = \sqrt{M_k M_j} D_{k,j}, \tag{2.57}$$

where M_i is a mass of nuclei. Then phonon frequencies can be found by solving the eigenvalue problem,

$$D_{k,j} X_{ki} = M_k \omega_i^2 X_{ki}, \tag{2.58}$$

where X_{ki} is the element of the ith eigenvector and ω_i is the phonon frequency of the ith mode. Recall the simple harmonic equation of motion.

$$\frac{d^2 x}{dt^2} + \omega^2 x = 0 \tag{2.59}$$

Eq.(2.59) show that if the phonon frequency is an imaginary value, the nuclei do not oscillate around the equilibrium position. It implies that the structure is unstable because the nuclei will move away from its equilibrium position. In addition, a displacement composition u_{ki} in the direction of the ith eigenvector can then be written as

$$u_{kj} = X_{ki} Q_i, \tag{2.60}$$

where Q_i is referred to a normal-mode coordinate. The phonon frequency at each k-point along the high symmetry point was plot for constructing the phonon dispersion.

2.12 Raman spectroscopy

Raman technique developed by Raman and Kirishnam [41] is a vibrational spectroscopy for assessing molecular motions and fingerprinting atomic or bonding species. This can be used to analyse the composition, structural and phase transition [42] of materials. The foundation of this technique is inelastic scattering.

In the experiment, a laser with monochromatic light in the visible, near infrared or ultraviolet region [43] is used to excite molecules and the scattering laser is detected. The energy of the scattering laser can change due to change in rotational or vibrational states of molecules. If the energy of the scattering laser is lower (higher) than the incidence, it is called Stoke (anti-Stoke) Raman scattering. Considering one molecular system, when it is perturbed by an external electric field, $\mathrm{E} = \mathrm{E}_0 \cos(2\pi\omega_0 t)$, the induced dipole moment, μ, can be expressed as

$$\mu = \alpha \mathbf{E}, \tag{2.61}$$

where α is the polarizability. The small vibration of the nuclei due to this perturbation also modifies the polarizability. Thus, α can be approximated by the first two terms in a Taylor series expansion as

$$\alpha = \alpha_{q=0} + \frac{\partial \alpha}{\partial q}_{q=0} q. \tag{2.62}$$

The variable q is a vibrational motion with eigenfrequency ω_i which is written as

$$q = q_0 \cos(2\pi\omega_i t). \tag{2.63}$$

Substituting Eq.(2.62) and Eq.(2.63) into Eq.(2.61), we have

$$\mu = \alpha_{q=0}\mathbf{E}_0 \cos(2\pi\omega_0 t) + \frac{1}{2}\frac{\partial \alpha}{\partial q}_{q=0} q_0 \mathbf{E}_0 [\cos(2\pi(\omega_0 - \omega_i)t) + \cos(2\pi(\omega_0 + \omega_i)t)]. \tag{2.64}$$

The first term in Eq.(2.64) corresponds to Rayleigh scattering, which is an elastic scattering. The second and third term are Stokes and anti-Stokes scatterings, respectively. As seen in Eq.(2.64), the coefficient $\dfrac{\partial \alpha}{\partial q}$ plays an important role for the calculation of Raman spectrum.

In order to examine the Raman spectrum in solid, the first-order differential Raman cross section [44] is calculated to identify the Raman spectra. It is written as

$$\frac{d\sigma_i}{d\Omega} = \frac{(2\pi\omega_s)^4}{c^4} \left| \hat{e_s} \frac{\partial \hat{\alpha}}{\partial Q_i} \hat{e_L} \right| \frac{h(n_i^b + 1)}{8\pi^2 \omega_i} \quad , n_i^b = \left[\exp\left(\frac{h\omega_i}{kT} \right) - 1 \right]^{-1}. \tag{2.65}$$

In Eq.(2.65), ω_s is the frequency of the scattered light, $\hat{e_s}$ and $\hat{e_L}$ are the unit vectors of electric-field directions (polarizations) for the scattered and the incident lights, $\hat{\alpha}$ is the polarizability tensor, and n_i^b the Bose-Einstein statistical factor. The Eq.(2.65) is zero if $\dfrac{\partial \hat{\alpha}}{\partial Q_i}$ is zero. This means that Raman cannot detect the vibration in Q_i^{th} mode. This term can be expressed as

$$\frac{\partial \hat{\alpha}}{\partial Q_i} = \sum_{i=1}^{3N} \frac{\partial \hat{\alpha}}{\partial R_k} X_{ki} \quad , \frac{\partial \hat{\alpha_{mn}}}{\partial R_k} = \frac{\partial^3 E}{\partial G_m \partial G_n \partial R_k}, \tag{2.66}$$

where $m, n = x, y, z$, and R_k is the atomic coordinates (Cartesian) and G_m is a component of the external electric field.

2.13 Band structure

From the Kohn-Sham solution, we obtained the eigenvalue, ε_i, which is refered to as Kohn-Sham orbital energy. The band structure was generated by plotting this energy eigenvalue versus the sampling k-point along the high symmetry points. However, it is well-known that LDA and GGA underestimate the band gap by a factor of 2 [21]. The band gap, in the Kohn-Sham method, is calculated by

$$E_{\mathrm{g}} = \varepsilon_{\mathrm{N+1,N+1}} - \varepsilon_{\mathrm{N,N}}, \tag{2.67}$$

where $\varepsilon_{\mathrm{N,M}}$ is the M^{th} Kohn-Sham orbital energy of the N-particles Kohn-Sham system [45]. Actually, the band gap can be calculated using only solution from the N-particle system, N+1-particle system is not necessary, as shown in FIG.2.5. The Eq.(2.67) is written as

$$E_{\mathrm{g}} = (\varepsilon_{\mathrm{N,N+1}} - \varepsilon_{\mathrm{N,N}}) + \Delta_{\mathrm{xc}} \quad , \Delta_{\mathrm{xc}} = \varepsilon_{\mathrm{N+1,N+1}} - \varepsilon_{\mathrm{N,N+1}}. \tag{2.68}$$

Δ_{xc} in Eq.(2.68), is called the derivative discontinuity. It is zero ($\Delta_{\mathrm{xc}} = 0$) in the LDA and GGA calculation [46] so their band gaps have large discrepancy with the experiments. The sX-LDA can improve this problem [21] as it gives reasonable and non-zero Δ_{xc}. This is because the parameter k_{TF} in Eq.(2.31) already contains some information of the excited states. The sX-LDA gives accurate band gaps in Si, C and their compounds.

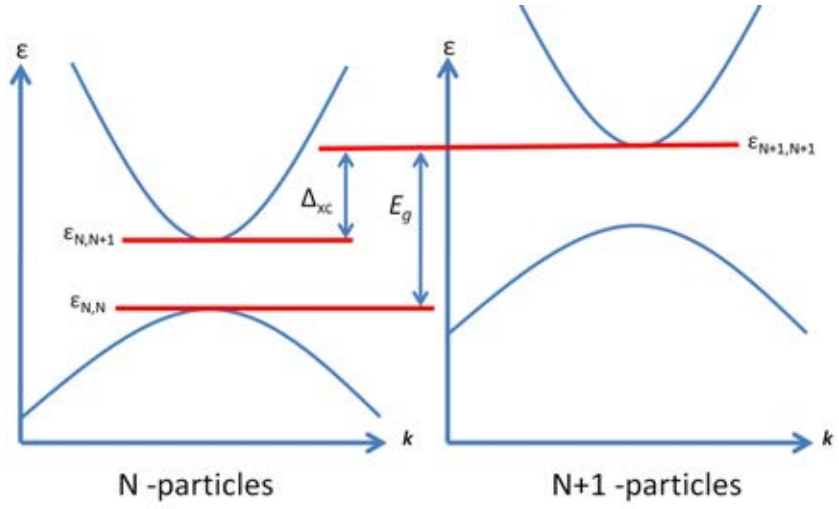

Figure 2.5: The foundation of the band gap calculation.

Chapter III

MECHANICAL PROPERTIES

The carbon nitride methanediide compound, $C_2N_2(CH_2)$, was successfully synthesized under high pressure and high temperature for the first time by Sougawa [1]. After that there have been many research works about the properties of this compound, i.e., bulk modulus, the contraction of the C-N single bond, elastic property, structural stability and band gap [2, 3, 5, 6]. However, the knowledge of its properties under high pressure is still incomplete. In addition, there is a disagreement on the strength of the C-C single bond in the $C_2N_2(CH_2)$ compound. Sougawa who synthesized this compound [2] claimed that its compressibility is comparable to diamond but recent work [6] shows that the C-C bond has higher compressibility than diamond. In this work, Cambridge serial total energy package (CASTEP), which is based on the density functional theory, is employed. It is well-known that the accuracy of DFT depends on choices of suitable exchange-correlation functionals. In this work, we use three different functionals, local density approximation (LDA), generalized gradient approximation (GGA) and screened-exchange local density method (sX-LDA). In this chapter, the results of $C_2N_2(CH_2)$ mechanical properties, i.e. lattice parameters, bulk modulus, the contraction of the C-N and C-C single bonds and the structural stability of this compound under high pressure are presented.

3.1 Computational detail

First of all, before CASTEP is used to examine the property of $C_2N_2(CH_2)$. We must test the cut-off energy and the number of k-point to find optimum values. The single-point energy calculation method is used in this test. To find the convergence of the k-point, we fix the cut-off energy at 770 eV [4] and calculate the ground state energy by varying the number of k-point. The results are shown in FIG.3.1. To test the cut-off energy, we repeat the computation by fixing the k-point to $4\times4\times4$. The cut-off energy converges at 3,600 eV which as in FIG.3.2.

However, we found that the band gap calculation time is 15 times more than that for the cut-off energy at 770 eV as shown in FIG.3.3. The difference in the band gap value is only 0.001 eV. Thus we chose the cut-off energy at 770 eV, which is the same as that of another work [4].

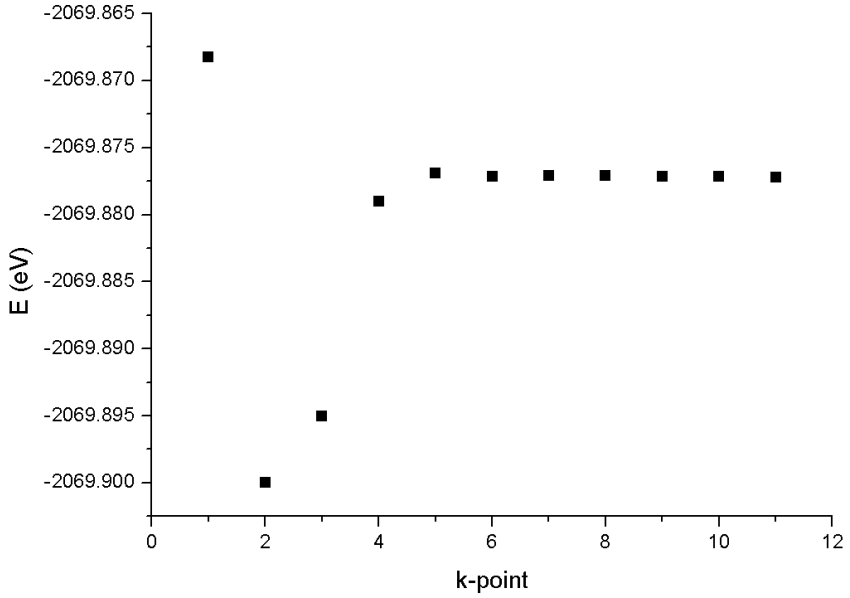

Figure 3.1: The convergence test of the k-point

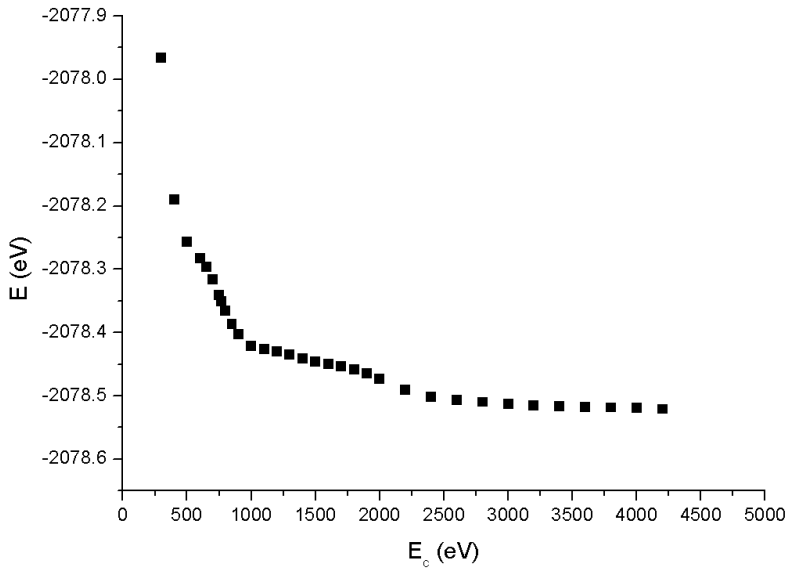

Figure 3.2: The convergence test of the cut-off energy

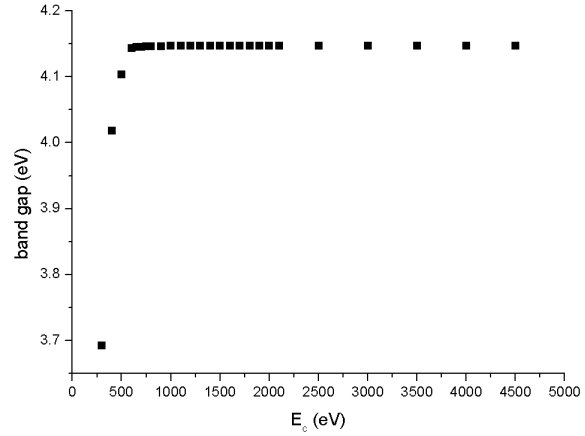

(a)

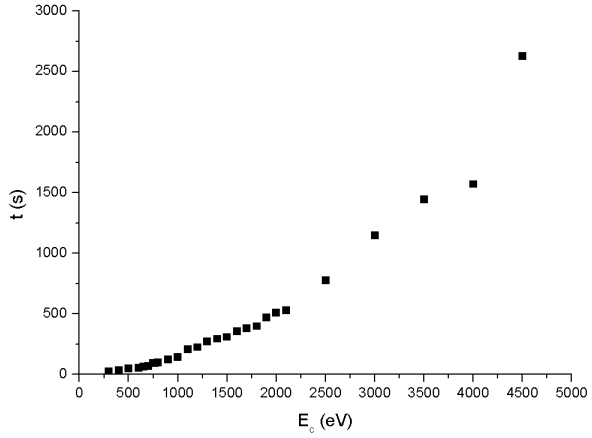

(b)

Figure 3.3: (a) The band gap versus the cut-off energy and (b) the time used for the calculation.

The condition for the convergence of the SCF calculation is set to the total energy change of less than 5×10^{-7} eV/atom. The convergence condition for calculating the geometry optimization is set to the total energy change of less than 5×10^{-6}eV/atom, the atomic maximum force change of less than 0.01 eV/Å, the atomic maximum stress change of less than 0.02 GPa, and the atomic maximum displacement change of less than 5×10^{-4}Å. For the LDA functional, we choose the functional proposed by Ceperley, Alder, Perdew and Zunger (CA-PZ) [47, 48]. For the GGA functional, we choose the functional proposed by Perdew, Burke and Ernzerhof (PBE) [49].

3.2 Lattice parameters and volume under pressure

The structure of the $C_2N_2(CH_2)$ compound is orthorhombic with the space group $Cmc2_1$ as shown in FIG.1.2. The experiment reported that the lattice parameters a, b and c are 7.625 Å, 4.490 Åand 4.047 Å, respectively [1]. The C atom in this compound can be separated into two types, C^1 and C^b. They are located at the center of a tetrahedral due to their sp^3 hybridization. The tetrahedral has four corners. For C^1 tetrahedral, three corners are occupied by three N atoms (one atom per corner), and the other is occupied by a C^b atom. For C^b tetrahedral, two corners are occupied by two H atoms, and the other two are occupied by two C^1atoms (one atom per corner). The tetrahedral of C^1 and C^b are shown in FIG.3.4.

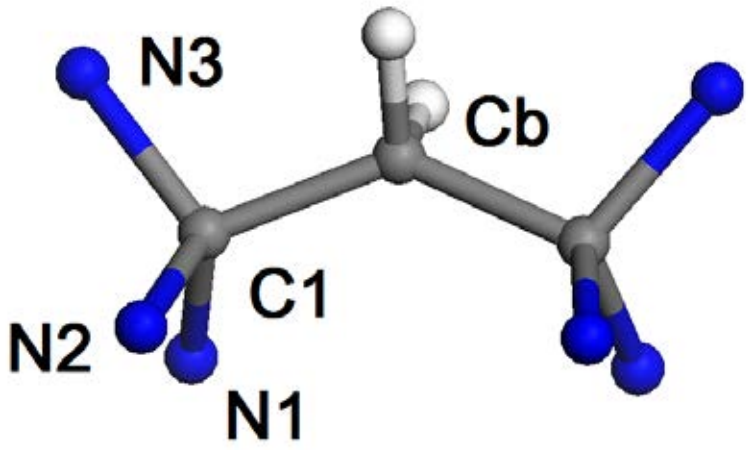

Figure 3.4: Structure of $C_2N_2(CH_2)$ with $Cmc2_1$ space group.

The lattice parameter is calculated to compare with the experiment and theory results [5] which are shown in Table 3.1. The results show that the sX-LDA calculation is more accurate than the LDA and GGA in terms of lattice parameter. The lattice parameters a, b and c are 7.980 Å, 4.561 Å and 4.067 Å with errors of 4.7%, 1.6% and 0.5% respectively in the sX-LDA calculation. The volume under pressure is calculated to compare with the experiment as shown in FIG.3.5a. These results show that three functionals, LDA, GGA and sX-LDA, have similar trends to experiment result and the sX-LDA has better agreement in this calculation.

Table 3.1: The lattice parameters and the bulk moduli at 0 GPa, compared with theoretical [5] and experimental [1, 3] works.

	Exp[1, 3]	LDA	GGA	sX-LDA	LDA[5]	GGA[5]
a	7.625	8.029	8.148	7.980	8.0168	8.1259
b	4.490	4.584	4.660	4.561	4.5662	4.6381
c	4.047	4.090	4.141	4.067	4.0667	4.1178
bulk modulus	258 ± 3.4	254 ± 0.1	229 ± 0.8	301 ± 4.1	263	239

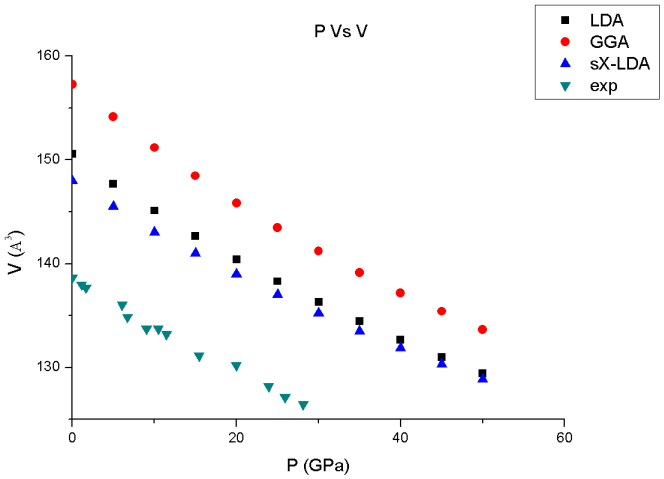

(a)

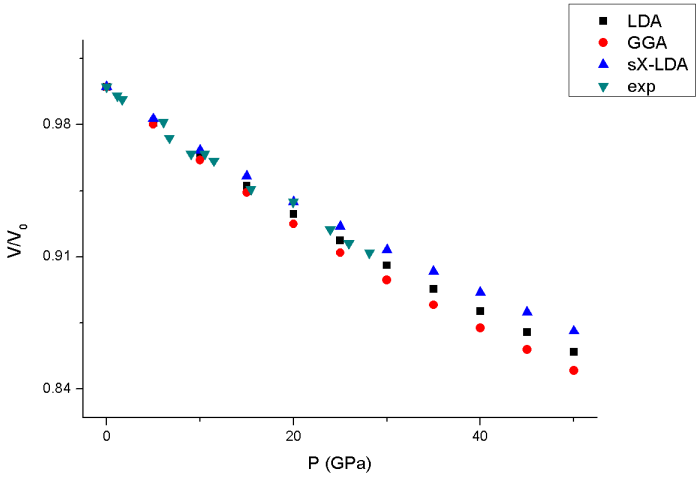

(b)

Figure 3.5: (a) V-P relation between 0 GPa and 50 GPa, compared with the experimental data [3]. (b) The volume under pressure related to volume at 0 GPa of each functional.

3.3 Bulk modulus

In order to calculate the bulk modulus, the energy is plotted as a function of volume, as shown in FIG.3.6. This graph is fitted to the third-order Birch-Murnaghan equation of states, Eq.(2.55). The results with standard error are also shown in Table 3.1. In addition, a residual which is a difference between the observed value and the predicted value are plotted in FIG.3.7. It shows that our data is good agreement with the Birch-Murnaghan equation of states. The LDA calculation shows that the bulk modulus of $C_2N_2(CH_2)$ is 254 GPa with an error of less than 2.8 %, the lowest compared with the experimental result [2]. This value is only 45 % of that of diamond.

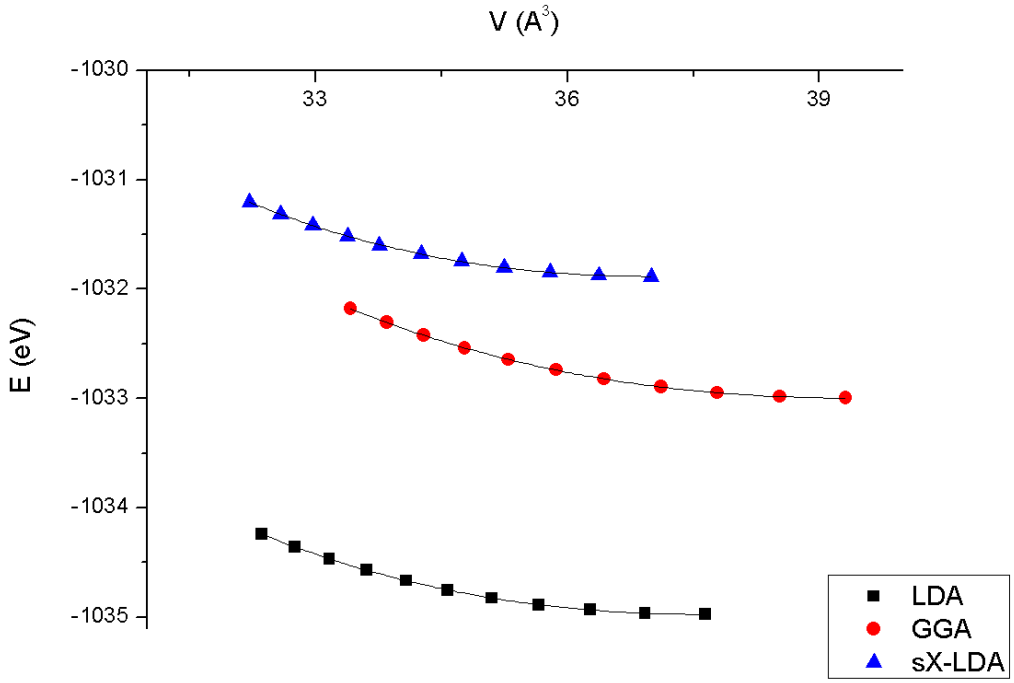

Figure 3.6: E-V relation between 0 GPa and 50 GPa. The solid lines are the fitting from Birch-Murnaghan equation of states.

Then we compared the volume change under pressure of $C_2N_2(CH_2)$ compound with those of β-C_3N_4 and diamond. The β-C_3N_4 volume decreases similarly to that of diamond which implies that it has the compressibility comparable with that of diamond but the volume reduction of $C_2N_2(CH_2)$ under pressure is faster than those of β-C_3N_4 and diamond as shown in FIG.3.8 . This result is reasonable compared with the bulk modulus of $C_2N_2(CH_2)$ from our calculation.

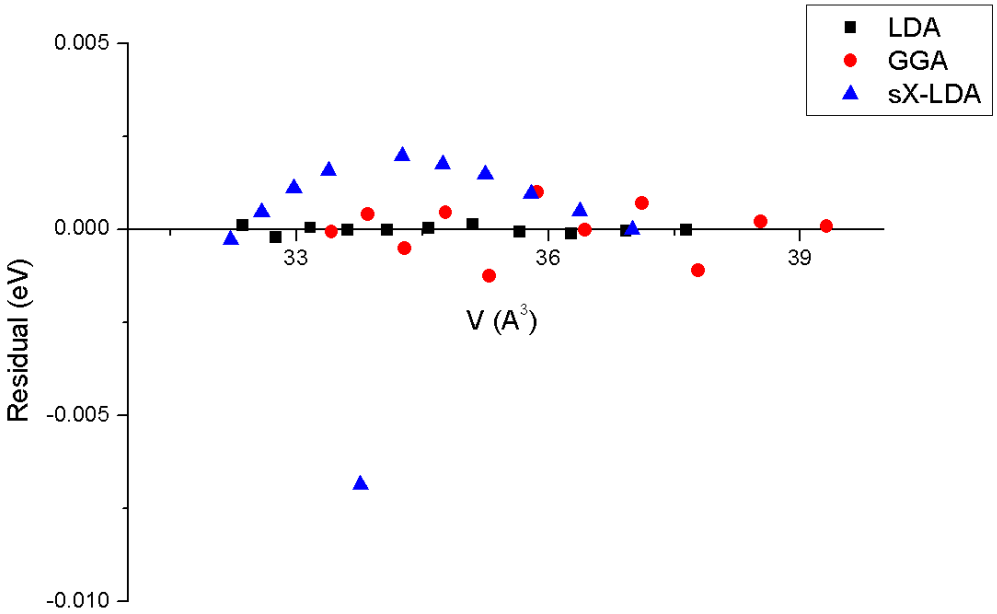

Figure 3.7: E-V relation between 0 GPa and 50 GPa. The solid lines are the fitting from Birch-Murnaghan equation of states.

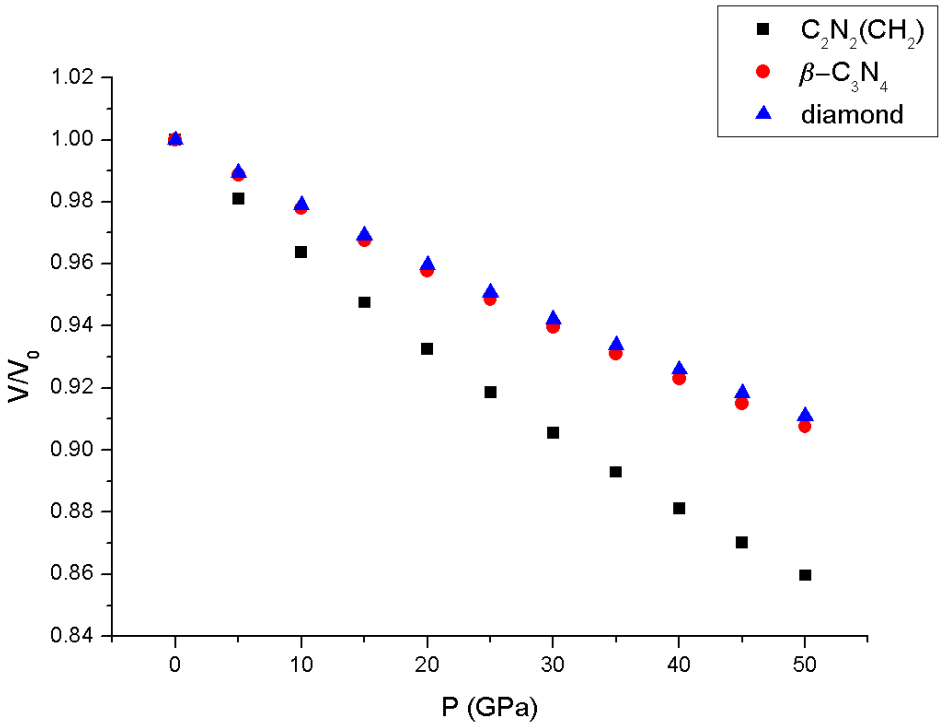

Figure 3.8: Reduction of volume under pressure of $C_2N_2(CH_2)$, β-C_3N_4 and diamond.

3.4 The contraction of the single bond

In 1989, Liu and Cohen proposed a structure of β-C_3N_4 and found that it has bulk modulus of 427 ± 15 GPa [12] which is close to that of diamond. They studied in more detail that the C-N single bond in β-C_3N_4 is shorter than the C-C bond in diamond, resulting in larger bulk modulus. It is very interesting to compare the compressibility of the C-N single bond in the $C_2N_2(CH_2)$ with those in β-C_3N_4. To examine the contraction of the C-N single bond, the varied pressure is applied and the unit cell is relaxed. Changes in the interatomic distances between C and N of the relaxed structure relative to those at 0 GPa are calculated. These values are compared with those of β-C_3N_4.

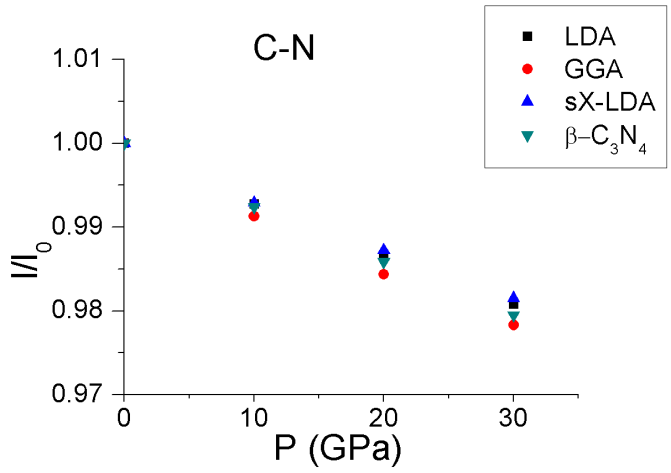

(a)

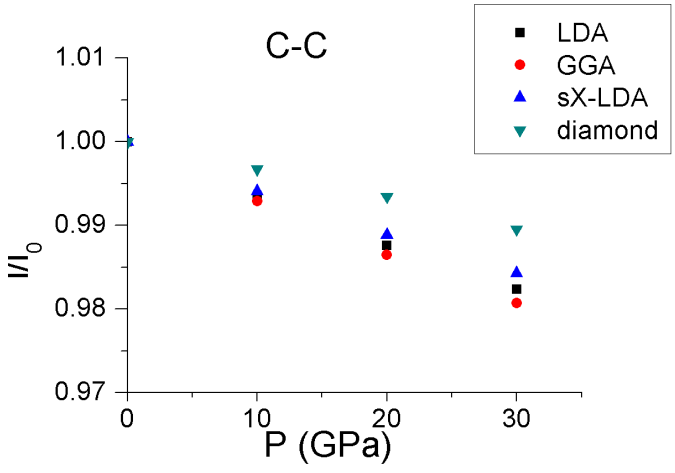

(b)

Figure 3.9: The contraction ration l/l_0 of (a) the average C-N bond length in $C_2N_2(CH_2)$ compared with that of β-C_3N_4 (b) the C-C bond length in $C_2N_2(CH_2)$ compared with that of diamond.

The reduction of the interatomic distances between C and N in $C_2N_2(CH_2)$ is the same as in β-C_3N_4, as shown in FIG 3.9a . This means that the compressibility of the C-N single bond in $C_2N_2(CH_2)$ is comparable with the super hard material β-C_3N_4, but the bulk modulus in this compound is very small compared with that of diamond. Thus this implies that the other bonds, i.e. C-C and C-H, have higher compressibility. Then the compressibility of the C-C single bond in the $C_2N_2(CH_2)$ was examined in the same way as the C-N bond. These results were compared with that of diamond which is shown in the FIG.3.9b. The results show clearly that there is a significant difference between the $C_2N_2(CH_2)$ and diamond. The interatomic distance of the C-C bond in the $C_2N_2(CH_2)$ changes more than in diamond so it has higher compressibility than diamond. This result is in good agreement with the low value of the hardness of the C-C bond [6].

3.5 Angle

When the pressure is applied, not only the interatomic distances change but so does the angle. We found that all angles in diamond do not change even if pressure is increased to 30 GPa. The angles in β-C_3N_4 change very little, the highest value is 0.4 % relative to the ambient structure when pressure is increased to 30 GPa. In the $C_2N_2(CH_2)$ compound, the angles significantly change; especially, the C^1-C^b-C^1 angle changes approximately 3.5% from the normal structure, as shown in FIG.3.10. This also supports our claim of low bulk modulus in this compound.

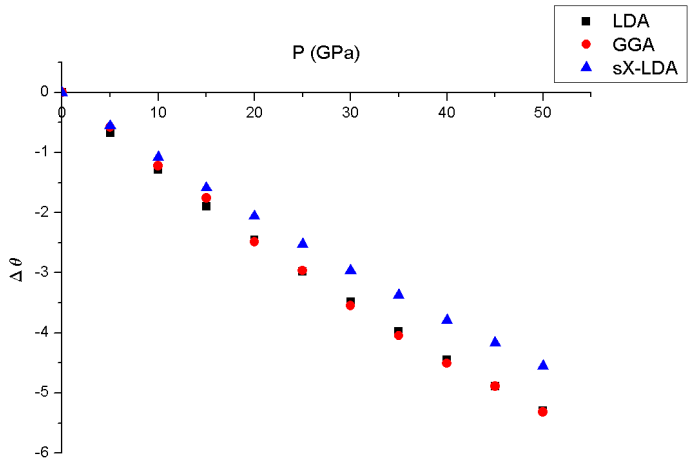

Figure 3.10: The percentage of C^1-C^b-C^1 angle change under pressure

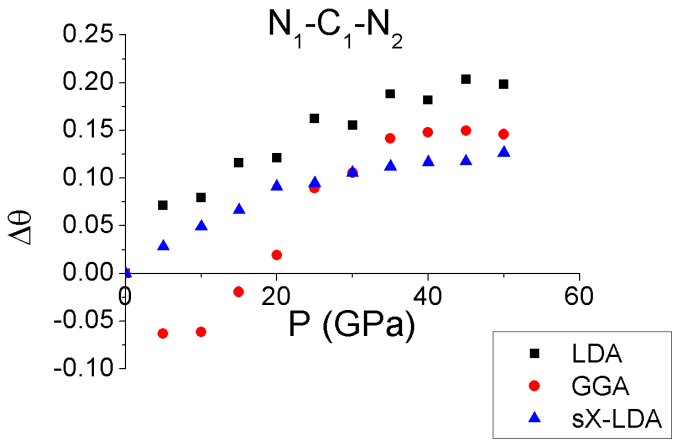

(a)

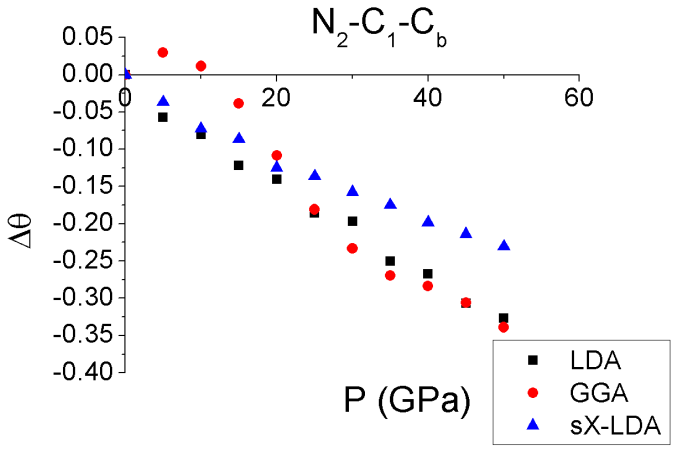

(b)

Figure 3.11: (a) the angle difference of N^1-C^1-N^2 and (b) the angle difference of N^2-C^1-C^b at various pressures. The angles of 0 GPa are set as a reference.

In this calculation, we found discrepancies of the results. The LDA and the sX-LDA calculations predict similar angle change in N^1-C^1-N^2, N^1-C^1-N^3, N^3-C^1-N^1, N^1-C^1-C^b, N^2-C^1-C^b and N^3-C^1-C^b angles. However, the GGA calculation has different results in the N^1-C^1-N^2 and the N^2-C^1-C^b angles which are shown in FIG.3.11. The LDA and the sX-LDA calculations predict that when pressure increases the N^1-C^1-N^2 increases and N^2-C^1-C^b decreases. In the GGA calculation, it has a different trend prior to 5 GPa. In more detail, the N^1-C^1-N^2 decreases and N^2-C^1-C^b increases. This distinction can be related with the electronic property which will be discussed in the next chapter.

3.6 Structure stability

The other interesting property of the $C_2N_2(CH_2)$ under high pressure is the phase stability. Usually when pressure increases the structure of the material often leads to the change of its property. This compound is newly discovered and complex so we have not found other candidate structures under high pressure. Thus, we studied the stability of the $Cmc2_1$ structure under high pressure by observing its phonon dispersion. In this part, we used LDA and GGA calculations only. The phonon dispersion of the relaxation structure between 0 to 50 GPa is calculated. The results are shown in FIG.3.12 and FIG.3.13. The number of branches in the phonon dispersion is three times of the number of atoms in the unit cell. Thus, there are 42 branches corresponding to the 14 atoms, in 2 units of $C_2H_2(CH_2)$, in our calculation. As shown in FIG.3.12 (3.13), there are only 3 branches that originate from gamma (G) point. These are the acoustic phonon modes and the others are optical phonon modes. The alphabets in the FIG.3.12 (3.13) denote the high symmetry points in the brillouin zone. The $Cmc2_1$ is classified as the base-centered orthorhombic and the high symmetry points are shown in Table.3.2.

Table 3.2: The symmetry points of the base-centered orthorhombic.

Lable	coordinates
Γ	0 0 0
Y	$-\frac{1}{2}$ $\frac{1}{2}$ 0
Z	0 0 $\frac{1}{2}$
T	$\frac{1}{2}$ $\frac{1}{2}$ $\frac{1}{2}$
S	0 $\frac{1}{2}$ 0
R	0 $\frac{1}{2}$ $\frac{1}{2}$

We did not find a negative phonon frequency, which indicates the evidence of the dynamical instability, but we find the disagreement between LDA and GGA calculations at around 20 GPa which is shown in FIG.3.14. The LDA calculation shows that the phonon frequency increases when pressure increases. However, the GGA calculation shows that the phonon frequency decreases to the lowest value at 20 GPa. The phonon of the Y-point decreases by 30 % compared with the frequency at ambient conditions. We select the Y-point phonon and plot its frequency versus pressure, as shown in FIG.3.15. This may be a signal of the structure instability so we check the mechanical stability of this structure using

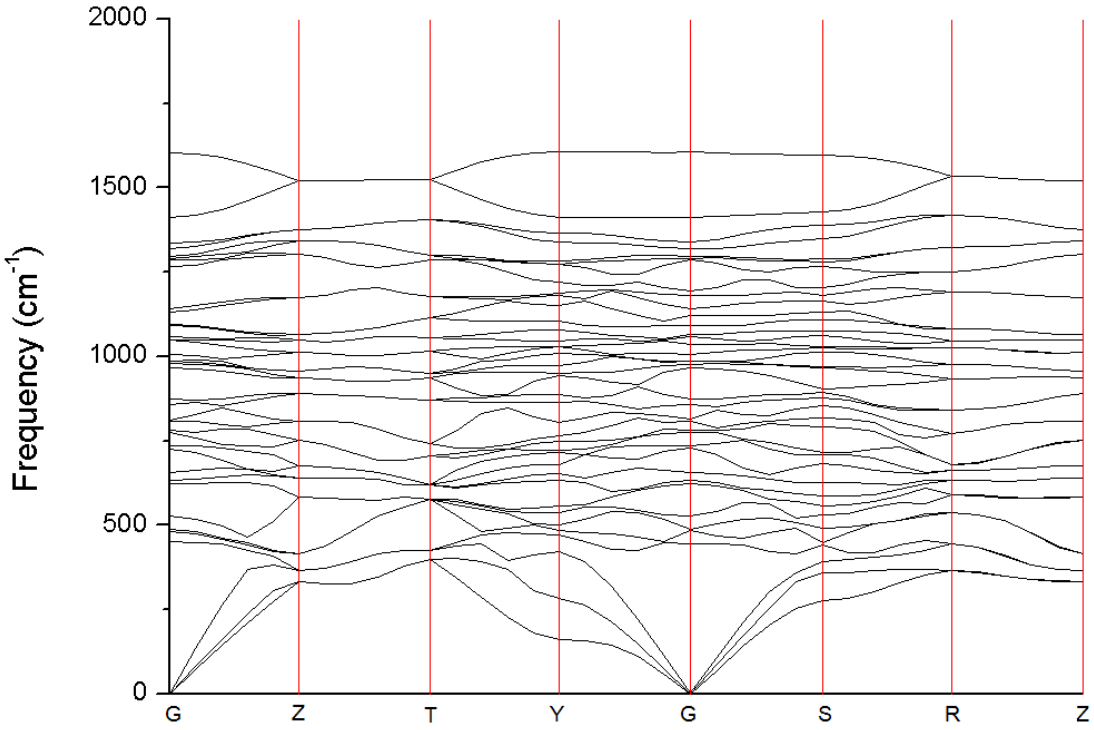

(a)

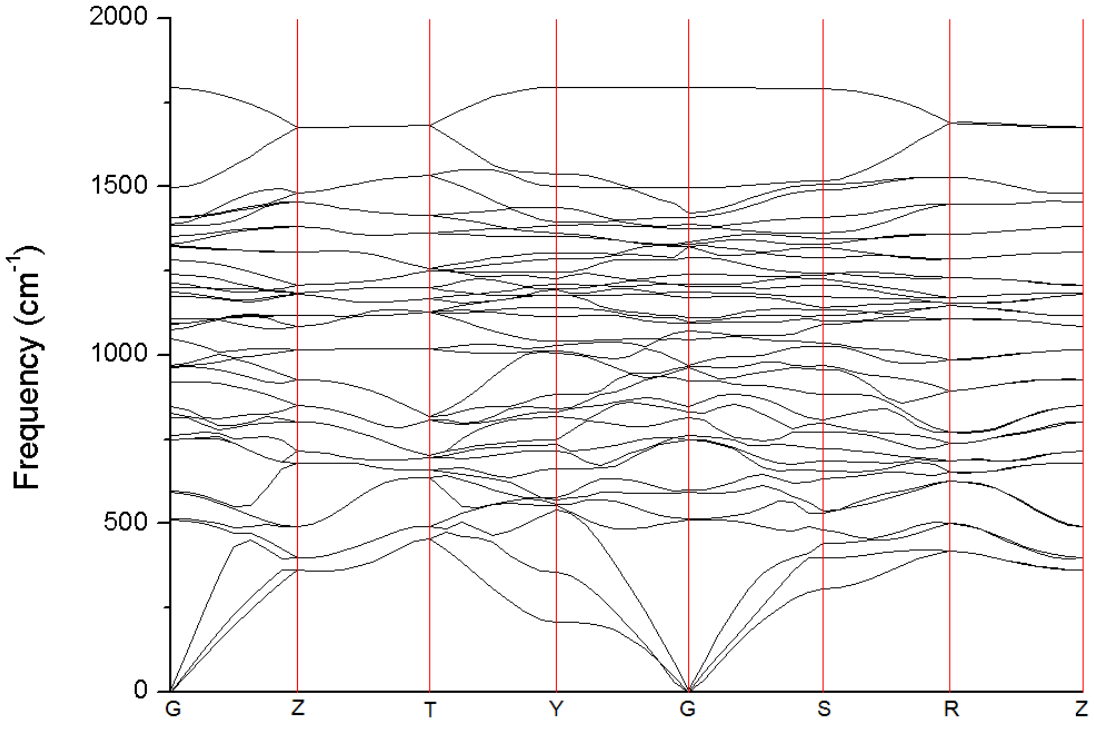

(b)

Figure 3.12: Phonon dispersion at (a) 0 GPa and (b) 50 GPa from the LDA.

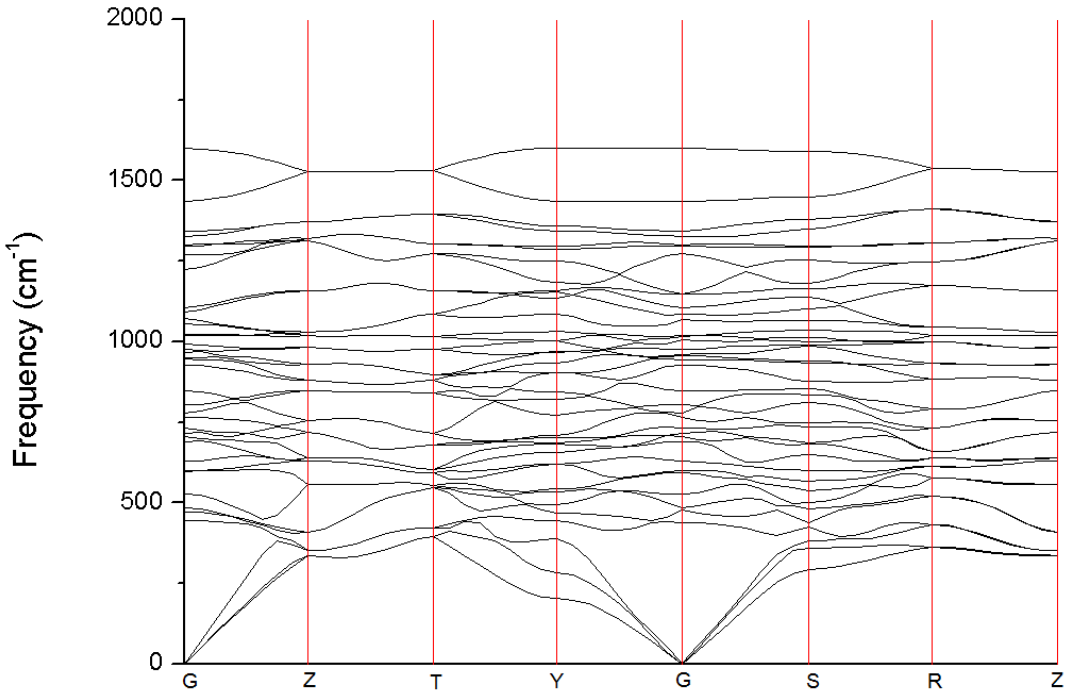

(a)

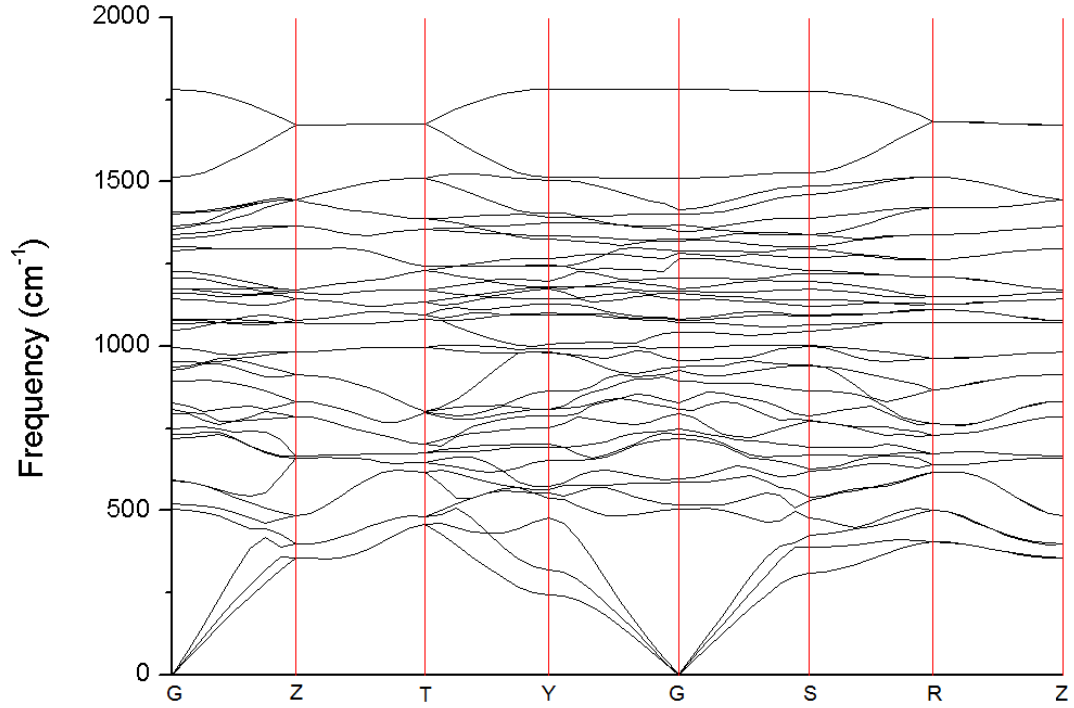

(b)

Figure 3.13: Phonon dispersion at (a) 0 GPa and (b) 50 GPa from the GGA .

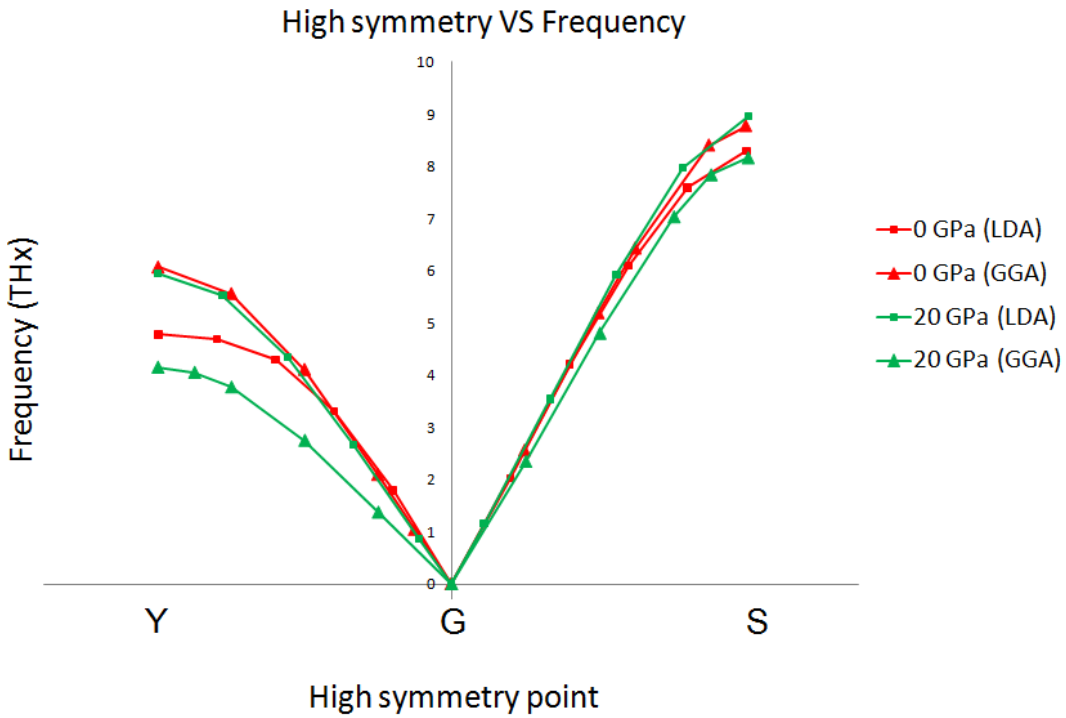

Figure 3.14: The Y-G-S branch at 0 and 20 GPa from the LDA and the GGA

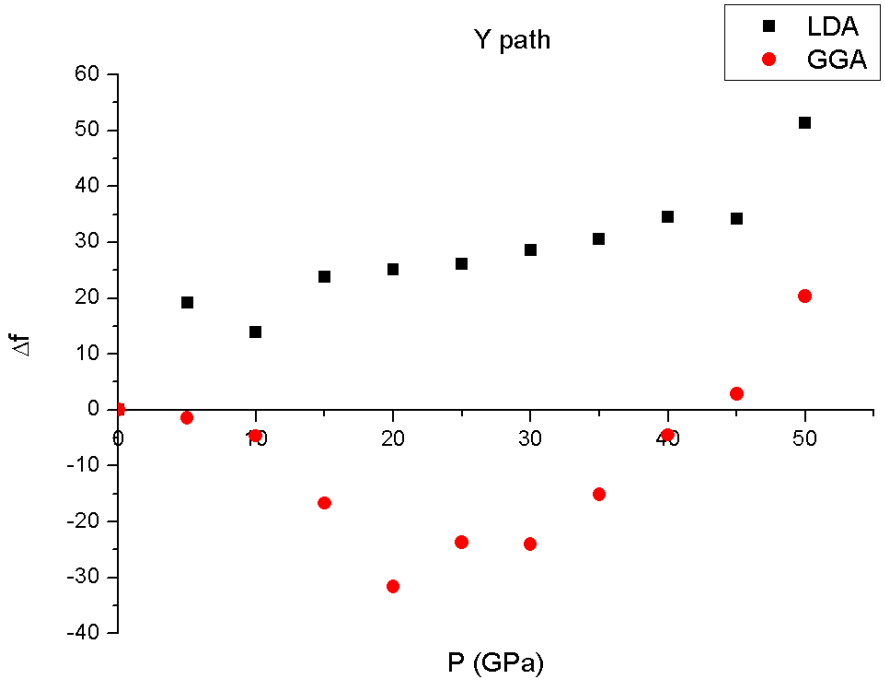

Figure 3.15: Frequency differences of the Y-point phonons under pressure. The frequency at 0 GPa is set as a reference. The results come from LDA and GGA calculations.

Born stability criteria [50]. In the orthorhombic system, it is mechanically stable if the elastic constants satisfy these conditions:

1. $C_{11}+C_{22}+C_{33}+2(C_{12}+C_{13}+C_{23}) > 0$,
2. $C_{11}+C_{22}-2C_{12} > 0$,
3. $C_{11}+C_{33}-2C_{13} > 0$,
4. $C_{22}+C_{33}-2C_{23} > 0$,

where C_{ij} are the elastic constants. The structure of the $C_2N_2(CH_2)$ at 20 GPa from the GGA calculation satisfies all these conditions. This confirms that the $Cmc2_1$ structure is stable at least upto 50 GPa.

3.7 Raman spectrum

The Raman spectroscopy is a method that uses the inelastic scattering of the photon, in the visible, near infrared or near ultraviolet range, to identify the structure of the material. In more detail, this technique can specify the vibrational and rotational modes in the system by observing the frequency shift of the incident photon. We calculate the Raman spectrum to compare with some available data [51, 52, 53]. In this part, LDA and GGA calculations were performed. The results of the relaxation structure at 0 GPa is shown in FIG.3.16. The star marks in the FIG.3.16 are the references from the experimental data [51, 52, 53]. We compared the peak of the Raman spectrum from our calculation and the experiment data which is shown in Table.3.3.

Table 3.3: The Raman shift from our calculation compared with available data [51, 52, 53]

Lable	Wavenumber (LDA)	Wavenumber (GGA)	Ref	Bond	Mode	Wavenumber (Ref)
1	402	393	⋆	C-C-C	Deform	375 [51]
2	671	648				
3	880	832	⋆	C-C	Stretch (a_1)	867 [51]
4	1012	1013	⋆	C-C	Stretch (b_1)	1054 [51]
5	1250	1269	⋆	C-H_2	Twist	1278 [51]
6	1375	1405	⋆	C-H_2	Wag	1338 [51]
7	1552	1560	⋆	C-N	-	1500-1600 [52, 53]
8	3050	3110	⋆	C-H_2	s-stretch	3008 [51]
9	3145	3203	⋆	C-H_2	a-stretch	3087 [51]

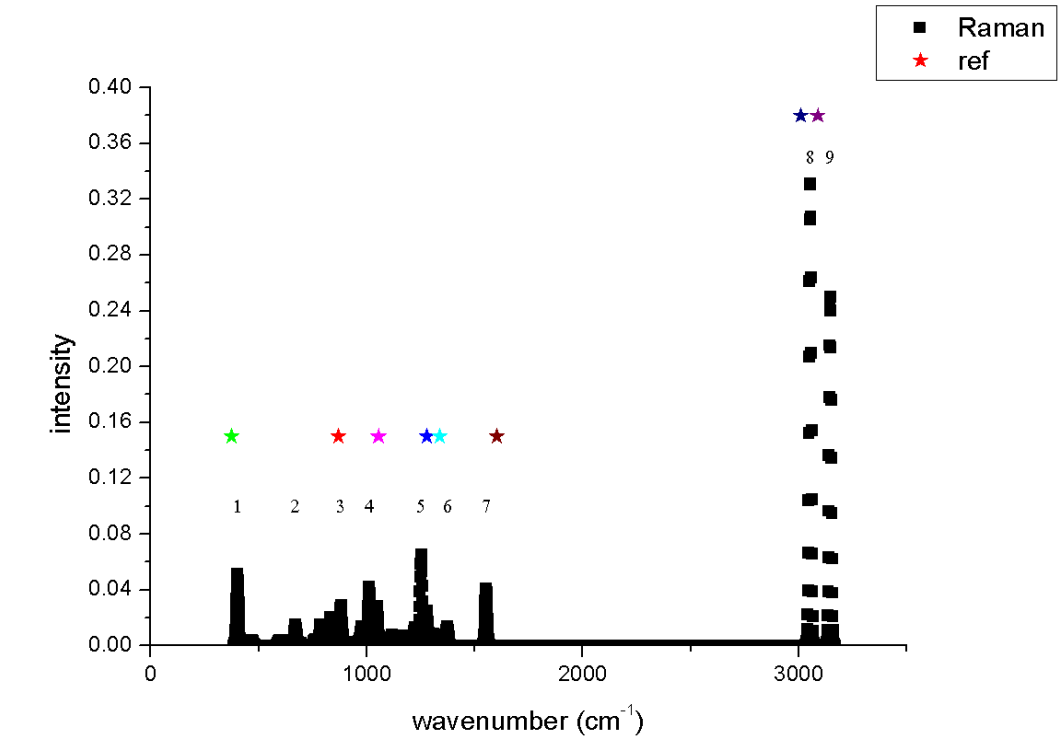

(a)

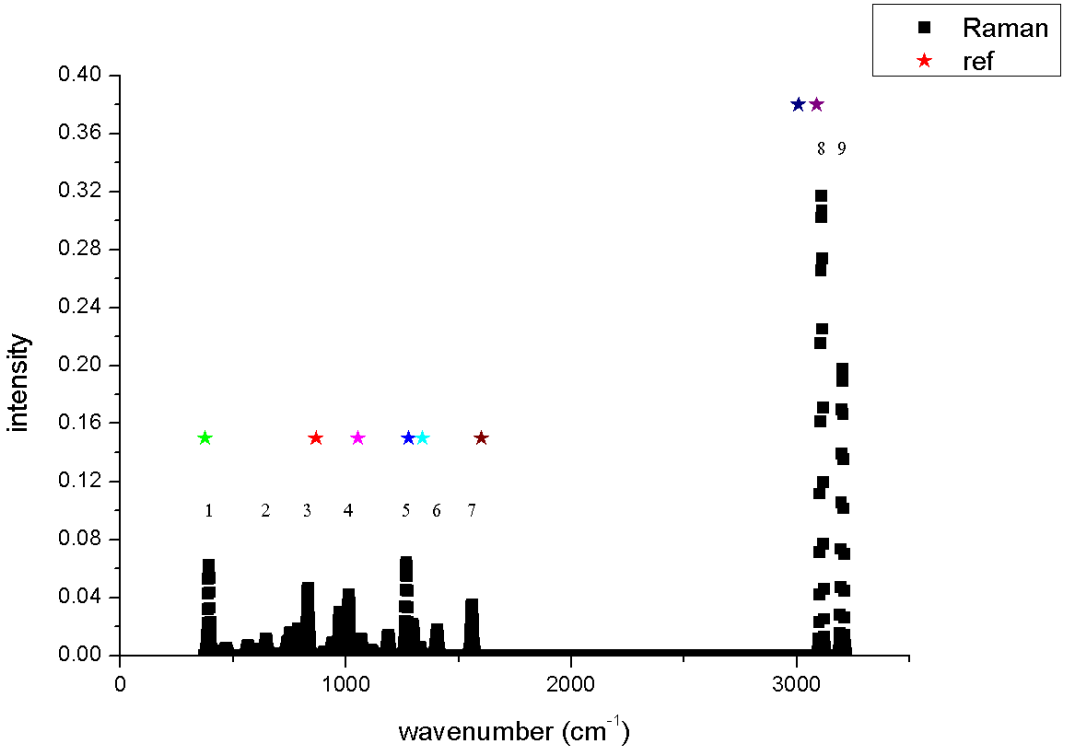

(b)

Figure 3.16: Raman spectrum of the relax structure at 0 GPa using (a) LDA and (b) GGA calculations.

In more detail, we chose the Raman spectrum from propane, $CH_3CH_2CH_3$, as a reference because its C atoms form the sp^3 hybridization and has CH_2 function as a link between two C atoms. It is similar to $C_2N_2(CH_2)$. However, it is well-known that the chemical environment affects the Raman spectrum so it might be slightly difference even if it is detected from the same type of bond as shown in FIG.3.17.The first peak of the Raman spectrum from our calculation corresponds to the deformation mode of C-C-C in the reference molecule. The peaks at 880 cm^{-1} from the LDA and 832 cm^{-1} from the GGA match with the C-C symmetrical stretching mode. The C-C antisymmetrical stretching mode is matched with the peak at 1012 cm^{-1} and 1013 cm^{-1} from the LDA and the GGA respectively. The twisting and wagging modes of C-H_2 appear at 1250 cm^{-1} and 1375 cm^{-1} from the LDA, and 1269 cm^{-1} and 1405 cm^{-1} from the GGA, respectively. Unfortunately, some special peaks cannot be specified using spectrum from $CH_3CH_2CH_3$. Also, we found that the peak at the wavenumber in the range of 2900-3100 cm^{-1} could correspond to the vibration of C-H_2 bond. Thus, we resort to other molecules that has CH_2 function, e.g. CH_2Br, CH_2Cl, CH_2Br CH_2Br and CH_2Cl CH_2Cl as references. Then we find that the peaks at 3050 cm^{-1} and 3110 cm^{-1} match the C-H_2 symmetrical stretching mode. The peaks at 3050 cm^{-1} and 3110 cm^{-1} match the C-H_2 antisymmetrical stretching mode. It was reported that the CN molecules has a peak at 1500-1600 cm^{-1} [52] which is in good agreement with the peaks at 1552 cm^{-1} and 1560 cm^{-1} from LDA and GGA respectively. Finally, we could not specify the peak in the range of 500-700 cm^{-1}.

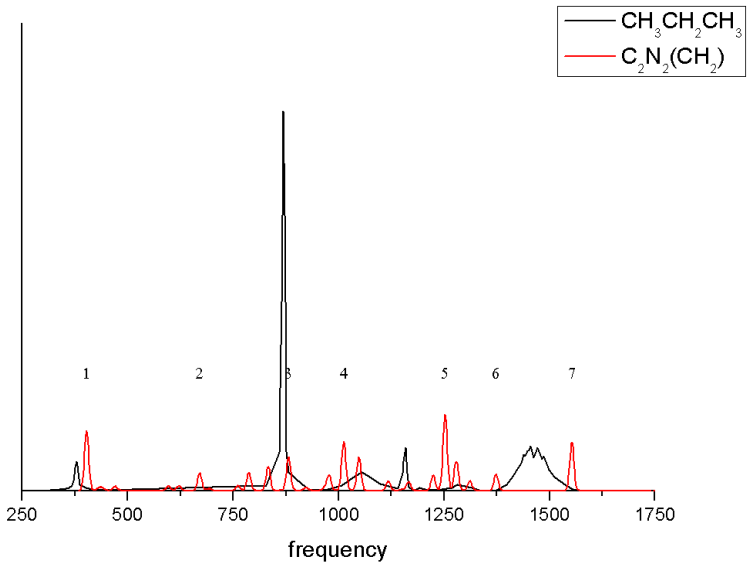

Figure 3.17: The Raman spectrum of propane [54] at 298 K versus $C_2N_2(CH_2)$ of LDA at 0 K.

We, therefore, chose and project some of normal modes from the LDA calculation. FIG.3.18-3.19 show the normal modes of the phonon at 833 cm^{-1} and 1048 cm^{-1}. There two mode have the C-C vibration. The normal mode of phonon at 1167 cm^{-1} show that two H atoms vibrate perpendicular to a plane, defined by C and two H atoms, with opposite vibrational directions as shown in FIG.3.20. This corresponds to the C-H_2 twisting mode. Next, FIG.3.21 illustrate the normal mode of phonon at 1311 cm^{-1}. This shows that two H atoms vibrate perpendicular to a plane the same as twisting mode but they vibrate in the same vibrational directions. This corresponds to the C-H_2 wagging mode. The normal modes of the phonon at 3052 cm^{-1} and 3147 cm^{-1} show the C-H_2 bond vibration in the direction that changes the bond length as shown in FIG.3.22-3.23. They correspond with the stretching mode vibration. In more detail, the mode at 3050 (3147) cm^{-1} is (anti)symmetrical stretching mode due to the two H atoms vibrate in the same (opposite) direction. Finally, we project a normal mode of phonon at 670 cm^{-1} as shown in FIG.3.24. This mode shows the vibration of the C and N atoms. Thus, we conclude that the peak in the range of 500-700 cm^{-1} is the result from the C-N single bond vibration.

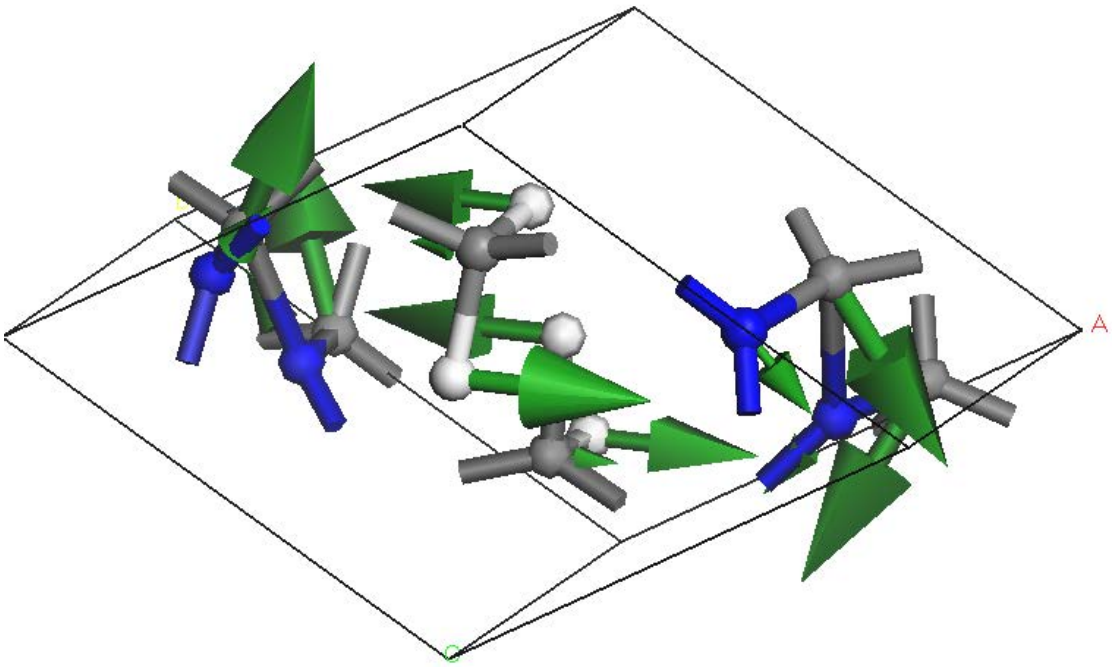

Figure 3.18: The normal mode at 833 cm^{-1} is the C-C symmetrical stretching mode.

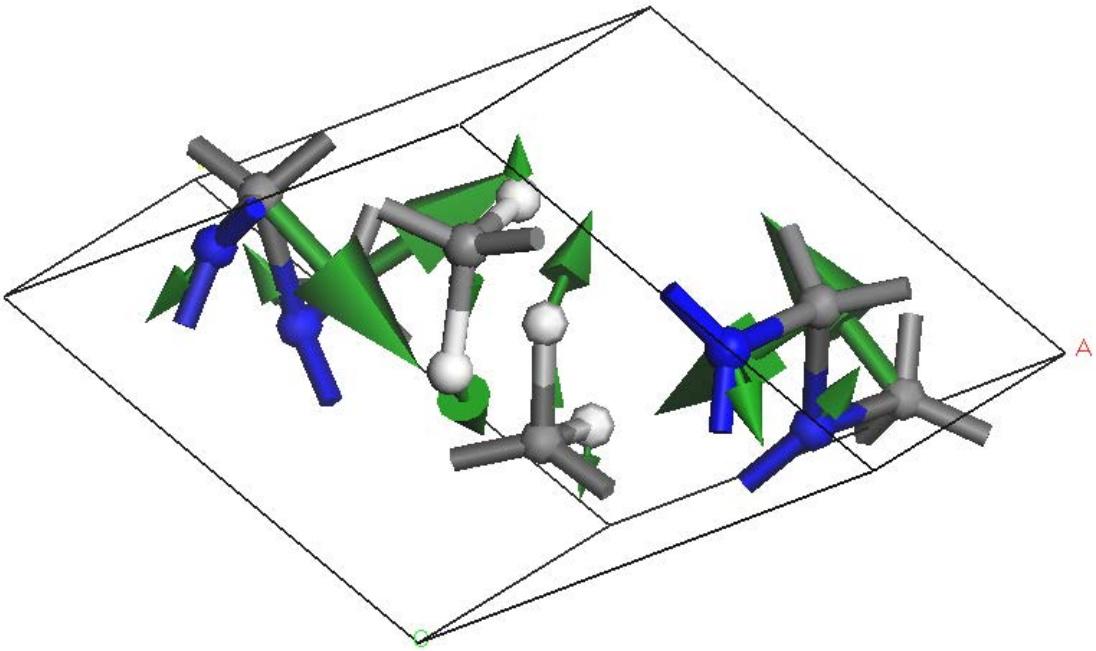

Figure 3.19: The normal mode at 1048 cm^{-1} is the C-C antisymmetrical stretching mode.

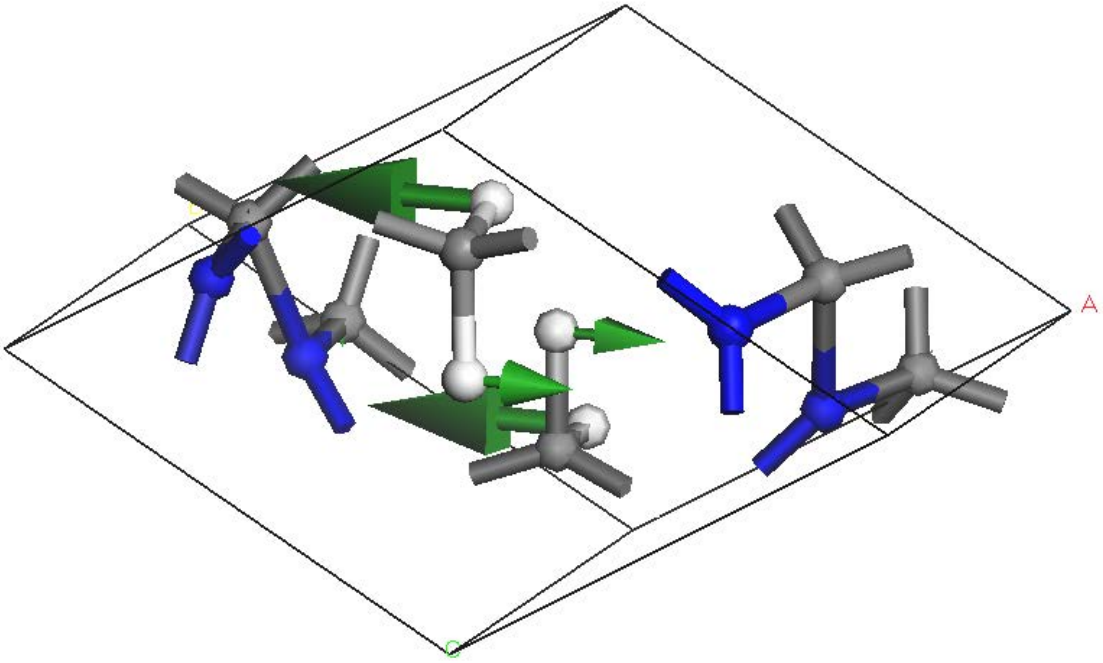

Figure 3.20: The normal mode at 1167 cm^{-1} shows the vibration of two H atom which corresponds to C-H_2 twisting mode.

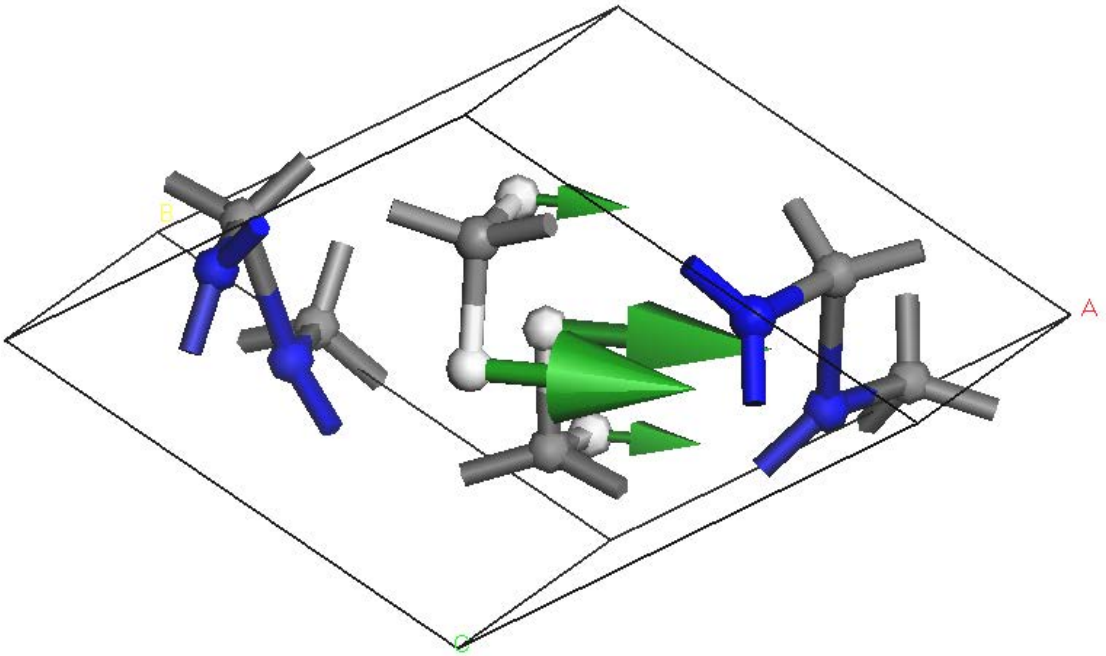

Figure 3.21: The normal mode at 1311 cm^{-1} shows the vibration of two H atom which corresponds to C-H_2 wagging mode.

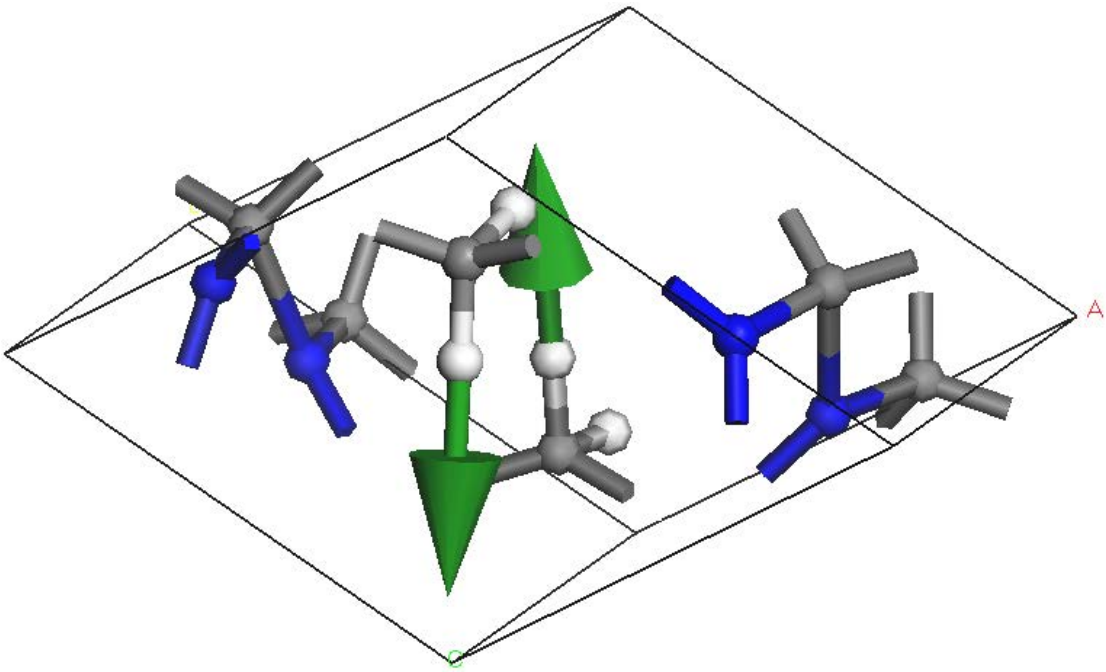

Figure 3.22: The normal mode at 3052 cm^{-1} is a vibration that changes the length of a bond. This matches with the C-H_2 symmetrical streching mode.

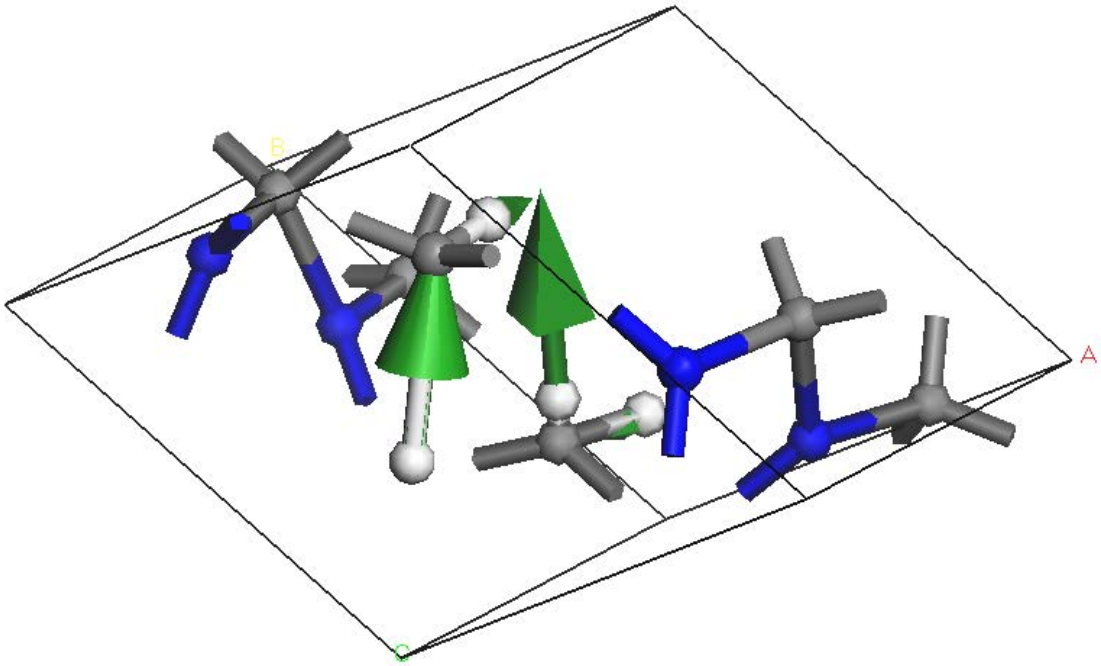

Figure 3.23: The normal mode at 3147 cm^{-1} is the C-H_2 antisymmetrical streching mode.

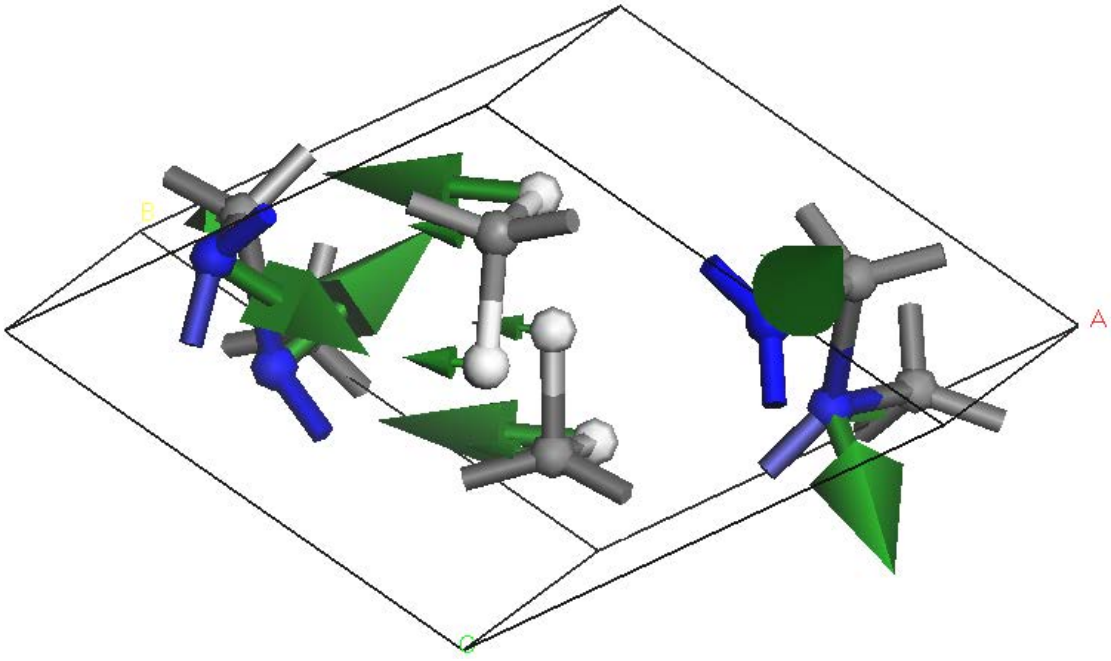

Figure 3.24: The vibration of the C-N single bond corresponds to the normal mode at 670 cm^{-1}.

Calculating Raman spectrum, would require a large amount of resources so we choose the phonon frequency at the G-point and plot it against pressure to predict the trend under high pressure. The results are shown in FIG.3.25. The results from the LDA calculation show that the phonon frequency increases when pressure increases but the GGA calculation predicts that the phonon frequency decreases at 10 GPa. Then we calculate the Raman spectrum of this compound at 5 and 10 GPa using GGA calculation and compare with those at 0 GPa as shown in FIG.3.26. We do not find the decrease of the Raman spectrum at 10 GPa.

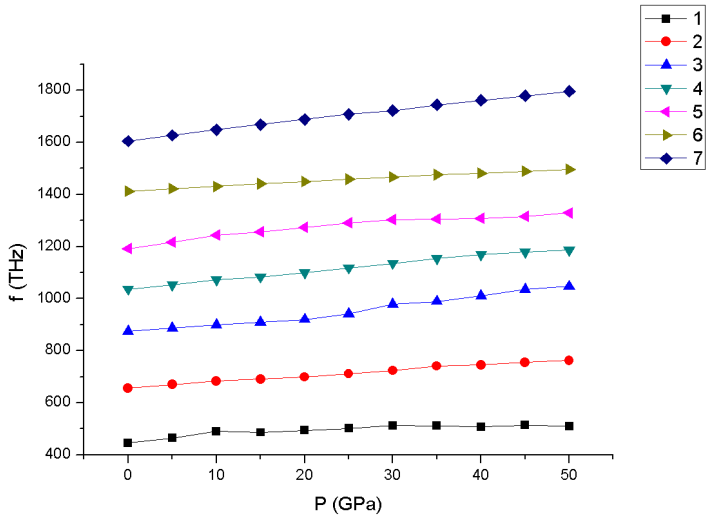

(a)

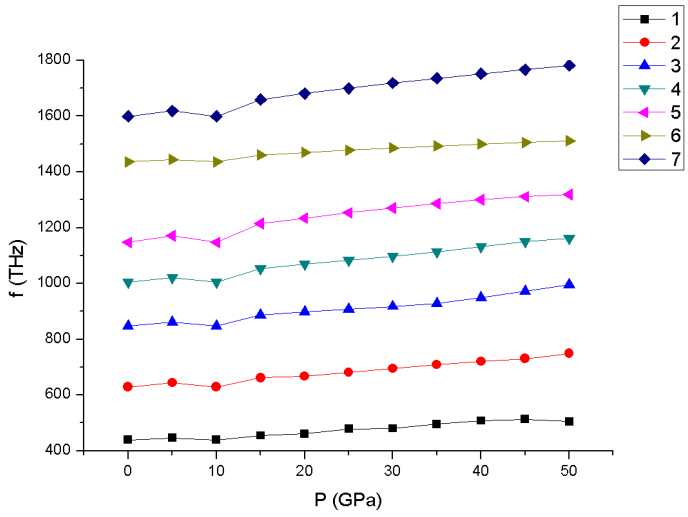

(b)

Figure 3.25: The phonon frequency at G-point using (a) LDA and (b) GGA calculations.

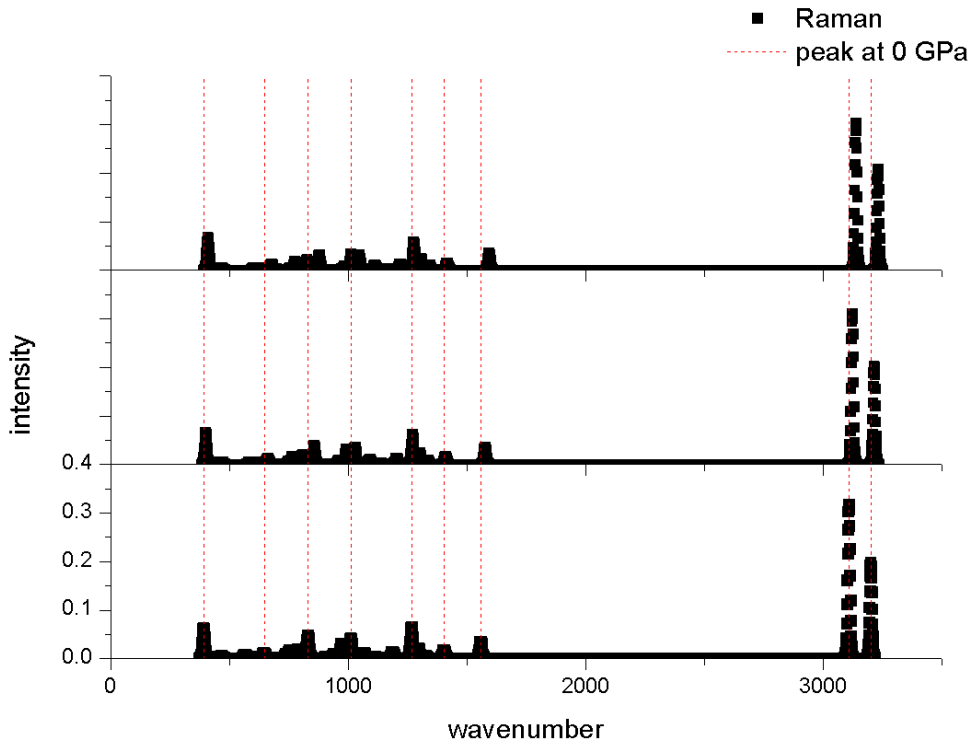

Figure 3.26: The Raman spectrum from the GGA calculation at 0, 5, 10 GPa.

Chapter IV

ELECTRONIC PROPERTIES

As we mentioned before, a wide-band gap semiconductor is very interesting because it has many applications. The previous works [4, 5] showed clearly that $C_2N_2(CH_2)$ has a wide-band gap. Wei's work [5] explained the origin of the valence band maximum (VBM) and the conduction band minimum (CBM). However, the nature of the $C_2N_2(CH_2)$ band gap under high pressure has not been described yet. In this part, the mechanism of band gap changing is explained. In order to explain it, the origin of the VBM and CBM is carefully examined. Then the band gap under pressure is described. Furthermore, the direct-indirect band gap crossing over effect is tested using the sX-LDA calculation since it is known to be the most accurate tool to study the band structure.

4.1 The mechanism of band gap reduction

The valence electrons in $C_2N_2(CH_2)$ consist of $2s^2$, $2p^2$ states from C, $2s^2$, $2p^3$ states from N, and $1s^1$ state from H. Thus, the electronic state around the edge of valence and conduction states, corresponding to VBM and CBM, respectively, results from mixing of these states. To explain the VBM and the CBM of $C_2N_2(CH_2)$, the partial density of states (PDOS) is examined, as shown in FIG.4.1. We find that the valence band is dominated by the p states of N, C^1 and C^b and the conduction band consists of all states, except the s state of C^b. This could be implied that the pressure affects the VBM and CBM differently. In order to extract the effect of the pressure on the VBM and CBM, we calculate the density of states (DOS) of the $C_2N_2(CH_2)$ and observe its behavior under high pressure. The DOS of this compound at 0, 25 and 50 GPa are shown in FIG.4.2. We found that the positions of the VBM and the CBM increase as pressure increases. We, therefore, plot the VBM and CBM energy as a function of pressure which is shown in FIG.4.3 and calculate the rates $a_p = \frac{dE}{dp}$ [55], also known as pressure coefficient. We found that the incremental rate of the VBM is greater than that of the CBM,

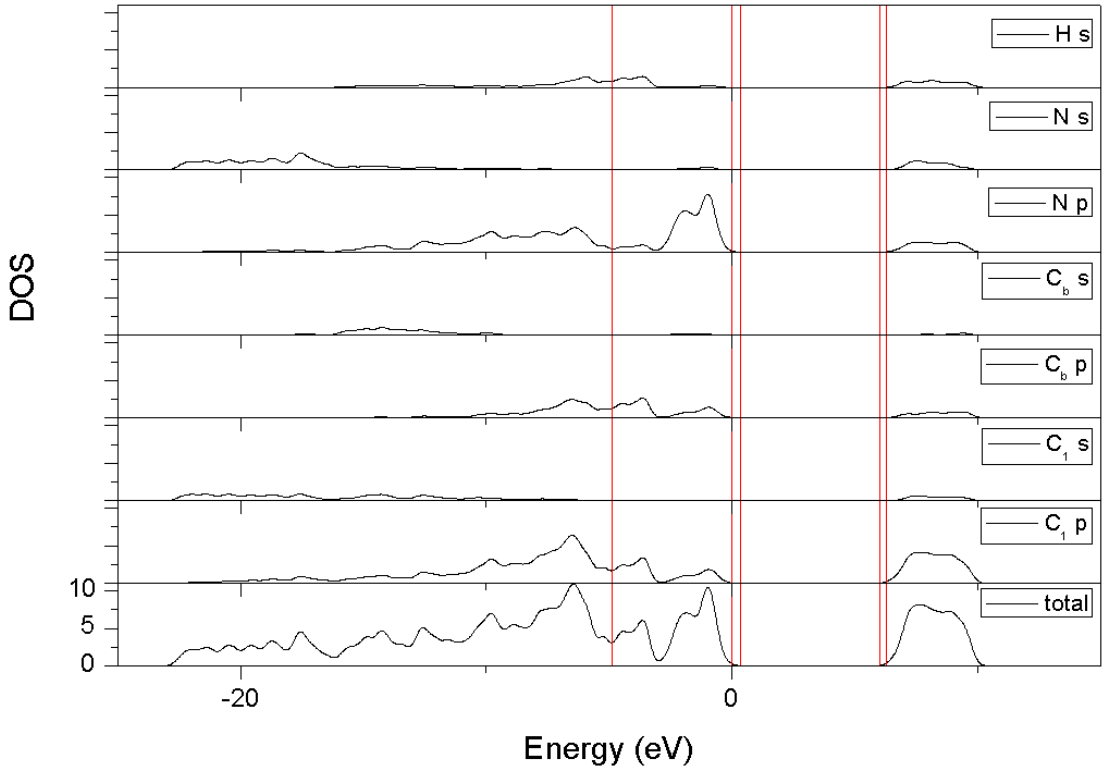

Figure 4.1: The partial density of states (PDOS) of $C_2N_2(CH_2)$.

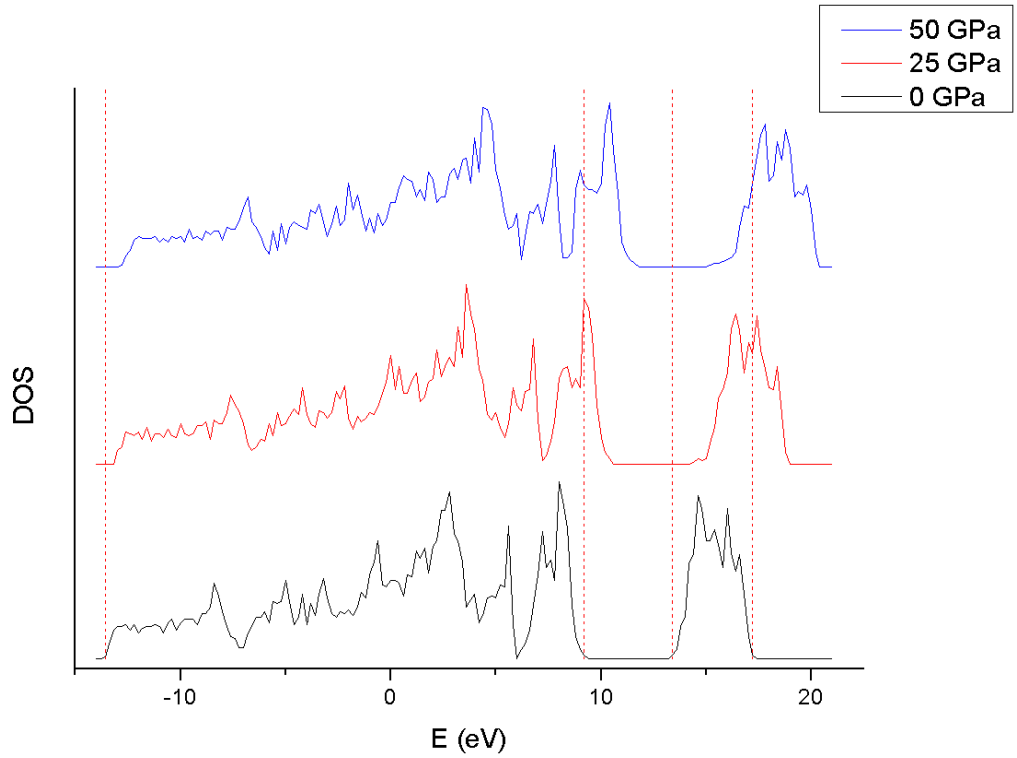

Figure 4.2: The density of states at 0, 25 and 50 using the LDA calculation.

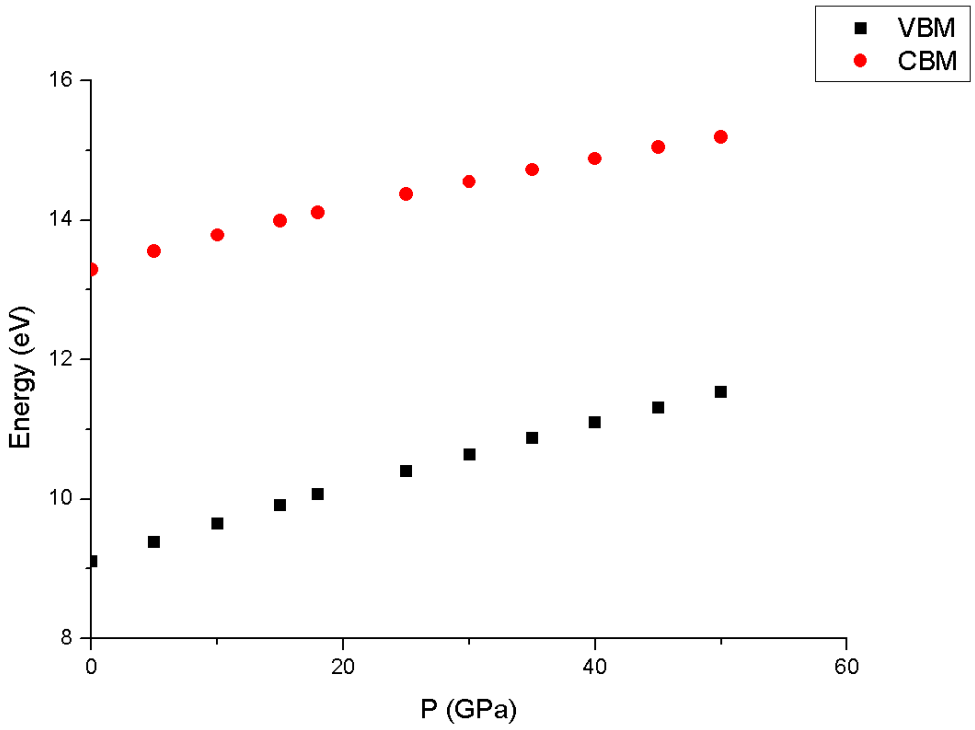

Figure 4.3: The VBM and the CBM under pressure from LDA calculation.

Table 4.1: The incremental rate of the VBM and the CBM.

	LDA (meV/GPa)	GGA (meV/GPa)
a_p^{VBM}	50.2	49.8
a_p^{CBM}	36.6	42.3

as seen in Table. 4.1. This leads to the reduction of the band gap. On the other hand, the band gap could increase, if the incremental rate of the CBM is higher than VBM.

4.2 Band structure

The band gap of $C_2N_2(CH_2)$ is calculated using three functionals, LDA, GGA and sX-LDA and compared with theoretical works [4, 5]. The band gap of $C_2N_2(CH_2)$ at 0 GPa and other pressure points are reported in Table 4.2. The results show that the band gaps of the relaxed structure at 0 GPa are 4.15, 4.26 and 6.04 according to LDA, GGA and sX-LDA calculations, respectively. The band structure of this compound at 0 GPa using the sX-LDA is shown in FIG.4.4. Under high pressure, the band gap of $C_2N_2(CH_2)$ decreases as pressure increases. We find paradoxical

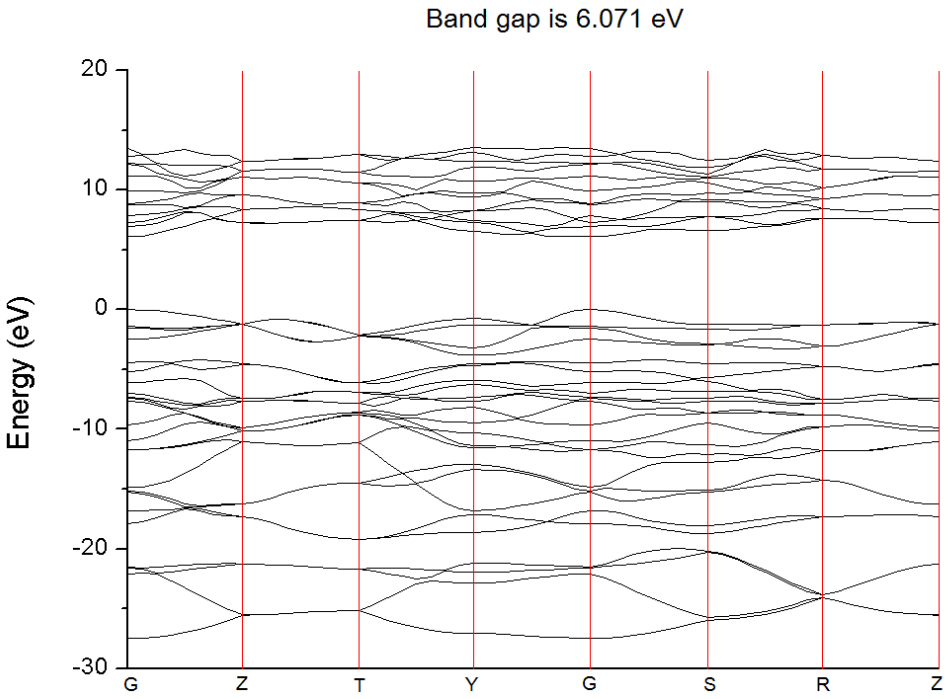

Figure 4.4: Band gap of the $C_2N_2(CH_2)$ compound at 0 GPa from the sX-LDA

results between GGA calculation and the others in pressure range of 0-5 GPa. The LDA and sX-LDA band gaps decrease when pressure increases while the GGA calculation shows that the band gap increases to the highest value at 5 GPa, and after that it starts to decrease. The band gap under pressure relative to that of at 0 GPa is shown in FIG.4.5.

As we showed in Chapter 3, GGA calculation gave different results of the N^1-C^1-N^2 and N^2-C^1-C^b angle changes in this range of pressure too. The reason is that the angles N^1-C^1-N^2 and N^2-C^1-C^b, and the band gap under pressure are

Table 4.2: The $C_2N_2(CH_2)$ band gap under pressure, compared with the results from the previous works [4, 5].

P(GPa)	$C_2N_2(CH_2)$				
	LDA	GGA	sX-LDA	GGA [5]	sX-LDA[4]
0	4.15	4.26	6.07	4.24	∼6
10	4.07	4.28	6.04	-	-
20	3.97	4.20	5.96	-	-
30	3.85	4.10	5.87	-	-
40	3.72	4.00	5.76	-	-
50	3.60	3.89	5.66	-	-

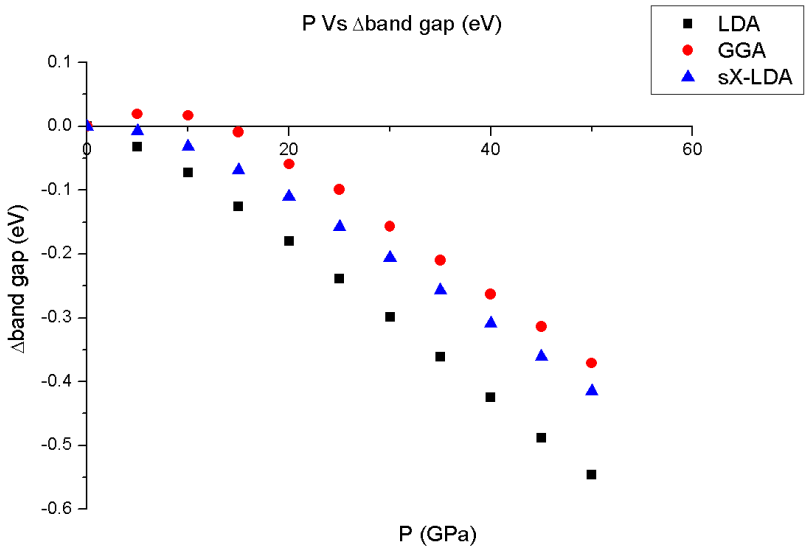

Figure 4.5: The band gap difference denoted by Δband gap at various pressures. The band gap at 0 GPa is set as a reference.

related. In more detail, N^1-C^1-N^2 and N^2-C^1-C^b share the N^2 atom. Thus, to study the effect of these angles on the band gap, we modify the N^1-C^1-N^2 and N^2-C^1-C^b angles by moving the N^2 atom and use LDA calculation to compute the band gap. We need to study the atomic movement only, thus, we keep the pressure fixed at 0 GPa. The relation between band gap changes and the N^2-C^1-C^b angle change, while fixing the N^1-C^1-N^2 angle, is shown in Table 4.3. The results show that the N^2-C^1-C^b angle change has little effect on the band gap.

Table 4.3: Relation between the N^2-C^1-C^b angles and the band gap from the LDA.

	N^2-C^1-C^b	band gap	ΔN^2-C^1-C^b	Δband gap
LDA	114.772	4.147	0	0
	114.807	4.147	0.035	0
	114.842	4.146	0.07	-0.001
	114.877	4.145	0.105	-0.002
	114.912	4.144	0.14	-0.004

Then we modify the N^1-C^1-N^2 and the N^2-C^1-C^b angles at the same time. We move the N^2 atom in such a way that the N^1-C^1-N^2 angle increases and the N^2-C^1-C^b angle decreases (the same trend as the GGA angle changes between 0-5 GPa). The results, as shown in Table.4.4, show that the LDA band gap increases. This leads to the conclusion that the discrepancy between the LDA and the GGA

band gaps between 0-5 GPa due different behavior of the N^1-C^1-N^2 and N^2-C^1-C^b angles.

Table 4.4: Relation between the N^1-C^1-N^2 and the N^2-C^1-C^b angles and the band gap from the LDA.

	N^1-C^1-N^2	N^2-C^1-C^b	band gap	ΔN^1-C^1-N^2	ΔN^2-C^1-C^b	Δband gap
LDA	109.429	114.772	4.147	0	0	0
	109.401	114.810	4.152	-0.028	0.038	0.005
	109.374	114.847	4.155	-0.055	0.075	0.008
	109.347	114.885	4.158	-0.082	0.113	0.011
	109.919	114.922	4.162	-0.110	0.150	0.015

Next, we change the N^1-C^1-N^2 angle, while the N^2-C^1-C^b angle was fixed, by moving the N^2 atom. Table 4.5 shows the relation between the N^1-C^1-N^2 angle and the band gap. The results show that the band gap changes significantly according to the N^1-C^1-N^2 angle change. Then we explore in more detail why the N^1-C^1-N^2 angle has a significant effect but the N^2-C^1-C^b angle has little effect on the band gap. Consider the N^1-C^1-N^2 angle change by moving the N^2 atom. When this angle decreases, the N^2 atom moves closer to the N^1 atoms, as shown in FIG.4.6a. This makes the overlapping integral increases, resulting in the band gap increase. On the opposite side, we find that if the N^1-C^1-N^2 increases, the band gap decreases. Consider the N^2-C^1-C^b angle change by moving the N^2 atom. The N^2 atom moves toward a free space which reduces the interaction with other atoms, regardless of whether this angle increases or decreases. The N^2 atom movement according to the increase of the the N^2-C^1-C^b angle is shown in FIG.4.6b.

From our knowledge, LDA calculation overestimates the binding energy [56] while GGA calculation underestimates it [57]. This means that in GGA calculation the bonding in $C_2N_2(CH_2)$ is softer than in LDA calculation. Thus, when

Table 4.5: Relation between the N^1-C^1-N^2 angles and the band gap from the LDA.

	N^1-C^1-N^2	band gap	ΔN^1-C^1-N^2	Δbandgap
LDA	109.429	4.147	0	0
	109.395	4.151	-0.034	0.004
	109.361	4.155	-0.068	0.018
	109.328	4.158	-0.101	0.011
	109.284	4.161	-0.145	0.014

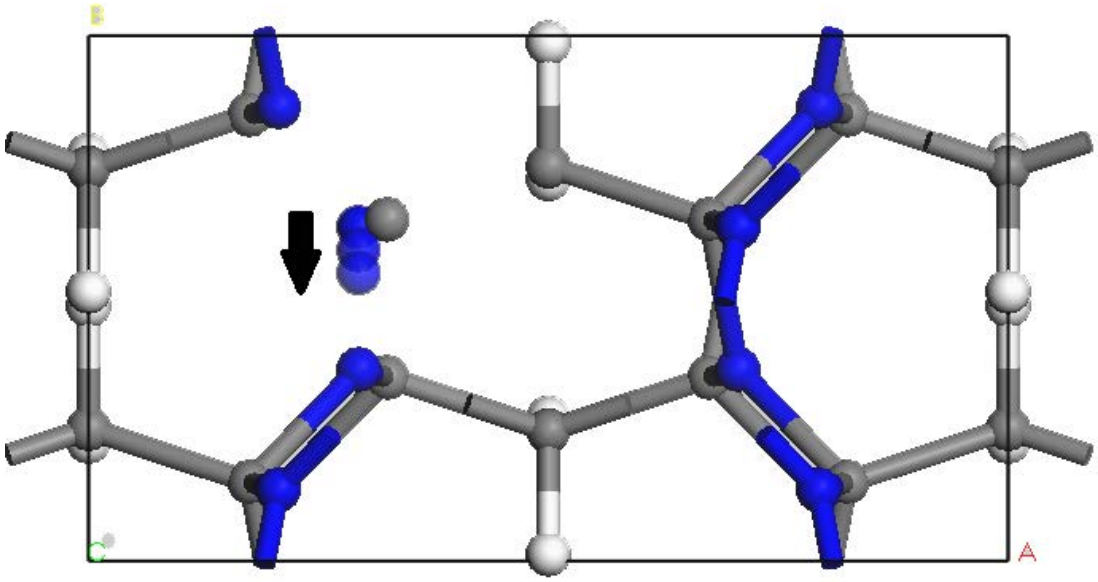

(a)

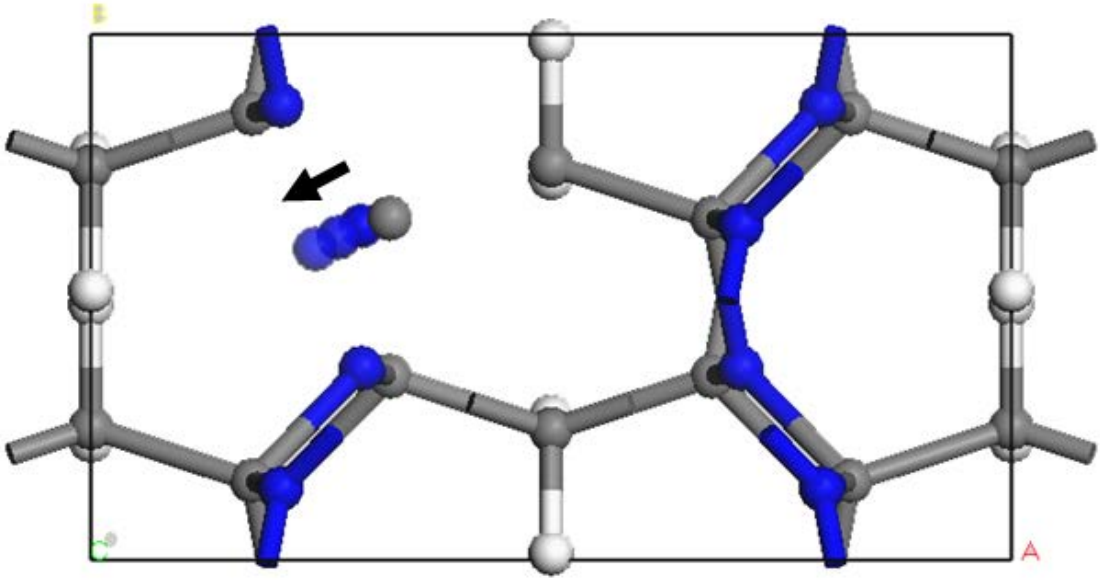

(b)

Figure 4.6: The N^2 movement, from equilibrium position (0.293603, 0.635494, 0.856859), according to (a) the N^1-C^1-N^2 angle decrease, to (0.293699, 0.634598, 0.857529), and (b) the N^2-C^1-C^b increase, to (0.293064, 0.635503, 0.856249).

pressure increases, the N^2 atom in the GGA calculation can move close to N^1 atom more easily than in the LDA calculation. This is a possible explanation for the discrepancy between the LDA and the GGA calculation.

4.3 The direct-to-indirect crossover

We find that the $C_2N_2(CH_2)$ compound is a direct band gap semiconductor at ambient condition. However, some materials [58] transform from a direct to an indirect semiconductor, which is called the direct-to-indirect band gap crossover, under high pressure. Also we monitor this phenomenon in the $C_2N_2(CH_2)$ compound. In this part, we use the sX-LDA calculation. It is clear that the band gap crossover occurs if the VBM and CBM exist at a point other than at the gamma point (G-point). We, therefore, examine the VBM and the CBM of the $C_2N_2(CH_2)$ compound under high pressure. The changes in the valence and the conduction states at the high symmetry points, i.e. Z, T, Y, S and R points, under high pressure relative to those at the G-point are calculated. The results are shown in FIG.4.7. These results show that the changes of the valence and the conduction states, decrease and increase, respectively, if the energy eigenvalues are higher than those at the G-point. It can be concluded that the $Cmc2_1$ structure of $C_2N_2(CH_2)$ is a direct semiconductor under high pressure.

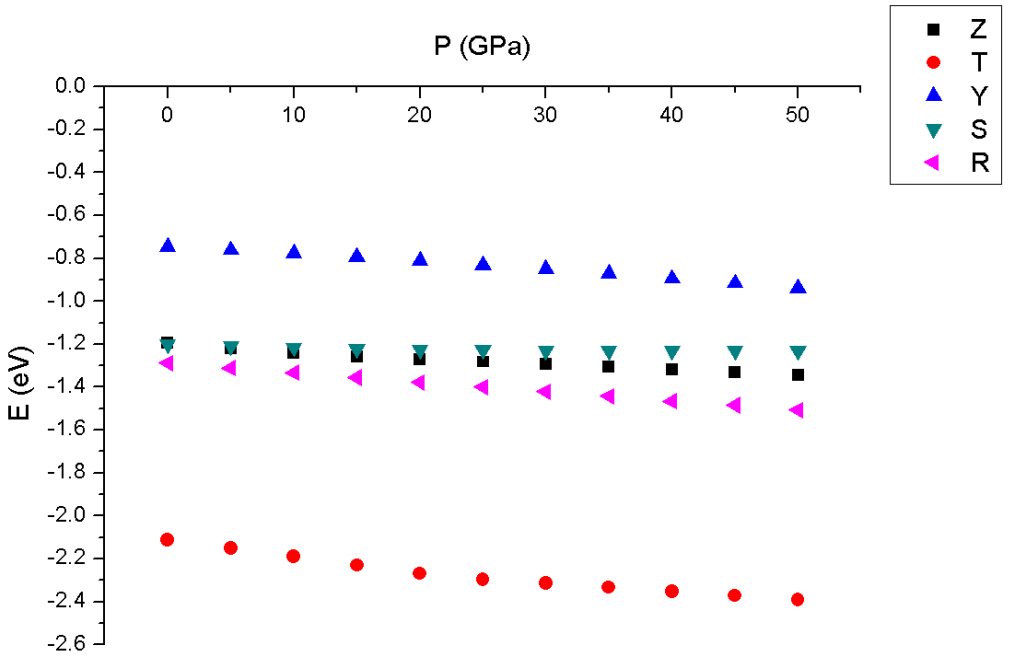

(a)

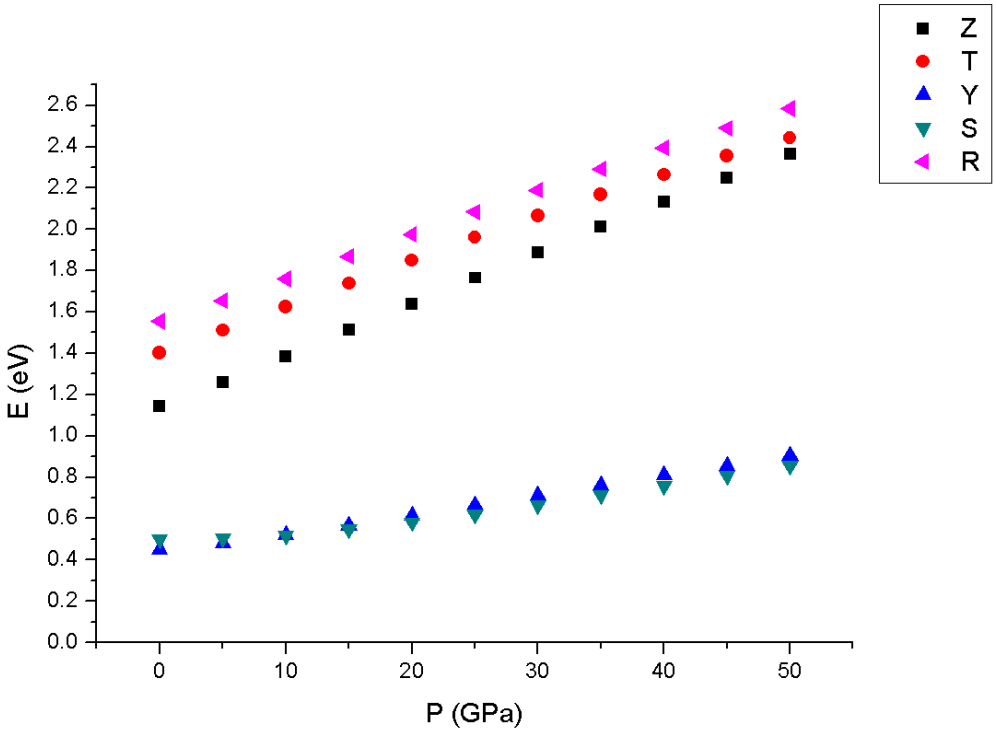

(b)

Figure 4.7: The difference of the (a) VBM and (b) CBM at high symmetry point under pressure relative to those at gamma point.

Chapter V

CONCLUSIONS

We investigated the mechanical and electronic properties under high pressure of carbon nitride methanediide, $C_2N_2(CH_2)$, using first principle method. In this thesis, three different exchange-correlation functionals, i.e. LDA, GGA and sX-LDA, are preformed. The sX-LDA is most accurate to calculate the lattice parameters giving, $a = 7.980$Å, $b = 4.561$Å and $c = 4.067$Å. Under pressure, the C-N single bond of $C_2N_2(CH_2)$ has similar contraction to that of β-C_3N_4. However, the C-C single bond has higher compressibility than that of diamond which is in good agreement with Ding's work [6]. Besides, the C^1-C^b-C^1 angle changes significantly. Thus, $C_2N_2(CH_2)$ has larger compressibility than that of diamond, i.e. the bulk modulus of $C_2N_2(CH_2)$ was only 45 % of that of diamond. The $Cmc2_1$ structure of this material was examined using the phonon dispersion and Born stability criteria. The results showed that it has dynamical and mechanical stability in pressure range of 0-50 GPa. The Raman spectrum of $C_2N_2(CH_2)$ is described for the first time by our calculation. We detect 9 peak from the Raman calculation, i.e., 402 (393), 671 (648), 880 (832), 1012 (1013), 1250 (1269), 1375 (1405), 1552 (1560), 3050 (3110) and 3145 (3203) cm^{-1} using LDA (GGA).The Raman shift at 671 (648) cm^{-1} and 1552 (1560) cm^{-1} could be due to the C-N single bond. Further, the Raman spectrum's results under pressure support that the $Cmc2_1$ structure has stability under pressure.

For the electronic property, the band gap of $C_2N_2(CH_2)$ is 6.071 eV from the sX-LDA calculation. Clearly the band gap decreases as pressure increases. To understand the reducing mechanism of the band gap, we examined the PDOS of this material under pressure. From our analysis, the VBM is dominated by the p states of N, C^1 and C^b but the CBM is composed of all states, except the s state of C^b. Under pressure, the results show that the incremental rate of the VBM is higher than that of the CBM, resulting in decreasing band gap. Moreover, we found the linkage between the interatomic angle N^1-C^1-N^2 and the band gap. The changing of this angle strongly affects the CBM and the CBM

increases as the N^1-C^1-N^2 decreases. Thus, the band gap increases. The direct-indirect band gap crossing over effect was tested and found that it did not occur in this material. In this thesis, we found many discrepancies, i.e., angle changes, phonon dispersion, Raman spectrum and band gap, between the GGA results and the LDA results. In our opinion, the main reason is because the LDA calculation overestimates the binding energy while the GGA calculation underestimates it so that they predict different ground states of the atomic positions leading to differences in other results. Further experimental works will be a tool to judge our prediction. Furthermore in the GGA results, we found the phonon softening which is a precursor to the structural instability around 20 GPa. To our knowledge, no phonon and Raman spectrum measurements have been performed experimentally. Therefore, our study suggested that these experiment should be carried out at low temperature and other structures of $C_2N_2(CH_2)$ could be detected.

REFERENCES

[1] Sougawa, M., Sumiya, T., Takarabe, K., Mori, Y., Okada, T., Gotou, H., Yagi, T., Yamazaki, D., Tomioka, N., Katsura, T., Kariyazaki, H., Sueoka, K. and Kunitsugu, S. Crystal structure of new carbon-nitride-related material $C_2N_2(CH_2)$. **Jpn. J. Appl. Phys.** 50 (2011): 095503.

[2] Sougawa, M., Takarabe, K., Mori, Y., Yagi, T., Kariyazaki, H. and Sueoka, K. Bulk modulus and structural changes of carbon nitride $C_2N_2(CH_2)$ under pressure: The strength of C-N single bond. **J. Appl. Phys.** 113 (2013): 053510.

[3] Sougawa, M., Sumiya, T., Takarabe, K., Mori, Y., Okada, T., Gotou, H., Yagi, T., Yamazaki, D., Tomioka, N., Katsura, T., Kariyazaki, H., Sueoka, K. and Kunitsugu, S. Bond strengths of new carbon-nitride-related material $C_2N_2(CH_2)$. **J. Phys.: Conf. Ser.** 377 (2012.): 012028.

[4] Takarabe, K., Sougawa, M., Kariyazaki, H., and Sueoka, K. Electronic structure C_2N_2X (X=O, NH, CH_2): Wide band gap semiconductors. **J. Appl. Phys.** 112 (2012): 013537.

[5] Wei, Q., Zhang, M., Guo, L., Yan, H., Zhu, X., Lin, Z. and Guo, P. Ab initio studies of novel carbon nitride phase $C_2N_2(CH_2)$. **Chem. Phys.** 415 (2013): 36-43.

[6] Ding, Y., Chen, M. and Wu, W. Stability and mechanical properties of C_2N_2X(X=O, NH and CH_2) from first-principles calculations. **Physica B** 428 (2013): 97-105.

[7] Yoder, M. N. Wide bandgap semiconductor material and devices. **IEEE. T. Electron Dev.** 43 (1996): 1633-1636.

[8] Ponce, F.A. and Bour, D.P. Nitride-based semiconductors for blue and green light-emitting devices. **Nature** 386 (1997): 351-359.

[9] Omnes, F., Monroy, E., Munoz, E. and Reverchon, J.-L. Wide bandgap UV photodetectors: A short review of devices and applications. **Proc. of SPIE** 6473 (2007): 64730E-1 - 64730E-15.

[10] Goldberg, Y. A. Semiconductor near-ultraviolet photoelectronics. **Semicond. Sci. Technol.** 14 (1999): R41.

[11] Casady, J.B. and Johnson, R.W. Status of silicon carbide (SiC) as a wide-bandgap semiconductor for high-temperature applications: A review. **Solid-State Electron** 39 (1996): 1409-1422.

[12] Liu, A.Y. and Cohen, M. L. Prediction of new low compressibility solids. **Science** 245 (1989): 841-842.

[13] Occelli, F., Loubeyre, P. and Letoullec, E. Properties of diamond under hydrostatic pressures up to 140 GPa. **Nat. Mater.** 2 (2003): 151-154.

[14] Guo, Y. and Goddard W.A. Is carbon nitride harder than diamond? No, but its girth increases when stretched (negative Poisson ratio). **Chem. Phys. Lett.** 237 (1995): 72-76.

[15] Teter, D.M. and Hemley, R.J. Low-compressibility nitrides. **Science** 271 (1996): 53-55.

[16] Liu, A.Y. and Wentzcovitch, R.M. Stability of carbon nitride solids. **Phys. Rev. B** 50 (1994): 10362-10365.

[17] Yao, H. and Ching, W.Y. Optical properties of β-C_3N_4 and its pressure dependence. **Phys. Rev. B** 50 (1994): 11231-11234.

[18] Xu, Y. and Gao, S.-P. Band gap of C_3N_4 in the GW approximation. **Int. J. Hydrogen Energy** 37 (2012): 11072-11080.

[19] Gao, F., He, J., Wu, E., Liu, S., Yu, D., Li, D., Zhang, S. and Tian, Y. Hardness of Covalent Crystals. **Phys. Rev. Lett.** 91 (2003): 015502.

[20] Simunek, A. and Vackar, J. Hardness of Covalent and Ionic Crystals: First-Principle Calculations. **Phys. Rev. Lett.** 96 (2006): 085501.

[21] Seidl, A., Gorling, A., Vogl, P., Majewski, J.A. and Levy, M. Generalized Kohn-Sham schemes and the band-gap problem. **Phys. Rev. B** 53 (1996): 3764-3774.

[22] Staroverov, V.N. Density-functional approximations for exchange and correlation. In M. Sukumar (ed.)., A Matter of Density: Exploring the Electron Density Concept in the Chemical, Biological and Materials Sciences, 2012.

[23] Bylander, D.M. and Kleinman, L. Good semiconductor band gap with a modified local-density approximation. **Phys. Rev. B** 41 (1990): 7868-7871.

[24] Herring, C. A New Mathod for Calculating Wave Functions in Crystals. **Phys. Rev.** 57 (1940): 1169.

[25] Slater, J.C. and Koster, G.F. Simplified LCAO Method for the Periodic Potential Problem. **Phys. Rev.** 94 (1954): 1498.

[26] Saffren, M.M. and Slater, J.C. An Augmeted Pland-Wave Method for the Periodic Potential Problem. II. **Phys. Rev.** 92 (1953): 1126.

[27] Clark, S.J., Segall, M.D., Pickard, C.J. Hasnip, P.J., Probert, M.I.J., Refson, K. Payne, M.C. First principles methods using CASTEP. **Z. Kristallogr.** 220 (2005):567-570.

[28] Wigner, E. and Seitz, F. On the Constitution of Metallic Sodium. **Phys. Rev.** 42 (1933): 804.

[29] Barth, U.V. and Gelatt C.D. Validity of the frozen-core approximation and pseudopotential theory for cohesive energy calculations. **Phys. Rev. B** 21 (1980): 2222.

[30] Phillips, J.C. and Kleinman, L. New Method for Calculating Wave Functions in Crystals and Molecules. **Phys. Rev.** 116 (1959): 287.

[31] Goedecker, S. and Maschke, K. Transferability of pseudopotentials. **Phys. Rev. A** 1 (1992):88-93.

[32] Hamann, D.R., Schluter, M. and Chiang, C. Norm-Conserving Pseudopotentials. **Phys. Rev. Lett.** 43 (1979): 1494.

[33] Troullier, N. and Martins, J.L. Efficient pseudopotentials for plane-wave calculations. **Phys. Rev. B** 43 (1991): 1993.

[34] Monkhorst, H.J. and Pack, J.D. Special points for Brillouin-zone integrations. **Phys. Rev. B** 13 (1976) 5188.

[35] Pfrommer, B.G., Cote, M., Louie, S.G. and Cohen, M.L. Relaxation of Crystals with the Quasi-Newton Method. **J. Comput. Phys.** 131 (1997): 223-240.

[36] Broyden, C.G. A class of methods for solving nonlinear simultaneous equations. **Math. Comput.** 19 (1965): 577-593.

[37] Dai, Y. Convergence properties of the BFGS algorithm. **SIAM J. Optim.** 13 (2002): 693-701.

[38] Birch, F. Finite Elastic Strain of Cubic Crystals. **Phys. Rev.** 71 (1947): 809.

[39] Murnaghan, F.D. The compressibility of media under extreme pressures. **Proc. Ncad. Sci. USA** 30 (1994): 244-247.

[40] Baroni, S., De Gironcoli, S., Dal Corso, A. and Giannozzi, P. Phonons and related crystal properties from density-functional perturbation theory. **Rev. Mod. Phys.** 73 (2001): 515-562.

[41] Raman, C.V. and Krishnan, K.S. A New Type of Secondary Radiation. **Nature** 121 (1928): 501-502.

[42] Ibanez, J., Oliva, R., Manjon, F.J., Segura, A., Yamaguchi, T., Nanishi, Y., Cusco, R. and Artus, L. High-pressure lattice dynamics in wurtzite and rocksalt indium nitride investigated by means of Raman spectroscopy. **Phys. Rev. B** 88 (2013): 115202.

[43] Lin, C.C., Kuo, M.T. and Chang, H.C. Review: Raman spectroscopy - A novel tool for noninvasive analysis of ocular surface fluid. **J. Med. Biol. Eng.** 30 (2010): 343-354.

[44] Porezag, D. and Pederson, M.R. Infrared intensities and Raman-scattering activities within density-functional theory. **Phys. Rev. B** 54 (1996):7830.

[45] Eisenberg, H.R. and Baer, R. A new generalized Kohn-Sham method for fundamental band-gaps in solids. **Phys. Chem. Chem. Phys.** 11 (2009): 11661.

[46] Perdew, J.P., Parr, R.G., Levy, M. and Balduz, J.L. Density-Functional Theory for Fractional Particle Number: Derivative Discontinuities of the Energy. **Phys. Rev. Lett.** 49 (1982): 1691.

[47] Ceperley, D.M. and Alder, B.J. Ground state of the electron gas by a stochastic method. **Phys. Rev. Lett.**. 45 (1980): 566-569.

[48] Perdew, J.P. and Zunger, A. Self-interaction correction to density-functional approximations for many-electron systems. **Phys. Rev. B**. 23 (1981): 5048-5079.

[49] Perdew, J.P., Burke, K. and Ernzerhof, M. Generalized gradient approximation made simple. **Phys. Rev. B** 77 (1996): 3865-3868.

[50] Wu, Z.J., Zhao, E.J., Xiang, H.P., Hao, X.F., Liu, X.J. and Meng, J. Crystal structures and elastic properties of superhard IrN2 and IrN3 from first principles. **Phys. Rev. B** 76 (2007): 054115.

[51] Shimanouchi, T. Table of Molecular Vibrational Frequencies Consolidated Volume I. **Nat. Stand. Ref. Data. Ser., Nat. Bur. Stand. (U.S.)** 39 (1972).

[52] Yap, Y.K., Kida, S., Aoyama, T., Mori, Y. and Sasaki, T. Influence of negative dc bias voltage on structural transformation of carbon nitride at 600 °C. **Appl. Phys. Lett.** 73 (1998): 915.

[53] Ferrari, A.C., Rodil, S.E. and Robertson, J. Resonant Raman spectra of amorphous carbon nitrides: the G peak dispersion. **Diam. Relat. Mater.** 12 (2003): 905-910.

[54] Martin J. Raman Intensities of Propane in the Gas Phase. **J. Raman Spectrosc.** 16 (1985): 139-142.

[55] Wei, S.H. and Zunger, A. Predicted band-gap pressure coefficients of all diamond and zinc-blende semiconductors: Chemical trends. **Phys. Rev. B** 60 (1999): 5404.

[56] Jones, R.O. and Gunnarsson, O. The density functional formalism, its applications and prospects. **Rev. Mod. Phys.** 61 (1989): 689-746.

[57] Gao, Y. and Zeng, X.C. Ab initio study of hydrogen adsorption on benzenoid linkers in metal-organic framework materials. **J. Phys.: Condens. Matter** 19 (2007): 386220.

[58] Olguin D., Cantarero, A., Ulrich, C. and Syassen, K. Effect of pressure on structural properties and energy band gap of γ-InSe. **Phys. Stat. Sol. B** 235 (2003): 456-463.

APPENDICES

Appendix A

VARIATIONAL PRINCIPLE

The variational principle is a tool to find a variable and a function that yields the extremum value of a function and a functional, respectively. To understand the principle, we study how to apply this method in a function. Suppose x_0 is a value that yields extremum value of function $y(x)$. If x_0 is varied with slightly, the difference between the values of the function at x_0 and $x_0 + \varepsilon$ will be zero,

$$\lim_{\varepsilon \to 0} \frac{y(x_0 + \varepsilon) - y(x_0)}{\varepsilon} = \left. \frac{\partial y}{\partial x} \right|_{x=x_0} = 0. \tag{A.1}$$

The variational principle can be applied to functional in the same way as function but the functional is a method to map function $y(x)$ to scalar $F[y(x)]$, Unlike function which maps variable x to scalar $y(x)$, defined by

$$F[y(x)] = \int_{x_1}^{x_2} f(y(x), y'(x), x)\, dx. \tag{A.2}$$

First, suppose $y_0(x)$ is a function that yields extremum value of functional which is perturbed by an arbitrary function $\eta(x)$, differentiable function and has small magnitude and satisfies boundary conditions,

$$\eta(x_1) = \eta(x_2) = 0. \tag{A.3}$$

The difference between functionals must be zero similar to Eq.(A.1),

$$\begin{aligned} \lim_{\varepsilon \to 0} \frac{F[y_0 + \varepsilon\eta] - F[y_0]}{\varepsilon} &= \frac{d}{d\varepsilon} F[y_0 + \varepsilon\eta]|_{\varepsilon=0} \\ &= \int \frac{\delta F}{\delta y} \eta \, dx \\ &= 0, \end{aligned} \tag{A.4}$$

when $\dfrac{\delta F}{\delta y}$ is derivative of functional F compared with function y at point x. From Eq.(A.2), $F[y_0 + \varepsilon\eta]$ is explained by,

$$\begin{aligned} F[y_0 + \varepsilon\eta] &= \int f(y_0 + \varepsilon\eta, y_0' + \varepsilon\eta', x)\, dx, \\ &= \int f(y_0, y_0', x) + \varepsilon \frac{\partial f}{\partial y}\eta + \varepsilon \frac{\partial f}{\partial y'}\eta' + O\left(\varepsilon^2\right) dx. \end{aligned} \tag{A.5}$$

If Eq.(A.4) is substituted by Eq.(A.2) and Eq.(A.5), it follows that

$$\begin{aligned}\lim_{\varepsilon\to 0}\frac{\int f\left(y_0,y_0',x\right)+\varepsilon\frac{\partial f}{\partial y}\eta+\varepsilon\frac{\partial f}{\partial y'}\eta'+O\left(\varepsilon^2\right)-f\left(y_0,y_0',x\right)dx}{\varepsilon}\\ =\lim_{\varepsilon\to 0}\frac{\int \varepsilon\frac{\partial f}{\partial y}\eta+\varepsilon\frac{\partial f}{\partial y'}\eta'+O\left(\varepsilon^2\right)dx}{\varepsilon}=\int\frac{\partial f}{\partial y}\eta+\frac{\partial f}{\partial y'}dx,\\ =\int\left(\frac{\partial f}{\partial y}-\frac{\partial}{\partial x}\left(\frac{\partial f}{\partial y'}\right)\right)\eta+\frac{\partial}{\partial x}\left(\frac{\partial f}{\partial y'}\eta\right)dx.\end{aligned}$$

The second term vanishes because of the boundary conditions of η, Eq.(A.3), when the integration operator is operated,

$$\int\left(\frac{\partial f}{\partial y}-\frac{\partial}{\partial x}\left(\frac{\partial f}{\partial y'}\right)\right)\eta\,dx=0. \tag{A.6}$$

The function η is an arbitrary function which is not necessary zero so Eq.(A.6) will be satisfied if and only if

$$\frac{\partial f}{\partial y}-\frac{\partial}{\partial x}\left(\frac{\partial f}{\partial y'}\right)=0. \tag{A.7}$$

This equation is called Euler-Lagrange equation, Euler's equation or Lagrange's equation, which is the condition to find the function that yields extremum value of a functional. Eq.(A.7), is proved in a special case that the functional depends on one function and this function depend on one variable, $(F=F[y(x)])$. In a more general case, if the functional depends on many functions but the function depends on only one variable,$(F=F[y_1,y_2,...,y_n])$, Euler's equation can be written as

$$\frac{\partial f}{\partial y_i}-\frac{\partial}{\partial x}\left(\frac{\partial f}{\partial y_i'}\right)=0. \tag{A.8}$$

If the functional has the constraint, $\left(G[y(x)]=\int g(y(x))=C\right)$ or in general form $(H[y(x)]=G[y(x)]-C=0)$, in order to find the extremum value, it will be satisfied by

$$\frac{\partial f}{\partial y_i}-\frac{\partial}{\partial x}\left(\frac{\partial f}{\partial y_i'}\right)-\lambda_i\frac{\partial g}{\partial y_i}=0. \tag{A.9}$$

The variable λ is a dummy variable called a Lagrange multiplier. In density functional theory, the total energy of the system depends on density, not on derivative of density so the second term in Eq.(A.9) vanishes. The Euler's equation in this case is written as

$$\frac{\partial f}{\partial y_i}-\lambda_i\frac{\partial g}{\partial y_i}=0. \tag{A.10}$$

Appendix B

DERIVATIVE OF A REAL VALUE FUNCTION WITH COMPLEX PARAMETERS

The derivation of function of complex variable ($f = f(z)$) is more complicated than the function of real variable because it consists of two variables, real part z and imaginary part z^*; therefore, the condition from Eq.(A.1) is not enough in this case. The condition to find the extremum value in this case has two approaches.

The first approach, the variable z is represented in form $z = x + iy$ when x and y are real variables. Now, the function depends on the variable x and y, $f(z) = f(x, y)$. The extremum value of this function occurs when

$$\left.\frac{\partial f}{\partial x}\right|_{z=z_0} = \left.\frac{\partial f}{\partial y}\right|_{z=z_0} = 0. \tag{B.1}$$

Where z_0 is a point that the function's value is extremum. This method is complex because z must be replaced before the condition, Eq.(B.1), can be used.

The second approach which is equivalent to first approach but it is in form of complex variable,

$$\frac{\partial f}{\partial z} = \frac{\partial f}{\partial z^*} = 0. \tag{B.2}$$

If the function f is real, the derivative of this function will be real too, $\left(\frac{\partial f}{\partial x} = \left(\frac{\partial f}{\partial x}\right)^*, \frac{\partial f}{\partial y} = \left(\frac{\partial f}{\partial y}\right)^*\right)$. There two conditions can be reduced to a single condition,

$$\frac{\partial f}{\partial z^*} = 0. \tag{B.3}$$

Appendix C

CASTEP

CASTEP Cambridge serial total energy package (CASTEP), based on DFT with plane wave basis is a software that is widely used to study a property of materials. It is one of the modules in Materials Studio program which has a graphic user interface (GUI). There have two steps for using CASTEP. The first step is created the material which requests structural information, i.e., space group, lattice parameter and atomic position. The second one is choose the option to calculate.

In order to create a material, the first step, open Materials Studio program from the desktop and then create a new 3D Atomistic Document. Call the **Build Crystal** bar by click the Build button and go to the **Crystals** and then chose the **Bulid Crystals** as shown in FIG.C.1. The first tap, Space Group tap, allows

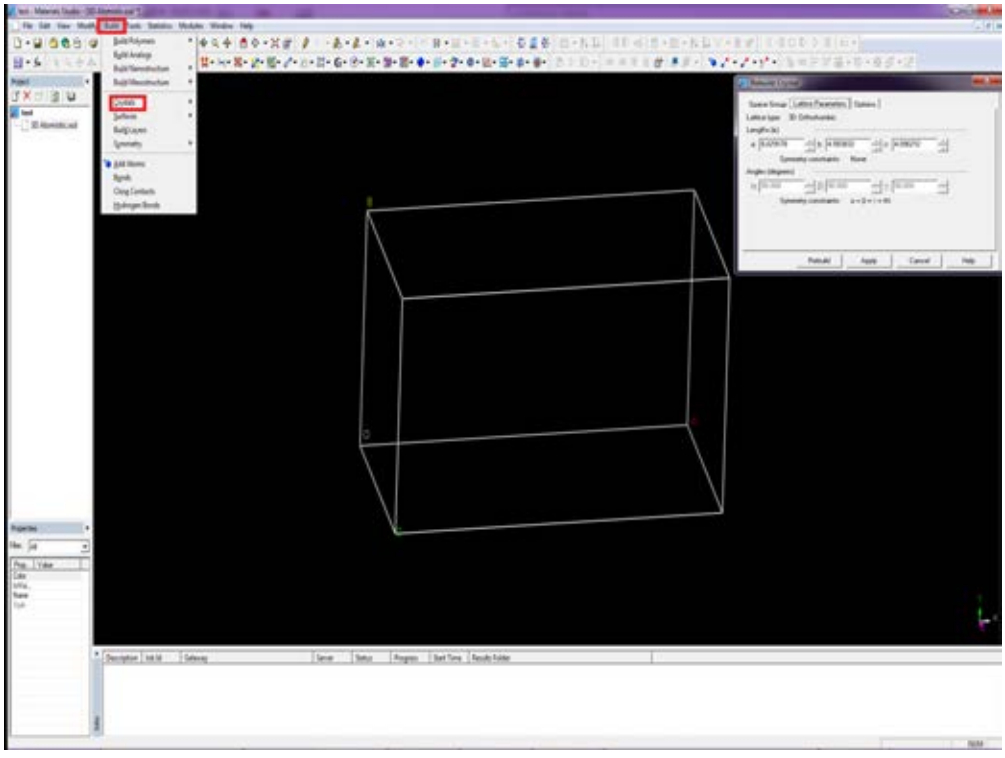

Figure C.1: Define the space group and lattice parameters.

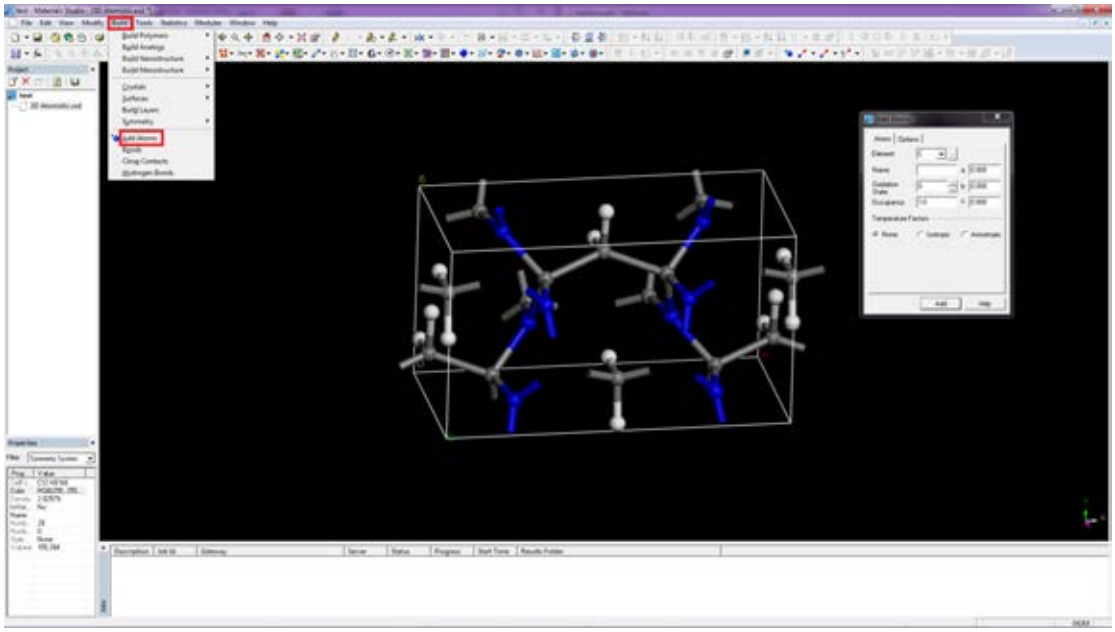

Figure C.2: Set the atomic positions.

us to select a space group which has 230 distinct types using Hermann-Mangain notation. The second tap, **Lattice Parameters** tap, is used to set lattice parameters, i.e. a, b and c, and angle, i.e., α, β and γ. Next, call **Add Atoms** bar which can be chosen in the **Bulid** button as shown in FIG.C.2. The first tap, **Atoms** tap, is used to define type of atom and its position.

To select option to calculate in the CASTEP, call the CASTEP program by click **Modules** button and go to **CASTEP** and then chose Calculation as shown in FIG.C.3. The first tap, **Setup** is used to choose the method and exchange-correlation functional in the calculation. The CASTEP has many method for, using to calculate, i.e., Energy, Geometry Optimization, Dynamics, Elastic constants, TS search and Properties. In this thesis, we only use Energy, Geometry optimization and Properties methods. The first one, Energy, is the calculation that only solves the Kohn-Sham equation without changing atomic position. The Geometry optimization is similar to the first one but it moves atom in order to search for the lowest energy position. The last method, Properties, is the calculation that uses the result from the Kohn-Sham equation to calculate the targeted property that we are interested. However, Energy or Geometry optimization must be used to solve Kohn-Sham equation before this method is operated. The method to calculate is chose by press the **Task** button. Press the **Functional** button to select the exchange-correlation functional, e.g., LDA, GGA-PBE, sX-LDA.

The Next tab, **Electronic** tab, allows us to set the parameter, i.e., energy

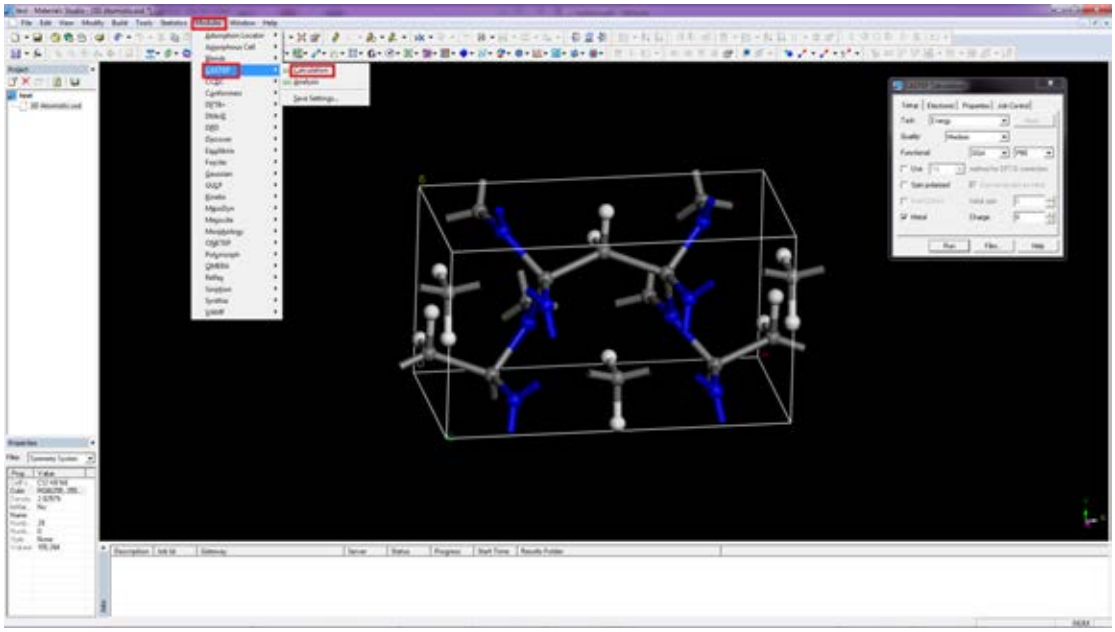

Figure C.3: Chose the method to calculate and functional.

cut off, k-point and pseudo-potential. For k-points, there are two methods to set this parameter. The first method is setting by fix number of point in each direction. The second method is specifying the length between the k-point grips. The following tab, **Properties** tab, is used for choosing the targeted properties to calculate. This program can calculate many properties, i.e., band structure, core level spectroscopy, density of state, electron density difference, electron localization function, NMR, optical properties, orbitals, phonons, population analysis, stress, polarizability, IR and Raman spectra. The last one, **Job Control** tab, allows us to select a server for the CASTEP and number of node to perform.

Bioghaphy

Mr. Sorajit Arrerut was born on 8 November 1989. He graduated from Assumption College school. Then he got his Bachelor of Science in physics (B.Sc. physics) from Chulalongkorn University in 2010. His senior project in B.Sc. is on the vibration of molecules in liquid metal. Afterwards, he continued Master of Science in physics (M. Sc. physics) and worked in the Exterme Condition Physics Research Laboratory (ECPRL) at Chulalongkorn University. The advisor in M. Sc. is Assoc.Prof. Udomsilp Pinsook in the subject of electronic and mechanical properties of carbon nitride methanediide.

International Conferences:

1. A. Sorajit, K. Takarabe and U. Pinsook. "Mechanical and Electronic properties of $C_2N_2(CH_2)$ under high pressure using density functional theory." The 39^{th} Congress on Science and Technology of Thailand. Bangkok, Thailand (21-23 Oct 2013)

Manuscript :

1. A. Sorajit, K. Takarabe and U. Pinsook "Electronic and Mechanical Properties of carbon nitride methanediide $C_2N_2(CH_2)$ under High Pressure" to be submitted.

thesis

ORIGINALITY REPORT

20%	11%	18%	5%
SIMILARITY INDEX	INTERNET SOURCES	PUBLICATIONS	STUDENT PAPERS

PRIMARY SOURCES

1	Submitted to Chulalongkorn University Student Paper	1%
2	Sougawa, M, T Sumiya, K Takarabe, Y Mori, T Okada, H Gotou, T Yagi, D Yamazaki, N Tomioka, T Katsura, H Kariyazaki, K Sueoka, and S Kunitsugu. "Bond strengths of New Carbon-nitride-Related material $C_2N_2(CH_2)$", Journal of Physics Conference Series, 2012. Publication	1%
3	Wei, Qun, Meiguang Zhang, Lixin Guo, Haiyan Yan, Xuanmin Zhu, Zhengzhe Lin, and Ping Guo. "Ab initio studies of novel carbon nitride phase C2N2(CH2)", Chemical Physics, 2013. Publication	1%
4	Shwetha, Gummula, Venkatakrishnan Kanchana, Kunchala Ramesh Babu, Ganapathy Vaitheeswaran, and Mundachali Cheruvalath Valsakumar. "High Pressure Structural Stability, and Optical Properties of Scheelite type ZrGeO4 and HfGeO4 X-ray Phosphor Hosts", The Journal of Physical Chemistry C, 2014. Publication	1%

5	www.misasa.okayama-u.ac.jp Internet Source	<1%
6	Frosch, Torsten(Kiefer, Wolfgang, Kothe, Erika and Popp, Jürgen). "Entwicklung und Anwendung Raman-spektroskopischer Methoden zur Untersuchung von Antimalaria-Wirkstoffen, biologischen Zielgruppen und deren molekularen Wechselwirkungen", Digitale Bibliothek Thüringen, 2008. Publication	<1%
7	Pakornchote, T, U Pinsook, and T Bovornratanaraks. "The hcp to fcc transformation path of scandium trihydride under high pressure", Journal of Physics Condensed Matter, 2014. Publication	<1%
8	Dirk Porezag. "Infrared intensities and Raman-scattering activities within density-functional theory", Physical Review B, 09/1996 Publication	<1%
9	Xu, Yuan, and Shang-Peng Gao. "Band gap of C3N4 in the GW approximation", International Journal of Hydrogen Energy, 2012. Publication	<1%
10	Da Silva, Juarez Lopez Ferreira. "The Nature and Behavior of Rare-gas Atoms on Metal Surfaces", Technische Universität Berlin, 2003. Publication	<1%

11	wurm.info Internet Source	<1%
12	Shabaev, A., S. G. Lambrakos, N. Bernstein, V. L. Jacobs, D. Finkenstadt, Nibir K. Dhar, and Thomas W. Crowe. "", Terahertz Physics Devices and Systems V Advance Applications in Industry and Defense, 2011. Publication	<1%
13	www-apl.c.oka-pu.ac.jp Internet Source	<1%
14	www.postech.ac.kr Internet Source	<1%
15	www.fhi-berlin.mpg.de Internet Source	<1%
16	www.scribd.com Internet Source	<1%
17	Atodiresei, N.. "First Principles Theory of Organic Molecules on Metal surfaces", Forschungszentrum Jülich, Zentralbibliothek, Verlag, 2005. Publication	<1%
18	Yeqiong Wu. "Electronic structure and properties of LaNi5 compound from first principles", Rare Metals, 08/2010 Publication	<1%
19	Sun, C.Q.. "Thermo-mechanical behavior of low-dimensional systems: The local bond	<1%

average approach", Progress in Materials Science, 200902
Publication

20	Submitted to Universiti Malaysia Perlis Student Paper	<1%
21	Bondoux, C.. "MgO insulating films prepared by sol-gel route for SiC substrate", Journal of the European Ceramic Society, 2005 Publication	<1%
22	Nagy, A.. "Density functional. Theory and application to atoms and molecules", Physics Reports, 19980501 Publication	<1%
23	www.science.gov Internet Source	<1%
24	Xun Liu. "First principle calculation of elastic and thermodynamic properties of stishovite", Chinese Physics B, 12/2010 Publication	<1%
25	I. Zhirko. "Optical Investigation of Hydrogen Intercalation-Deinteracalation Processes in Layered Semiconductory-InSe Crystals", NATO Science Series II Mathematics Physics and Chemistry, 2005 Publication	<1%
26	etds.lib.ncku.edu.tw Internet Source	<1%
27	Schönecker, Stephan (Leibniz-Institut für	<1%

	Festkörper- und Werkstoffforschung Dresden (IFW Dresden), Institut für Theoretische Festkörperphysik, Prof. Dr. Helmut Eschrig, Prof. Dr. Jeroen van den Brink, Prof. Dr. Niels Egede Christensen and Technische Universität Dresden, Fakultät Mathematik und Naturwissenschaften). "Theoretical Studies of Epitaxial Bain Paths of Metals ", Saechsische Landesbibliothek- Staats- und Universitaetsbibliothek Dresden, 2011. Publication	<1 %
28	Changbo Chen. "New high-pressure phase of BaH_2 predicted by *ab initio* studies", Journal of Physics Condensed Matter, 06/09/2010 Publication	<1 %
29	SUEOKA, Koji, Yanbo WANG, Seiji SHIBA, and Seishiro FUKUTANI. "Ab Initio Analysis of Point Defects in Plane-Stressed Si Single Crystal", Journal of Computational Science and Technology, 2008. Publication	<1 %
30	leopardi.nest.sns.it Internet Source	<1 %
31	matdl.org Internet Source	<1 %
32	Botti, Silvana, and Julien Vidal. "Energy Generation: Solar Energy", Computational Approaches to Energy Materials Walsh/Computational, 2013.	<1 %

Publication

33	etd.lsu.edu Internet Source	<1%
34	Iafrate, G. J., and J. B. Krieger. "Extension of the KLI approximation toward the exact optimized effective potential", The Journal of Chemical Physics, 2013. Publication	<1%
35	Kang, Lei, Siyang Luo, Hongwei Huang, Ning Ye, Zheshuai Lin, Jingui Qin, and Chuangtian Chen. "Prospects for Fluoride Carbonate Nonlinear Optical Crystals in the UV and Deep-UV Regions", The Journal of Physical Chemistry C, 2013. Publication	<1%
36	www.wtec.org Internet Source	<1%
37	Yang, Jun. "Quantum Chemical Investigation of Electronic and Structural Properties of Crystalline Bismuth and Lanthanide Triborates", Kölner UniversitätsPublikationsServer, 2011. Publication	<1%
38	Zienert, Andreas (, Prof. Dr. Thomas Geßner). "Electronic Transport in Metallic Carbon Nanotubes with Metal Contacts", Universitätsbibliothek Chemnitz, 2013. Publication	<1%

39	Blügel, Stefan, Brückel, Thomas, Schneider, Claus M. and Urban, Knut. "Probing the Nanoworld", Forschungszentrum Jülich, Zentralbibliothek, Verlag, 2007. Publication	<1%
40	Zhao, Shuainan, and Karin Larsson. "Theoretical Study of the Energetic Stability and Geometry of Terminated and B-Doped Diamond (111) Surfaces", The Journal of Physical Chemistry C, 2014. Publication	<1%
41	www.cems.umn.edu Internet Source	<1%
42	Staroverov, Viktor N.. "Density-Functional Approximations for Exchange and Correlation", A Matter of Density Exploring the Electron Density Concept in the Chemical Biological and Materials Sciences, 2012. Publication	<1%
43	Anua, N Najwa, R Ahmed, A Shaari, M A Saeed, Bakhtiar Ul Haq, and Souraya Goumri-Said. "Non-local exchange correlation functionals impact on the structural, electronic and optical properties of III–V arsenides", Semiconductor Science and Technology, 2013. Publication	<1%
44	"Bibliography", Quantum Mechanics with Applications to Nanotechnology and	<1%

Information Science, 2013.
Publication

---

45 Gabriel Bester. "Electronic excitations in nanostructures: an empirical pseudopotential based approach", Journal of Physics Condensed Matter, 01/14/2009 <1%
Publication

---

46 Sang, Liwen, Meiyong Liao, and Masatomo Sumiya. "A Comprehensive Review of Semiconductor Ultraviolet Photodetectors: From Thin Film to One-Dimensional Nanostructures", Sensors, 2013. <1%
Publication

---

47 Heyden, Andreas. "Theoretical investigation of the nitrous oxide decomposition over iron zeolite catalysts", Technische Universität Harburg, 2005. <1%
Publication

---

48 Zhao Long. "First-principles study of electronic and optical properties in wurtzite $Zn_{1-x}Cu_xO$", Chinese Physics B, 05/2010 <1%
Publication

---

49 www.scichina.com:8081 <1%
Internet Source

---

50 Quirico, E.. "Precursor and metamorphic condition effects on Raman spectra of poorly ordered carbonaceous matter in chondrites and coals", Earth and Planetary Science Letters, 20090930 <1%

Publication

51	Rosner, Helge (Prof. Dr. Helmut Eschrig, Prof. Dr. Peter Fulde, Prof. Dr. W. E. Pickett and Technische Universität Dresden, Mathematik und Naturwissenschaften, Physik, Institut für Theoretische Physik). "Electronic structure and exchange integrals of low-dimensional cuprates", Saechsische Landesbibliothek-Staats- und Universitaetsbibliothek Dresden, 1999. Publication	<1%
52	nanoscience.huji.ac.il Internet Source	<1%
53	Wagner, Jan-Martin(Bechstedt, Friedhelm, Hoffmann, Axel and Strauch, Dieter). "Structure and Lattice Dynamics of GaN and AlN: Ab-Initio Investigations of Strained Polytypes and Superlattices", Digitale Bibliothek Thüringen, 2008. Publication	<1%
54	www.docstoc.com Internet Source	<1%
55	Submitted to Ramapo College Student Paper	<1%
56	crd.lbl.gov Internet Source	<1%
57	cel.archives-ouvertes.fr Internet Source	<1%

58	Vincent L. Lignères. "An Introduction to Orbital-Free Density Functional Theory", Handbook of Materials Modeling, 2005 Publication	<1%
59	Antons, Armin. "First-principles investigation of initial stages of surfactant mediated growth on the Si(111) substrate", Forschungszentrum Jülich, Zentralbibliothek, Verlag, 2005. Publication	<1%
60	Polyanin, . "Ordinary Differential Equations", Handbook of Mathematics for Engineers and Scientists, 2006. Publication	<1%
61	A P Litvinchuk. "Electronic structure, optical properties and lattice dynamics of $MgSO_3 \cdot 6H_2O$", Journal of Physics Condensed Matter, 12/07/2011 Publication	<1%
62	www.fc.up.pt Internet Source	<1%
63	worldwidescience.org Internet Source	<1%
64	Friedrich, Alexandra, Björn Winkler, Erick A. Juarez-Arellano, and Lkhamsuren Bayarjargal. "Synthesis of Binary Transition Metal Nitrides, Carbides and Borides from the Elements in the Laser-Heated Diamond Anvil Cell and Their Structure-Property Relations",	<1%

Materials, 2011.
Publication

---

65 Zhao, Zongyan, Zhaosheng Li, and Zhigang Zou. "Water Adsorption and Decomposition on N/V-Doped Anatase TiO_2 (101) Surfaces", The Journal of Physical Chemistry C, 2013. <1%
Publication

---

66 Iuga, Maria. "Ab Initio and Finite Element Simulations of Material Properties in Multiphase Ceramics", Universität Würzburg, 2008. <1%
Publication

---

67 Victor Milman. "Structural, electronic and vibrational properties of tetragonal zirconia under pressure: a density functional theory study", Journal of Physics Condensed Matter, 12/02/2009 <1%
Publication

---

68 Rossi Carvalho, Mariana. "Ab initio study of alanine-based polypeptide secondary-structure motifs in the gas phase", Technische Universität Berlin, 2012. <1%
Publication

---

69 Attig, Norbert, Blügel, Stefan, Grotendorst, Johannes and Marx, Dominik. "Multiscale Simulation Methods in Molecular Sciences", JUWEL - Volltextserver des Forschungszentrums Juelich, 2009. <1%
Publication

70	XiaoGuang Luo. "Hardness estimation for covalent crystals using empirical electron theory", Chinese Science Bulletin, 12/2010 Publication	<1%
71	Byounghak Lee. "Nonlocal exchange correlation in screened-exchange density functional methods", Physical Review B, 12/2007 Publication	<1%
72	www.esi.umontreal.ca Internet Source	<1%
73	beatztom.free.fr Internet Source	<1%
74	Ibáñez, J., R. Oliva, F. J. Manjón, A. Segura, T. Yamaguchi, Y. Nanishi, R. Cuscó, and L. Artús. "High-pressure lattice dynamics in wurtzite and rocksalt indium nitride investigated by means of Raman spectroscopy", Physical Review B, 2013. Publication	<1%
75	White, S.N.. "Laser Raman spectroscopy as a technique for identification of seafloor hydrothermal and cold seep minerals", Chemical Geology, 20090225 Publication	<1%
76	qchem.pnpi.spb.ru Internet Source	<1%
77	Chun-Hai Wang. "First-Principle Calculation	<1%

and Far Infrared Measurement for Infrared-Active Modes of Ba(Mg1/3Ta2/3)O3 : Calculation and Measurement for IR Modes of BMT", Journal of the American Ceramic Society, 11/2010
Publication

78 paper
Student Paper <1%

79 Weronika Walkosz. "Theoretical Methods and Approximations", Atomic Scale Characterization and First-Principles Studies of Si_3N_4 Interfaces, 2011
Publication <1%

80 Wortmann, Daniel. "An embedding green function approach for electron transport through interfaces", Forschungszentrum Jülich, Zentralbibliothek, Verlag, 2005.
Publication <1%

81 Anders, Frithjof, Jarrell, Mark (Eds.), Koch, Erik and Pavarini, Eva. "Correlated Electrons: From Models to Materials - Lecture Notes of the Autumn School Correlated Electrons 2012", Forschungszentrum Jülich GmbH, Institute for Advanced Simulation, 2012.
Publication <1%

82 www.lct.jussieu.fr
Internet Source <1%

83 Santra, Biswajit. "Density-Functional Theory Exchange-Correlation Functionals for <1%

Hydrogen Bonds in Water", Technische Universität Berlin, 2010.
Publication

84	theochem.chem.rug.nl Internet Source	<1%
85	Goglio, G.. "State of Art and recent trends in bulk carbon nitrides synthesis", Materials Science & Engineering R, 20080107 Publication	<1%
86	arxiv.org Internet Source	<1%
87	www.tlchm.bris.ac.uk Internet Source	<1%
88	Deslippe. "Ab initio Theories of the Structural, Electronic, and Optical Properties of Semiconductors: Bulk Crystals to Nanostructures", Comprehensive Semiconductor Science and Technology, 2011 Publication	<1%
89	R. Andreani. "An inexact-restoration method for nonlinear bilevel programming problems", Computational Optimization and Applications, 11/20/2007 Publication	<1%
90	Jindřich Kolorenč. "Applications of quantum Monte Carlo methods in condensed systems", Reports on Progress in Physics, 02/01/2011 Publication	<1%

91	Veprek, S.. "Chemistry, physics and fracture mechanics in search for superhard materials, and the origin of superhardness in nc-TiN/a-Si"3N"4 and related nanocomposites", Journal of Physics and Chemistry of Solids, 200705/06 Publication	<1%
92	René T. Boeré. "Tricarbonyl[*N*,*N*′,*N*″-tris(2,6-diisopropylphenyl)guanidine]molybdenum(0)", Acta Crystallographica Section E Structure Reports Online, 07/15/2011 Publication	<1%
93	A.-L. Auzende. "Atomistic calculations of structural and elastic properties of serpentine minerals: the case of lizardite", Physics and Chemistry of Minerals, 06/2006 Publication	<1%
94	Submitted to University of Witwatersrand Student Paper	<1%
95	Kronik, Leeor, and Yoshitada Morikawa. "Understanding the Metal-Molecule Interface from First Principles", The Molecule-Metal Interface KOCH INTERFACES O-BK, 2013. Publication	<1%
96	Azzi, S, A Zaoui, and M Ferhat. "High pressure phase of pnictides yttrium YAs and YBi: first-principles studies", Physica Scripta, 2013. Publication	<1%
97	Schuchardt, Karen L., Brett T. Didier, Todd Elsethagen, Lisong Sun, Vidhya Gurumoorthi,	<1%

Jared Chase, Jun Li, and Theresa L. Windus. "Basis Set Exchange: A Community Database for Computational Sciences", Journal of Chemical Information and Modeling, 2007.
Publication

---

98 WeiHu Zhang. "Electronic structure and magnetism of Fe-doped SiC nanotubes", Science China Physics Mechanics and Astronomy, 09/2010 <1%
Publication

---

99 Submitted to University of Central Florida <1%
Student Paper

---

100 Konrad H Marti. "Complete-graph tensor network states: a new fermionic wave function ansatz for molecules", New Journal of Physics, 10/05/2010 <1%
Publication

---

101 Parashari, S.S.. "Calculated structural, electronic and optical properties of Ga-based semiconductors under pressure", Physica B: Physics of Condensed Matter, 20080901 <1%
Publication

---

102 Submitted to Higher Education Commission Pakistan <1%
Student Paper

---

103 Submitted to University of Hong Kong <1%
Student Paper

---

104 Rosenblatt, . "Multivariable Integrals", <1%

Mathematical Modeling, 1998.
Publication

105 Hochedez, Jean-Francois E., F. D. Auret, Andrei Belsky, Philippe Bergonzo, Udo H. Schuehle, Jose L. Pau, Jose Alvarez, Olivier Hainaut, and Thierry P. Appourchaux. "", Innovative Telescopes and Instrumentation for Solar Astrophysics, 2003. <1%
Publication

106 Submitted to KTH - The Royal Institute of Technology <1%
Student Paper

107 Xiaoyan Cao. "Relativistic Pseudopotentials", Relativistic Methods for Chemists, 2010 <1%
Publication

108 Nadimi, Ebrahim (, Prof. Dr. -Ing. habil. John Thomas Horstmann). "Quantum Mechanical and Atomic Level ab initio Calculation of Electron Transport through Ultrathin Gate Dielectrics of Metal-Oxide-Semiconductor Field Effect Transistors", Universitätsbibliothek Chemnitz, 2008. <1%
Publication

109 Submitted to University of Arkansas, Fayetteville <1%
Student Paper

110 Hlushak, Stepan P., Clare McCabe, and Peter T. Cummings. "Fourier space approach to the classical density functional theory for multi- <1%

Yukawa and square-well fluids", The Journal of Chemical Physics, 2012.
Publication

111	ccm.uma.pt Internet Source	<1%
112	Progress in Theoretical Chemistry and Physics, 2003. Publication	<1%
113	M. M. Siddick. "Constrained dynamics and extraction of normal modes from ab initio molecular dynamics: Application to ammonia", The Journal of Chemical Physics, 2006 Publication	<1%
114	Zhang, Hongbin (Prof. Dr. Helmut Eschrig, Prof. Dr. Helmut Eschrig, Prof. Dr. Stefan Blügel and Technische Universität Dresden, Fakultät Mathematik und Naturwissenschaften). "Relativistic Density Functional Treatment of Magnetic Anisotropy", Saechsische Landesbibliothek- Staats- und Universitaetsbibliothek Dresden, 2009. Publication	<1%
115	Savini, Gianluca <1972>(Heggie, Prof. Malcolm I, Merli, Dott. Pier Giorgio and Pozzi, Prof. Giulio). "Theory of plastic and elastic properties of graphite and silicon carbide", Alma Mater Studiorum - Università di Bologna, 2012. Publication	<1%

116	www.ic.ac.uk Internet Source	<1%
117	www.ifw-dresden.de Internet Source	<1%
118	iss.bu.edu Internet Source	<1%
119	etd.gatech.edu Internet Source	<1%
120	lib.tkk.fi Internet Source	<1%
121	www.coursehero.com Internet Source	<1%
122	V.M. Aroutiounian. "Microwave characteristics of BARITT diodes based on silicon carbide", IEEE Transactions on Electron Devices, 3/1999 Publication	<1%
123	Koci, L.. "Ab initio calculations of the elastic properties of ferropericlase Mg"1"-"xFe"xO (x@?0.25)", Physics of the Earth and Planetary Interiors, 20071015 Publication	<1%
124	Zhu, Z.. "Enhanced gas-sensing behaviour of Ru-doped SnO"2 surface: A periodic density functional approach", Journal of Physics and Chemistry of Solids, 200909 Publication	<1%

125	Peng, Chengxiao, Yong Liang, Kefan Wang, Yang Zhang, Gaofeng Zhao, and Yuanxu Wang. "Possible Origin of Ferromagnetism in an Undoped ZnO d0 Semiconductor", The Journal of Physical Chemistry C, 2012. Publication	<1%
126	Andrey Ipatov. "Molecular excitation spectra by TDDFT with the nonadiabatic exact exchange kernel", International Journal of Quantum Chemistry, 2010 Publication	<1%
127	Submitted to University of South Florida Student Paper	<1%
128	Zu, Ningning, Jing Wang, and Zhi-Jian Wu. "Pressure Induced Half Metallic Ferrimagnetism in La2VMnO6", The Journal of Physical Chemistry C, 2013. Publication	<1%
129	sig3.ecanews.org Internet Source	<1%
130	E. I. Isaev. "Phonon related properties of transition metals, their carbides, and nitrides: A first-principles study", Journal of Applied Physics, 2007 Publication	<1%
131	星野 稔. "原子核と電子の量子効果を同時に取り扱う分子理論の高精度化と非平衡ダイナミクスへの展開", [出版者不明], 2009. Publication	<1%

132	Assfour, Bassem (Prof. Dr. Florian Mertens, Prof. Dr. rer. nat. habil. Gotthard Seifert and Technische Universität Dresden, Fakultät Mathematik und Naturwissenschaften). "Hydrogen Storage In Nanostructured Materials", Saechsische Landesbibliothek-Staats- und Universitaetsbibliothek Dresden, 2011. Publication	<1%
133	olivine.ethz.ch Internet Source	<1%
134	Yuan Xu Wang. "Elastic and electronic properties of TcB[sub 2] and superhard ReB[sub 2]: First-principles calculations", Applied Physics Letters, 2007 Publication	<1%
135	S H Shah. "First-principles density functional study of polarization–strain coupling in bismuth titanate", Journal of Physics Condensed Matter, 09/29/2010 Publication	<1%
136	Machón Valbuena, María. "Electron-phonon coupling, vibrational, and optical properties of carbon nanotubes and picotubes", Technische Universität Berlin, 2006. Publication	<1%
137	www.me.kuas.edu.tw Internet Source	<1%

138	Barber, . "SCATTERING BY AXISYMMETRIC PARTICLES: T-MATRIX METHOD", Advanced Series in Applied Physics, 1990. Publication	<1%
139	www.jove.com Internet Source	<1%
140	Mohr, Marcel. "Electronic and vibrational properties of carbon and CdSe nanostructures", Technische Universität Berlin, 2010. Publication	<1%
141	Cao Miao. "InGaN/GaN multi-quantum-well-based light-emitting and photodetective dual-functional devices", Frontiers of Optoelectronics in China, 09/23/2009 Publication	<1%
142	Kazuaki Kobayashi. "Lattice Anomaly of MgB (h -BN) and Related Compounds under Various Compression Conditions", Molecular Simulation, 1/1/2004 Publication	<1%
143	Li, Y.. "Crystal structure and physical properties of OsN: First-principle calculations", Solid State Communications, 201004 Publication	<1%
144	mpdc.mae.cornell.edu Internet Source	<1%
145	Henderson, Thomas M., Benjamin G. Janesko,	<1%

	and Gustavo E. Scuseria. "Range Separation and Local Hybridization in Density Functional Theory†", The Journal of Physical Chemistry A, 2008. Publication	<1 %
146	Erik E. Santiso. "Multi-scale Molecular Modeling of Chemical Reactivity", Molecular Simulation, 1/1/2004 Publication	<1 %
147	Balázs Hetényi. "Reconstruction of frozen-core all-electron orbitals from pseudo-orbitals", The Journal of Chemical Physics, 2001 Publication	<1 %
148	Bukowinski, Mark S.T., and Sofia Akber-Knutson. "The role of theoretical mineral physics in modeling the Earth's interior", Geophysical Monograph Series, 2005. Publication	<1 %
149	www.edu.upmc.fr Internet Source	<1 %
150	M D Segall. Journal of Physics Condensed Matter, 03/25/2002 Publication	<1 %
151	Yan, H.Y.. "Low-compressibility and hard material carbon nitride imide C"2N"2(NH): First principles calculations", Journal of Solid State Chemistry, 201103 Publication	<1 %

152	portellen.phycmt.dur.ac.uk Internet Source	<1%
153	Li, Hong, Paul Winget, and Jean-Luc Brédas. "Transparent Conducting Oxides of Relevance to Organic Electronics: Electronic Structures of Their Interfaces with Organic Layers", Chemistry of Materials, 2013. Publication	<1%
154	scholarworks.umass.edu Internet Source	<1%
155	Ying-Teng Zhai. "Structural diversity and electronic properties of Cu_{2}SnX_{3} (X=S, Se): A first-principles investigation", Physical Review B, 08/2011 Publication	<1%
156	www.thaitage.com Internet Source	<1%
157	Ortmann, Frank(Bechstedt, Friedhelm, Bobbert, Peter and Pflaum, Jens). "Charge Transport in Organic Crystals", Digitale Bibliothek Thüringen, 2009. Publication	<1%
158	Liu, Yong, Wen-Cheng Hu, De-jiang Li, Xiao-Qin Zeng, Chun-Shui Xu, and Xiang-Jie Yang. "First-principles investigation of structural and electronic properties of MgCu2 Laves phase under pressure", Intermetallics, 2012. Publication	<1%

159	louis14.nrl.navy.mil Internet Source	<1%
160	"Calculus of Variation", Mathematical Methods for Engineers and Scientists 3, 2007 Publication	<1%
161	www.chemistry.mcmaster.ca Internet Source	<1%
162	www.ncbi.nlm.nih.gov Internet Source	<1%
163	Tapati Mallik. "Synthesis, crystal structure and solubility of $C_6H_{14}N_4O_2$,$C_4H_4O_4$,$2H_2O$", Science and Technology of Advanced Materials, 07/31/2005 Publication	<1%
164	www.mms.gov Internet Source	<1%
165	www.vlab.msi.umn.edu Internet Source	<1%
166	www.scm.com Internet Source	<1%
167	LiangCai Ma. "First-principles study of the adsorption of oxygen atoms on copper nanowires", Science China Physics Mechanics and Astronomy, 02/06/2012 Publication	<1%
168	Steven Prawer. "Raman spectroscopy of diamond and doped diamond", Philosophical	<1%

	Transactions of The Royal Society A Mathematical Physical and Engineering Sciences, 11/15/2004 Publication	
169	El-Mallawany, . "Optical Properties of Tellurite Glasses in the Ultraviolet Region", Tellurite Glasses Handbook Physical Properties and Data Second Edition, 2011. Publication	<1%
170	edoc.ub.uni-muenchen.de Internet Source	<1%
171	Manfred Martin. "A chemically driven insulator–metal transition in non-stoichiometric and amorphous gallium oxide", Nature Materials, 05/2008 Publication	<1%
172	www.etsg.org Internet Source	<1%
173	www.nature.com Internet Source	<1%
174	www.ise.gmu.edu Internet Source	<1%
175	Hansen, Niels. "Multiscale modeling of reaction and diffusion in Zeolites", Technische Universität Harburg, 2010. Publication	<1%
176	envisat.esa.int Internet Source	<1%

177	Neise, Carsten (Prof. Dr. Helmut Eschrig, Prof. Dr. Hubert Ebert and Technische Universität Dresden, Fakultät Mathematik und Naturwissenschaften). "Magnetic Properties Studied by Density Functional Calculations Including Orbital Polarisation Corrections", Saechsische Landesbibliothek- Staats- und Universitaetsbibliothek Dresden, 2011. Publication	<1%
178	A Hachemi. "Elasticity of $SrTiO_3$ perovskite under high pressure in cubic, tetragonal and orthorhombic phases", Physica Scripta, 08/2010 Publication	<1%
179	Chen, Gang, and Shang-Peng Gao. "Structure and electronic structure of S-doped graphitic C_3N_4 investigated by density functional theory", Chinese Physics B, 2012. Publication	<1%
180	www.imperial.ac.uk Internet Source	<1%
181	Xu, Dongwei, Haiying He, Ravindra Pandey, and Shashi P Karna. "Stacking and electric field effects in atomically thin layers of GaN", Journal of Physics Condensed Matter, 2013. Publication	<1%
182	Kociper, Birgit. "Singlet - triplet gaps in polymers from range-separated time	<1%

dependent density functional theory", Publikationsserver der Universität Regensburg, 2012.
Publication

---

183 Sukumar, N.. "Density Functional Approach to the Electronic Structure of Matter", A Matter of Density Exploring the Electron Density Concept in the Chemical Biological and Materials Sciences, 2012. <1%
Publication

---

184 Elmer G. Valderrama. "Electron correlation studies by means of local-scaling transformations and electron-pair density functions", Journal of Mathematical Chemistry, 04/2005 <1%
Publication

---

185 Dang, Thi Uyen-Khanh. "Intersubband transitions in low-dimensional nanostructures Many-body effects in quantum wells and quantum dots", Technische Universität Berlin, 2012. <1%
Publication

---

186 C. J. Rupp. "First principles study of Si-doped BC[sub 2]N nanotubes", The Journal of Chemical Physics, 2009 <1%
Publication

---

187 J. Łażewski. "Ab initio elasticity of chalcopyrites", Journal of Applied Physics, 2003 <1%
Publication

188 Sougawa, Masaya, Kenichi Takarabe, Yoshihisa Mori, Taku Okada, Takehiko Yagi, Hiroaki Kariyazaki, and Koji Sueoka. "Bulk modulus and structural changes of carbon nitride C2N2(CH2) under pressure: The strength of C–N single bond", Journal of Applied Physics, 2013. <1%
Publication

189 Bu, Hongxia, Mingwen Zhao, Yan Xi, Xiaopeng Wang, Hua Peng, Chunlei Wang, and Xiangdong Liu. "Is yne-diamond a super-hard material?", EPL (Europhysics Letters), 2012. <1%
Publication

190 Johnson, C.M., N.G. Wright, M.J. Uren, K.P. Hilton, M. Rahimo, D.A. Hinchley, A.P. Knights, D.J. Morrison, A.B. Horsfall, S. Ortolland, and A.G. O'Neill. "Recent progress and current issues in SiC semiconductor devices for power applications", IEE Proceedings - Circuits Devices and Systems, 2001. <1%
Publication

191 Lazić, Jasmina(Mitra, G and Mladenović, N). "New variants of variable neighbourhood search for 0-1 mixed integer programming and clustering", Brunel University, School of Information Systems, Computing and Mathematics, 2010. <1%
Publication

192 Fu, Hongzhi; Liu, Wenfang and Gao, Tao. "Structural, elastic and thermodynamic properties of TiSC", Bulletin of Materials Science, 2011. <1%
Publication

193 Byounghak Lee. "Band gap bowing and electron localization of Ga[sub x]In[sub 1−x]N", Journal of Applied Physics, 2006 <1%
Publication

194 A. D. Yoffe. "Semiconductor quantum dots and related systems: electronic, optical, luminescence and related properties of low dimensional systems", Advances In Physics, 1/1/2001 <1%
Publication

195 島田 拓哉. "Theoretical analysis on the reaction mechanisms of reducing agents for electroless deposition processes", [出版者不明], 2009. <1%
Publication

196 Kremer, M., Münster, G. (Hrsg.) and Wolf, D.. "John von Neumann Institute for Computing NIC Symposium 2010 Proceedings, 24 - 25 February 2010 | Jülich, Germany", Forschungszentrum Jülich Zentralbibliothek, Verlag, 2010. <1%
Publication

197 Wang, B.T.. "First-principles study of ground-state properties and high pressure behavior of <1%

ThO"2", Journal of Nuclear Materials, 20100430
Publication

198 Costa, S. N., F. A. M. Sales, V. N. Freire, F. F. Maia, E. W. S. Caetano, L. O. Ladeira, E. L. Albuquerque, and U. L. Fulco. "l-Serine Anhydrous Crystals: Structural, Electronic, and Optical Properties by First-Principles Calculations, and Optical Absorption Measurement", Crystal Growth & Design, 2013. <1%
Publication

199 Kordt, Pascal. "Single-Site Green Function of the Dirac Equation for Full-Potential Electron Scattering", Forschungszentrum Jülich GmbH Zentralbibliothek, Verlag, 2012. <1%
Publication

200 John P. Perdew. "Density Functionals for Non-relativistic Coulomb Systems in the New Century", Lecture Notes in Physics, 2003 <1%
Publication

201 Borowka, Julia. "Quantum Chemical Calculations on the Copper(II) Catalyzed Michael Reaction", Technische Universität Berlin, 2007. <1%
Publication

202 M. Preuss. "Vibrational spectra of ammonia, benzene, and benzene adsorbed on Si(001) by first principles calculations with periodic <1%

boundary conditions", Physical Review B, 04/2006

Publication

EXCLUDE QUOTES	OFF	EXCLUDE MATCHES	OFF
EXCLUDE BIBLIOGRAPHY	OFF		